

**Hot-Wire Chemical Vapor Deposition of
Silicon and Silicon Nitride for Photovoltaics:
Experiments, Simulations, and Applications**

Thesis by

Jason Knowles Holt

In Partial Fulfillment of the Requirements

for the Degree of

Doctor of Philosophy

California Institute of Technology

Pasadena, California

2003

(Defended October 10, 2002)

© 2003

Jason K. Holt

All rights reserved

Acknowledgements

I am now about to undertake the singularly most difficult task in my last 5 years here at Caltech – to thank all of the people who have contributed to my thesis, directly and indirectly.

Harry Atwater took me into his group comparatively late into my graduate career, at a time when I was debating whether this whole Ph.D. thing was for me or not. From the day I entered, I was encouraged, challenged, and given the opportunity to attend numerous conferences where I experienced a whole new element to my graduate studies. His enthusiasm and willingness to tailor this project to my background cannot be overstated. I was also in the unique situation to be co-advised by David Goodwin, who provided guidance with the simulation and modeling aspects of this thesis. Together, they provided an ideal balance for me.

Funding for this work came principally from the National Renewable Energy Laboratory (NREL) and through an Applied Materials Research Fellowship. I would like to thank the number of people at NREL I had the pleasure of meeting and discussing photovoltaic research with during 4 annual summer trips to the Rocky Mountains for the Crystalline Silicon Solar Cell Materials Conference. Late into this project, I also had the pleasure of collaborating with Andrew Gabor at *Evergreen Solar, Inc.* and Mike Stavola at Lehigh University who helped us put together a nice story on silicon solar cell passivation.

And now, for the people that I saw on a regular basis with whom I could talk about things ranging from mass spectrometry to where to go for a beer: the Atwater group. Torsten Bistrichan helped get me up to speed on the hot-wire reactor when I first joined the group and was always a good drinking buddy. Maribeth Mason was probably the second person in the group I met, and we had a number of productive (and often humorous) conversations together, particularly at the many conferences we attended. Claudine Chen was always available to talk to me during various tumultuous points in my life while here, and provided the environmental “conscience” for our office; new people wonder why I often still work with the lights off. I only briefly overlapped with Kyu Min, but I have to thank him for letting me attend his wedding and reception after being in the group for only a month; this got me hooked on karaoke forever. Thanks to Liz Boer-Duchemin for letting me bounce ideas off her – hard to imagine a physicist and a chemical engineer communicating well.

Regina Ragan was always available for a coffee (*even if we had had one 15 minutes prior!*), and occasionally some late-night beers, and listened to my complaining without fail. Of all the members of the group, I have known Rhett Brewer the longest, as we toiled through first year Chemical Engineering courses and qualifying exams together. Although we weren’t really coffee or beer buddies (*inside joke*), we had many scientific and non-scientific discussions together. He has a vast knowledge of vacuum processes, having built two

systems from scratch, and I was able to draw on his experience on a number of occasions. He was particularly helpful with more personal discussions, however, which often took the form, “Hey, you should watch yourself with that woman...” I hope that I was able to be equally useful, if not in scientific conversation, then in personal matters. Thanks to Julie Casperson for providing smiles on days in which I was feeling like anything but smiling and also for a being the group’s club diva that made me realize there was a world outside “Goth.” However, I thank Cecily Ryan for being the most “Goth” person in the group, next to myself, and encouraging trips to these clubs in Hollywood. Jimmy Zahler’s and Robb Walter’s contributions to the lunchtime discussions cannot go without credit (*forget what all the etiquette books say about discussing politics and religion*). Stefan Maier’s hard work and efficiency provided motivation to me on some of my less exciting days. Harry brought in a visitor from Sweden last year, Joakim Nilsson, with whom I had many entertaining late night conversations.[†] He offered up his apartment for me to stay at in Stockholm, during a particularly difficult point in time for me, and was able to show me how to have a good time, Swedish style.

Harry sure knows how to pick postdocs! Upon joining the group, I had the pleasure of meeting Mark Brongersma, who has a breadth of knowledge that

[†] I had never before met someone who had seen *Top Gun* more than 5 times, let alone boast about it and have the ability to recite any line of the movie.

allowed him to make many useful comments on my group presentations. He was also an avid consumer of the Belgian ales at Lucky Baldwin's in Old Town Pasadena, where we hung out on countless occasions. I later met Pieter Kik, from the same institute as Mark in The Netherlands, and as luck would have it, also a fan of Belgian ale. Must be something in the water there in Amsterdam because Pieter is not only an exemplary scientist, but also a talented musician. He also helped me figure out the most effective way to communicate my ideas during presentations, and was one to sit and listen to personal issues of mine. Another postdoc in the group, Anna Foncuberta i Morral, was able to provide many useful insights and answers to issues that I had long wondered about in this field, as her thesis work was very similar; like Julie, she also had a way of cheering me up on the gloomiest of days.

Word soon got out around campus about how fun Harry's research group was, and we saw an explosion of new students in the last two years. Although I wasn't able to get to know all of them personally, I enjoyed conversations with Luke Sweatlock, Andrea Martin, Julie Biteen, Tao Feng, Beth Lachut, and Ben Kaufmann.

I was fortunate to be able to stay in touch with a number of friends from high school and college during my stay at Caltech. I'd like to thank Nicole Kim, Duke Dougherty, Larry Tu, Long Le, and Steve Costuma for staying in touch and being around when I wanted to escape to familiar Orange County. In particular, I have

to acknowledge Steve Costuma for meeting with me at the local Diedrich's coffee shop a week before classes were to start for me (back in September of 1997), and convincing me that I couldn't afford to pass up the opportunity to attend Caltech.

Finally, I have to thank the members of my family, most of which were close by during the past 5 years. I'd like to thank my grandmother and great-grandmother for their support of my studies. I wish my uncle could have been here to see the culmination of my work. He made lots of jokes, but I later learned that he was secretly proud of the work I was doing, and I miss the fun times we had together during weekend trips to Phoenix. My other grandmother from the Bay Area was also supportive of my studies, even when it seemed crazy to enter another 5+ year program right after college (*sorry, I had to pass up Stanford in favor of Caltech*). And, of course, my mom and dad were always there for me, providing love and support, attending my jazz concerts on campus, and bringing up "care packages" to a poor graduate student who might have otherwise starved.

Abstract

Hot-wire chemical vapor deposition is a promising technique for deposition of thin amorphous, polycrystalline, and epitaxial silicon films for photovoltaic applications. Fundamental questions remain, however, about the gas-phase and surface-kinetic processes involved. To this end, the nature of the wire decomposition process has been studied in detail by use of mass spectrometry. Atomic silicon was the predominant radical formed for wire temperatures above 1500 K, and catalysis was evident for SiH_3 production with the use of a new wire. Aged wires appear to produce radicals by a non-catalyzed route and chemical analysis of these wires reveal large quantities of silicon at the surface, consistent with the presence of a silicide layer. This study is the first of its kind to correlate radical desorption kinetics with filament aging for the hot-wire chemical vapor deposition technique.

Threshold ionization mass spectrometry revealed large quantities of the SiH_2 radical, attributed to heterogeneous pyrolysis on the walls of the reactor. At dilute (1%) silane pressures of up to 2 Torr, a negligible amount of ions and silicon agglomerates (Si_2 , Si_2H , Si_2H_6) were detected. Density functional theory calculations reveal an energetically favorable route for the reaction of Si and SiH_4 , producing Si_2H_2 and H_2 . The trace amounts of Si_2H_2 observed experimentally, however, may suggest that an intermediate spin state transition

involved in this reaction is slow under the hot-wire conditions used. Monte Carlo simulations of the hot-wire reactor suggest SiH_3 is the predominant growth species under conditions leading to amorphous and polycrystalline growth. The flux of atomic hydrogen, rather than the identity of the precursor, appears to be the more important factor in governing the amorphous-to-microcrystalline transition that occurs upon hydrogen-dilution. Two-dimensional Monte Carlo simulations were used to model a hot-wire reactor for the first time, showing that filament arrays can be used to improve film growth uniformity. Under conditions where agglomerate formation does not occur, continuum simulations predict a maximum growth rate of 10 nm/s for dilute (1%) silane conditions and a rate of 50 nm/s for pure silane.

Hot-wire chemical vapor deposition was used to deposit silicon nitride films with indices of refraction from 1.8-2.5 and hydrogen content from 9-18 atomic %. By tuning the SiH_4/NH_3 flow ratio, films in which the hydrogen was predominantly bound to N or Si could be produced, each of which reveal different hydrogen release kinetics. Platinum-diffused silicon samples, capped by a hydrogenated silicon nitride layer revealed, upon annealing at 700°C, platinum-hydrogen complexes with a bulk concentration of 10^{14} cm^{-3} . This constitutes the first direct evidence for bulk silicon passivation by hydrogen release from a silicon nitride layer and hydrogen complex formation.

Photovoltaic cells employing a hot-wire nitride layer were found to have comparable electrical properties to those using plasma nitride layers.

Finally, a method for *in situ* generation of SiH_4 by atomic hydrogen etching was evaluated. Using a cooled crystalline silicon target in an H/H_2 ambient produced negligible etching, while a cooled amorphous silicon film target was etched at a rate of up to 14 nm/min. In the latter case, net deposition at 0.6 nm/min onto a heated Ge(100) substrate resulted. A method for more efficient etching of crystalline silicon materials was proposed.

Related Publications

The work described in this thesis is derived, in part, from the publications listed below:

- “The aging of tungsten filaments and its effect on wire surface kinetics in hot-wire chemical vapor deposition”, J. K. Holt, M. Swiatek, D. G. Goodwin, H. A. Atwater, *J. Appl. Phys.* 92(8), 4803-4808 (2002). **(Chapter 2)**
- “Gas Phase and Surface Kinetic Processes in Polycrystalline Silicon Hot-Wire Chemical Vapor Deposition”, J. K. Holt, M. Swiatek, D. G. Goodwin, and H. A. Atwater, *Thin Solid Films* 395, 29-35 (2001). **(Chapters 3 and 4)**
- “Si + SiH₄ Reactions and Implications for Hot-Wire CVD of a-Si:H: Computational Studies”, R. P. Muller, J. K. Holt, D. G. Goodwin, and W. A. Goddard, III, *Mat. Res. Soc. Symp. Proc. Vol. 609* (2000). **(Chapter 4)**
- “Radical Species Distributions in Hot-Wire Chemical Vapor Deposition Probed Via Threshold Ionization Mass Spectrometry and Direct Simulation Monte Carlo Techniques”, J.K. Holt, M. Swiatek, D.G. Goodwin, R.P. Muller, W.A. Goddard, III, and Harry A. Atwater, *Mat. Res. Soc. Symp. Proc. Vol. 664* (2001). **(Chapter 4)**
- “Hot Wire Chemical Vapor Deposition of High Hydrogen Content Silicon Nitride for Solar Cell Passivation and Anti-Reflection Coating Applications”, J. K. Holt, D. G. Goodwin, A. M. Gabor, F. Jiang, M. Stavola, and Harry A. Atwater, *Thin Solid Films*, submitted for publication (2002). **(Chapter 5)**

List of Figures and Tables

Chapter 1

- Figure 1. Example of a n-p-p⁺ solar cell. Photons are absorbed and generate electron-hole pairs, primarily in the p region in this case. The internal field (E) separates the carriers, allowing current to be collected at the ohmic contacts. Grain boundaries, present in polycrystalline solar cells, can act as recombination centers. 5
- Figure 2. (a) Current-voltage characteristics of an ideal solar cell, with and without illumination; V_{OC} is the open circuit voltage, and I_{SC} is the short-circuit current, (b) the circuit equivalent of this idealized solar cell; adapted from Chen.⁸ 6
- Figure 3. Schematic of the HWCVD process, illustrating the various kinetic processes involved. 7

Chapter 2

- Figure 1. Diagram of the hot-wire reactor. 25
- Figure 2. Low pressure (5×10^{-6} Torr) radical species measurements obtained using a new W wire. Activation energy accurate to within +/- 10%,

due to wire temperature uncertainties (+/- 50 K); error bars are not shown.....	29
Figure 3. Summary of experimental studies on W wire surface kinetics.	30
Figure 4. SiH _x radical signals measured from an aged W wire at a total pressure of 5 x 10 ⁻⁶ Torr. Activation energies quoted are accurate to within +/- 10%, due to uncertainties (+/- 50K) in wire temperature; error bars are not shown.	33
Figure 5. Surface morphology of (a) new, (b) heat-treated, and (c) aged wires. .	35
Figure 6. Scanning electron microscopy (SEM) image of aged tungsten wire.....	37
Table 1. Composition of used tungsten wire, as determined by Auger Electron Spectroscopy (AES).....	37
Figure 7. Si-W phase diagram, created with TAPP v2.1 (Thermochemical and Physical Properties), ES Microwave, 1991.	38
Figure 8. Mass spectrometry evidence for Si incorporation by W wire.....	40
Figure 9. Rates of interest for wire surface kinetic processes.	41

Chapter 3

Figure 1. (a) Response of reactor to a pulse input of gas - 187 mTorr/47.1 sccm of 1% Ar in He mixture; (b) Normalized response function and residence time distribution (RTD) function for Ar tracer experiment and for an ideal CSTR.....	55
---	----

Figure 2. Simulated species disitributions as a function of reactor residence time for total pressures of (a) 0.1 Torr and (b) 1 Torr, for a 1% SiH ₄ in He mixture.	59
Figure 3: Detection of ions under conditions of 382 mTorr (1% SiH ₄ in He), filament temperature of 1700°C, and filament bias of 34 V. Both spectra were background corrected. Discontinuities are caused by negative baseline values, the absolute values of which are much less than the peak signal intensities.....	63
Table 1. Threshold energies (eV) for direct radical and dissociative ionization. From Robertson <i>et al.</i> ²⁵	66
Figure 4a, b. Threshold ionization spectra of (a) Si and (b) SiH ₂ , acquired at 28 mTorr (1% SiH ₄ in He).	69
Figure 4c, d. Threshold ionization spectra of (c) SiH ₃ and (d) H acquired at 28 mTorr (1% SiH ₄ in He).	70
Figure 5a, b. Threshold ionization spectra of (a) Si and (b) SiH ₂ , obtained at 220 mTorr (1% SiH ₄ in He).	73
Figure 5c, d. Threshold ionization spectra of (c) SiH ₃ and (d) H obtained at 220 mTorr (1% SiH ₄ in He).	74
Figure 6. (a) Distribution of Si ₂ H _x species observed at 2050 mTorr, (b) Cracking pattern of Si ₂ H ₆ within the mass spectrometer.....	80

Chapter 4

Figure 1. Energy profile (kcal/mole) for the insertion, rearrangement, and H ₂ elimination process that leads to Si ₂ H ₂	90
Figure 2. Simulation domain for two-dimensional DSMC model of the hot-wire reactor.	101
Figure 3. 1-D species profiles along the gas-inlet axis (Y=0) for conditions of 10 mTorr pure SiH ₄ , T _{wire} = 2000°C.	103
Table 1. Conditions leading to amorphous or polycrystalline silicon growth from Schropp <i>et al.</i> , ²² and corresponding radical flux ratios to the surface from DSMC simulations. Also listed are experimental conditions from a recent study ²³ by the present author.	104
Figure 4. Species profiles obtained along the gas-inlet axis (y=0) for feed gas conditions of (a) 35 mTorr SiH ₄ , and (b) 80 mTorr dilute SiH ₄ (9:1, H ₂ :SiH ₄).	106
Figure 5 (color). Contour plots of the SiH ₃ concentration (atomic %) for feed gas conditions of 84 mTorr SiH ₄ with (a) one wire and (b) three wires (0.25 mm diameter). The near-substrate region is shown here (X = 4-5 cm) to enhance contrast.....	108
Figure 6. Gas species profiles obtained with the continuum simulation for dilute (1%) SiH ₄ at 5 Torr pressure in (a) He and (b) Ar for a residence time of 2 ms in each case.	113

Figure 7. Growth rate as a function of pressure, determined from the continuum model. Conditions of dilute (1%) and pure SiH ₄ are simulated. Selected experimental growth rates from the literature are included as a reference; Ref. [9] Molenbroek <i>et al.</i> (1997), Ref. [8] Molenbroek <i>et al.</i> (1996), Ref. [22] Schropp <i>et al.</i> (1997), Ref. [27] B.P. Nelson <i>et al.</i> (2002).	116
--	-----

Chapter 5

Figure 1. Low pressure radical measurements probing NH ₃ decomposition....	126
Figure 2. XPS N 1s spectra for films grown via hot-wire and plasma CVD.....	128
Figure 3. FTIR spectra for films grown under different SiH ₄ /NH ₃ flow ratios.	130
Figure 4. Normalized FTIR spectra of the same films as in Figure 3.....	131
Table 1. Film growth conditions and resulting thickness/index.....	131
Table 2. Summary of RBS and HFS film analysis.....	133
Figure 5. FTIR spectra at various annealing temperatures (5 minute anneal at each temperature) for (a) film grown with a flow ratio of 0.02 SiH ₄ /NH ₃ , and (b) film grown with 0.08 SiH ₄ /NH ₃ ; corresponding hydrogen concentrations at each temperature are listed.	136
Figure 6. Schematic of Multiple Internal Reflection technique used to probe hydrogenation of defects.	138

Figure 7. FTIR spectra for p-Si Pt-diffused sample obtained by the ATR technique; leftmost peaks are attributed to the formation of Pt-H complexes, while those on the right come from the Si-H of the nitride top layer.....	140
Figure 8. String-ribbon silicon substrate with an illustration of the relative location of the filament array. The array is spaced 5 cm from the substrate, with a maximum filament spacing of 2 cm. Select points are shown with their apparent color, thickness, and index of refraction, determined by ellipsometry (at a wavelength of 633 nm).	144
Table 3. Comparison of electrical properties for hot-wire versus plasma nitride cells.....	146

Chapter 6

Figure 1. Schematic of <i>in situ</i> silane generation source.	154
Figure 2. Optical micrograph of etch pits created on Ge(100) substrate during exposure to atomic H for a period of 80 minutes; feed gas conditions were 100 mTorr/10 sccm of H ₂	157
Figure 3. Transition from deposition to etching that occurs upon H ₂ -dilution.	158
Table 1. Comparison of etch rates for amorphous and crystalline silicon - (100), unless otherwise noted. Pressures and flow rates are those of pure hydrogen. The etch rate for Holt <i>et al.</i> (a-Si) was calculated based	

on the resultant growth rate, assuming a 4% yield. Abrefah *et al.*²
 calculate the etching rate reported in this table by extrapolating data
 from $\sim 10^{-4}$ Torr. 163

Appendix A

Figure 1. Front view of the hot-wire reactor. 176
 Figure 2. Rear view of the hot-wire reactor..... 178
 Figure 3. Top view of the hot-wire reactor through the viewport, with the
 wire on. The wire is oriented normal to the plane of the photo..... 179
 Figure 4. Wire array used for growth onto large area (> 100 cm²) samples. 180
 Figure 5. Schematic of showerhead-catalyzer assembly developed by the
 ANELVA/JAIST group. Adapted from Matsumura.³ 181

Appendix B

Table 1. Assumed irreversible wire reactions, along with reaction
 probabilities. 184
 Table 2. Assumed irreversible surface reactions, along with reaction
 probabilities. H(s) represents a hydrogenated surface site, --(s)
 represents an open site, Si(s) is a silicon atom that has been
 incorporated into the film, and SiH₃(s) is a tri-hydride surface site. 184

Table 3. Gas-phase reactions used in the DSMC simulation. The rate constant is given by: $k = AT^n \exp(-E_a/RT)$. Reactions (1)-(10) constitute the bimolecular portion of the mechanism, while reactions (11)-(19) are the remaining reactions that require a third body, denoted by (+M)..... 185

Table of Contents

Acknowledgements	iii
Abstract	viii
Related Publications	xi
List of Figures and Tables	xii
Chapter 1 Introduction	1
1.1 Photovoltaics: A Renewable Energy Source	1
1.1.1 Feasibility	1
1.1.2 Thin-Film Polycrystalline Silicon	2
1.1.3 Operation Principle	3
1.2 Hot-Wire Chemical Vapor Deposition.....	7
1.2.1 Historical Perspective	8
1.2.2 Recent Work	9
1.2.3 Advantages to Hot-Wire Chemical Vapor Deposition	11
1.3 Motivation.....	12
1.4 Outline	14
References	17
Chapter 2 Wire Surface Kinetics	21
Abstract.....	21

2.1	Introduction	22
2.2	Experiment.....	24
2.2.1	Data Acquisition	27
2.3	Results.....	29
2.3.1	Radical Detection – new wire	29
2.3.2	Radical Detection – aged wire	32
2.3.3	Wire Characterization.....	34
2.4	Discussion	38
2.4.1	Rates for Surface Kinetic Processes.....	40
2.5	Conclusions.....	44
	References	47
Chapter 3 Gas-Phase Experiments		50
	Abstract.....	50
3.1	Introduction	50
3.2	Residence Time Distribution (RTD)	52
3.2.1	RTD Measurements.....	53
3.2.2	Stirred Tank Reactor Calculations.....	56
3.3	Detection of Radical Species.....	60
3.3.1	Introduction.....	60
3.3.2	Radical-to-Ion Flux in HWCVD	61
3.3.3	Threshold Ionization Mass Spectrometry	64

3.3.4	Detection of Higher Silicon Species.....	78
3.4	Conclusions.....	83
	References	84
Chapter 4	Computations and Simulations of Gas-Phase Processes	87
	Abstract.....	87
4.1	Reaction of Si + SiH ₄	87
4.1.1	Introduction.....	87
4.1.2	Computational Chemistry Studies.....	89
4.1.3	Summary.....	92
4.2	Gas-Phase Simulations	94
4.2.1	Direct Simulation Monte Carlo (DSMC) Modeling.....	94
4.2.2	Continuum Simulations.....	109
4.3	Conclusions.....	117
	References	119
Chapter 5	HWCVD of Silicon Nitride	122
	Abstract.....	122
5.1	Introduction	122
5.2	Experiment.....	124
5.3	Results.....	125
5.3.1	NH ₃ Decomposition	125

5.3.2	Initial Film Growth Results	127
5.3.3	Variation of SiH ₄ /NH ₃ Flow Ratio	129
5.3.4	Annealing of Hydrogenated SiN _x	134
5.3.5	Multiple Internal Reflection FTIR: Hydrogen-Defect Passivation	137
5.3.6	Silicon Nitride Deposition onto String Ribbon Silicon Substrates	143
5.4	Conclusions	146
	References	148
Chapter 6 <i>In situ</i> Silane Generation by Hot-Wire Atomic Hydrogen Etching of Solid Silicon Sources		151
	Abstract	151
6.1	Introduction	152
6.2	Experiment	153
6.3	Results	155
6.4	Discussion	160
6.5	Conclusions	164
	References	166
Chapter 7 Conclusions and Future Work		167
7.1	Wire Surface Kinetics	167
7.2	Gas-Phase Experiments	168

7.3	Computations and Simulations of Gas-Phase Processes.....	170
7.4	HWCVD of Silicon Nitride	171
7.5	<i>In situ</i> Silane Generation by Hot-Wire Atomic Hydrogen	
	Etching of Solid Silicon Sources	174
	References	175
Appendix A HWCVD Chamber Pictures and Design		
	Considerations	176
	References	183
Appendix B Wire, Substrate, and Gas-Phase Reactions Used in		
	Modeling Studies	184
	References	188

Chapter 1 Introduction

1.1 Photovoltaics: A Renewable Energy Source

Photovoltaics (PV) are devices capable of producing electricity when exposed to radiant energy. Although once reserved for the research laboratory, these devices were being considered as an alternative energy source during the oil crisis of the mid-1970s. The perception that fossil fuels were a limited energy resource stimulated programs in several countries to search for alternatives, with PV solar energy among those.¹ This technology was considered appealing (from a safety standpoint) when compared with nuclear energy, particularly after the Three Mile Island and Chernobyl incidents.¹ Recently, renewable energy has assumed even greater importance due to concerns over CO₂ emissions and global warming.²

1.1.1 Feasibility

Although generally believed to be a “clean” technology, PV has not been implemented on a wide scale due to the high costs associated with module

production. However, strides have been made in the past few decades, with commercial prices dropping an average of 7.5% per year, while production is increasing worldwide at an average of 18% per year.¹ A commonly employed figure-of-merit for assessing the sustainability of any renewable energy technology is the “energy payback time,” defined as the time needed for the device to produce the amount of energy used in its manufacture. In this regard, PV technology is promising, as crystalline silicon modules are estimated to achieve this break-even point in only 3 years, substantially smaller than their projected lifetimes of about 30 years.³ Another question concerns the module area required to produce a meaningful amount of energy. The study by Turner² estimates that for a 10% module efficiency (fixed, flat-plate collectors), a square array 100 miles on a side would generate in 1 year the amount of energy used annually in the US. When coupled with other alternative technologies available (wind, geothermal), the area becomes smaller, suggesting that PV technology could fill the void created by the eventual depletion of fossil fuel reserves.

1.1.2 Thin-Film Polycrystalline Silicon

For PV technology to eventually contribute substantially to global energy needs, the module cost reduction and production increases previously mentioned must be maintained. These demands are contingent, however, on the

global supply of the raw materials used in PV manufacturing. As a result, the most favorable technologies are those that use small quantities of less refined raw materials.¹ Specifically, thin-film polycrystalline silicon (poly-Si) is believed by many^{4,5} to be the most promising of the available PV technologies (e.g., crystalline silicon, amorphous silicon, cadmium telluride, copper indium diselenide). Thin-film poly-Si offers lower production costs than conventional thick, high-efficiency crystalline silicon, while offering higher efficiency than amorphous silicon (due to the inherent metastability of the latter).⁴ Additionally, from a materials standpoint, silicon is the second most abundant element in the earth's crust, with a bandgap (in crystalline material) almost ideal for photovoltaic conversion.⁴ As a demonstration of the viability of the thin-film poly-Si approach, the Kaneka Corporation fabricated in 1998 a microcrystalline cell of only 2 μm thickness, with an efficiency of 10.1%.⁶

1.1.3 Operation Principle

In the simplest sense, a PV solar cell works by absorbing incident photons and converting them into electron-hole pairs. The photogeneration of electron-hole pairs depends critically upon the bandgap energy (E_g) of the semiconductor used. Sub-bandgap photons will not contribute to photogeneration, while those above the bandgap contribute E_g to the electron-hole pair, with the remainder

lost to thermalization. Additionally, for a given spectrum of radiation, the smaller the bandgap, the greater the utilization of the spectrum will be, but the lower the photovoltage. Conversely, for large bandgaps there is a higher photovoltage, but lower short circuit current density (J_{sc}).⁷

Fortuitously, crystalline silicon has a bandgap energy (~ 1.1 eV) close to the optimal for which roughly half of the incident solar energy could be converted to electron-hole pairs. In practice, however, there are a number of limiting factors such as radiative recombination (limiting efficiencies to 33%) and Auger recombination (further limiting efficiency to 29%) that make the value of 50% unattainable.⁴ The latter process of Auger recombination has a high probability of occurrence in indirect bandgap materials like silicon. Also problematic with crystalline silicon in particular is its relative weak absorbance of light near the bandgap. This disadvantage can be overcome, however, by light-trapping structures and anti-reflection coatings.⁴

Once electron-hole pairs are generated, they must be separated in order to collect current, and thus power, from the device. Figure 1 shows a representative n-p-p⁺ solar cell, illustrating this process. This structure is preferred as the majority of carriers will be generated in the p-region (where electrons are minority carriers), and electron mobility is higher than that of holes.

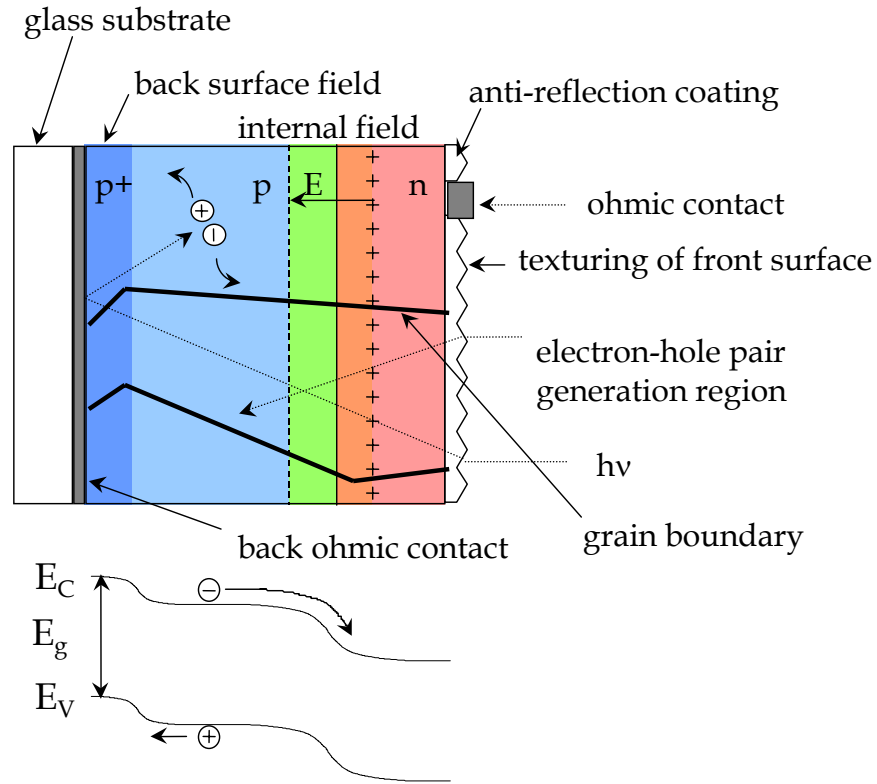


Figure 1. Example of a n-p-p⁺ solar cell. Photons are absorbed and generate electron-hole pairs, primarily in the p region in this case. The internal field (E) separates the carriers, allowing current to be collected at the ohmic contacts. Grain boundaries, present in polycrystalline solar cells, can act as recombination centers.

The diode structure of this solar cell (n-p-p⁺) creates an internal electric field (E) that sweeps electrons and holes in opposite directions. Electrons are swept to the n-region, where they become majority carriers, and conversely, holes are swept to the p-region. Material defects, such as grain boundaries or vacancies, can act as recombination centers, reducing the overall current attainable.

The current-voltage (I-V) characteristics of an idealized solar cell (no recombination or other losses), along with the circuit equivalent are shown in Figure 2. Without illumination, the device behaves as a simple diode, while under illumination, the photogenerated current (I_L , or I_{SC} when there are no losses) is added to the circuit. The maximum power (P_{max}) that can be obtained from the device is illustrated in Figure 2a, defined as the maximum area rectangle bounded by the curve in the fourth quadrant of the I-V plot. Along with I_{SC} and V_{OC} , the other key parameter characterizing solar cell performance is the fill factor (FF), defined as: $FF = P_{max}/(V_{OC} \times I_{SC})$. It should be noted that “real” solar cells will have ohmic losses at the front surface (the equivalent of a series resistance in the circuit of Figure 2b) and leakage currents in the bulk,

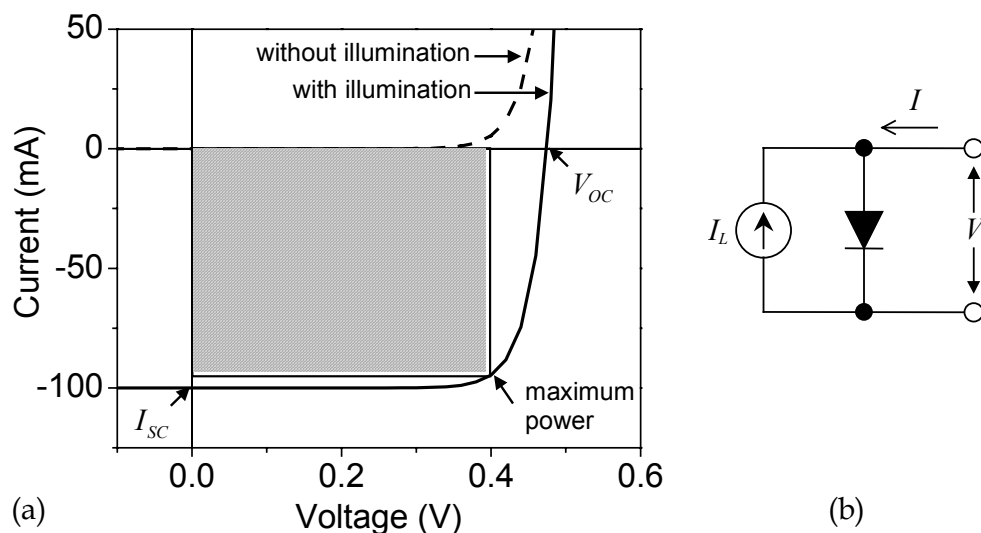


Figure 2. (a) Current-voltage characteristics of an ideal solar cell, with and without illumination; V_{OC} is the open circuit voltage, and I_{SC} is the short-circuit current, (b) the circuit equivalent of this idealized solar cell; adapted from Chen.⁸

associated with recombination at defect sites (the equivalent of a parallel shunt resistance in the circuit of Figure 2b).

1.2 Hot-Wire Chemical Vapor Deposition

Hot-wire chemical vapor deposition (HWCVD) is a technique that involves the decomposition of precursor gases (e.g., silane) on a heated filament (typically tungsten), with the constituent radical species often reacting in the gas phase and depositing onto a heated substrate, as depicted in Figure 3. There are a number of reactor variables that can ultimately impact the quality of the film obtained. These variables include, among others, wire temperature, total pressure, gas flow rates, and substrate temperature. The last 15 years have shown a great deal of

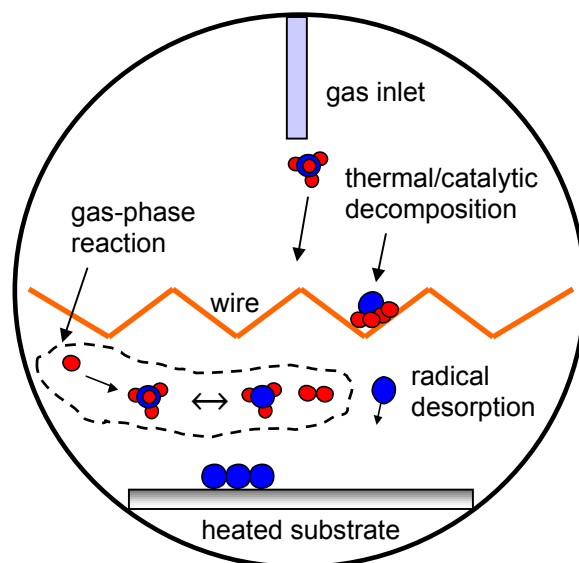


Figure 3. Schematic of the HWCVD process, illustrating the various kinetic processes involved.

effort put into studying which combination of these variables will yield films of the highest electronic quality.

1.2.1 Historical Perspective

The technique of HWCVD was introduced by Weismann *et al.*⁹ in 1979 as a means for producing hydrogenated amorphous silicon (a-Si:H) films at high deposition rates. Results of Weismann *et al.* were not encouraging, however, due to the inferior electronic properties of their films in comparison with those prepared by plasma enhanced chemical vapor deposition (PECVD). In addition, they claimed that nitrogen incorporation (via the addition of gaseous ammonia) was needed to improve upon these properties. These discouraging results led to several years of inactivity in this field until Matsumura and Tachibana¹⁰ in 1985 demonstrated high-quality hydrofluorinated amorphous silicon (a-Si:F:H) using silicon difluoride (SiF_2) and hydrogen (H_2) as gas precursors. They claimed that the H_2 reaction with the heated filament (tungsten) was catalytic in nature and thus termed the entire process catalytic CVD (cat-CVD). In a follow-up study in 1986,¹¹ Matsumura was able to grow high-quality a-Si:H using deposition conditions similar to those used in the a-Si:F:H study. These encouraging results renewed interest in the technique.

High-quality a-Si was also grown by Doyle *et al.*¹² at the University of Colorado in 1988, using slightly different deposition conditions than those of Matsumura. They termed the process “evaporative surface decomposition” (ESD) due to the highly efficient dissociation of the low-pressure feed gas and consequent large flux of deposition radicals. This same work was later continued at the Solar Energy Research Institute (SERI) (now the National Renewable Energy Laboratory – NREL) by Mahan *et al.*,¹³ where thorough comparative studies of a-Si prepared via ESD versus PECVD were carried out. The process termed ESD was later renamed “hot-wire assisted CVD,” largely because of uncertainty over whether catalysis was indeed occurring on the heated filament. The work of the group at SERI was instrumental in demonstrating the importance of this growth method and has led to tremendous growth in this field of research in the past 10 years.

1.2.2 Recent Work

Prior to 1991, amorphous silicon films produced via HWCVD were of inferior quality to those obtained by the well-established technique of plasma enhanced chemical vapor deposition (PECVD). This poor quality was attributed to an unsuitable reactor pressure and filament-substrate distance, producing too large a fraction of silicon atoms (among the other radical species) at the film surface.¹⁴

In 1991, device quality a-Si of low hydrogen content (< 1 at.%) was finally produced via the HWCVD technique by Mahan *et al.*¹³ The criterion of low hydrogen content is particularly important, as it is believed¹⁵ that hydrogen motion is involved in the formation of light-induced metastable defects in a-Si via the Staebler-Wronski effect.¹⁶

As a result of the fundamental problem of light-induced metastability in a-Si, research into the growth of microcrystalline ($\mu\text{-Si}$) and polycrystalline silicon (poly-Si)¹⁷ was simultaneously initiated. Matsumura¹⁸ in 1991 was the first to obtain poly-Si films by HWCVD, at a temperature of 300°C. Heintze *et al.*¹⁹ in 1996 identified the transition from amorphous to microcrystalline silicon growth that occurs at a critical hydrogen-to-silane ratio in the gas phase.

Once device quality a-Si could be produced, questions about how the electronic properties of the film depend on the various reactor parameters remained. The work of Molenbroek *et al.* in 1996-1997^{20,21} examined issues of film quality versus reactor parameters for highly diluted silane and pure silane conditions, respectively. A principal conclusion of these studies was that a-Si film quality (e.g., light-to-dark conductivity ratio) improves under conditions where gas-phase reactions with silane (SiH_4) occur, specifically that of atomic silicon (Si) and SiH_4 . Beyond a critical pressure (all other variables fixed), however, radical-radical reactions can lead to a deterioration in electronic properties.

Some of the more recent and promising results include the demonstration of epitaxial silicon growth via HWCVD by Thiesen *et al.*,²² the first such evidence for epitaxy by this technique. High growth rates were achieved (up to 10 Å/s) at relatively low temperatures (~200°C) in comparison with other techniques for epitaxial growth such as molecular beam epitaxy (MBE). In the area of device fabrication, thin film transistors (TFT) with both the a-Si and silicon nitride (SiN_x) layers deposited exclusively by HWCVD (“All-Hot-Wire-TFTs”) have been demonstrated.^{23,24} Additionally, a-Si/poly-Si multibandgap tandem solar cells (n-i-p/n-i-p structure) have been produced with the thick absorbing layer (i layer) deposited by HWCVD; initial efficiencies were 8.1%, with a total device thickness of only 1.1 μm. Promising results like these suggest the hot-wire technique could replace conventional film deposition techniques.

1.2.3 Advantages to Hot-Wire Chemical Vapor Deposition

The hot-wire technique offers a number of important advantages over conventional film deposition techniques, some of which have already been alluded to. In comparison with plasma-based processes such as radio-frequency glow discharge, HWCVD involves the deposition of only thermal (~ 0.2 eV) radical species. Plasma-based processes produce ions that can be accelerated

towards the substrate or form powders by confinement in the discharge,²⁵ both of which may be ultimately deleterious to film properties. Another important advantage to HWCVD is the high flux of atomic hydrogen (H) produced in comparison with that in a glow discharge.²⁶ This high flux of H helps promote poly-Si growth by etching silicon from the strained bond sites that are found in amorphous material. It is also commonly believed¹⁴ that a high flux of H promotes gas-phase H abstraction reactions such as $\text{H} + \text{SiH}_4 \rightarrow \text{SiH}_3 + \text{H}_2$, producing a growth species (SiH_3) believed to be involved in epitaxial silicon growth.²² For industrial application, the hot-wire process is more readily scalable to large area deposition than a plasma process. Simply by introducing more filaments, the deposition area can be extended to the desired shape, while the ball shape of a plasma discharge presents difficulties with respect to deposition on multiple large area substrates.²⁶

1.3 Motivation

Despite the large number of researchers in the field of HWCVD, fundamental questions about gas-phase and surface kinetic processes remain. In particular, the distribution of radicals produced at the wire surface has remained in question, due in part to inconsistencies in the results obtained.²⁷⁻³⁰ Also, no studies to date have correlated wire surface kinetics with the aging of wires that

occurs during prolonged exposure to silane. Knowledge of the radical species produced via gas-phase reactions at the pressures characteristic of film growth has also been lacking for silane-based HWCVD, particularly for highly diluted silane ambients. Inferences about the species present during growth have been made based on the resulting film properties,^{20,21} but no direct radical measurements have been made under these conditions.

As mentioned earlier, HWCVD has been employed in the area of TFT fabrication,^{23,24} but the technique also has promise for producing silicon nitride layers for use as anti-reflection and passivation coatings for photovoltaics. The passivation effect of the nitride layer is believed to occur during a post-deposition anneal, resulting in an increase in the internal quantum efficiency of the underlying Si solar cell.³¹ Whether this passivation effect can be attributed solely to H release into the underlying Si is unclear, as the mechanisms involved are still being debated. Also, hot-wire CVD silicon nitride layers have not yet been assessed for their passivation capabilities relative to those grown by conventional plasma CVD.

The single largest cost in PV technology is the raw material used (up to 50% of the finished module cost³²), often scrap silicon material received from the semiconductor industry. The demand of the PV industry for this scrap silicon is expected to exceed the supply, however, by a factor of 2-4 by 2010.³³ As a result, methods are needed to refine the relatively abundant metallurgical-grade silicon

(MG-Si) that is the precursor to electronic-quality silicon. One method that may offer promise exploits the known etching effect of atomic hydrogen on amorphous and crystalline silicon, and the inverse dependence on temperature.³⁴ It was recently suggested by Masuda³⁵ that a cooled silicon target can be etched with high yield by atomic H, generating silicon species that result in the growth of a polycrystalline film. It has not yet been demonstrated, however, whether MG-Si can be etched with a similar efficiency, or whether refining of this material can take place.

1.4 Outline

Chapter 2 focuses on the production of radical species on the wire in a HWCVD reactor, using the technique of quadrupole mass spectrometry. Atomic Si was found to be the predominant radical produced for wire temperatures above 1500 K, with evidence for catalysis using a new wire. Radical production using aged filaments appears to occur through a non-catalyzed route. This constitutes the first such study of the effect of wire aging on radical species production in HWCVD. Chapter 3 examines the production of radical and ion species via gas-phase and surface processes, using the same mass spectrometry technique. Both ions and disilicon (or larger) species were found to be trace in abundance for typical hot-wire film growth conditions, while appreciable

amounts of the SiH_2 radical were detected under a specific set of deposition conditions.

Chapter 4 explores simulation and computational chemistry tools used to examine gas-phase reactions. An energetically favorable reaction pathway for Si and SiH_4 was identified, resulting in Si_2H_2 and H_2 as the products. Monte Carlo simulations of the hot-wire reactor suggest SiH_3 is the predominant growth species under conditions leading to amorphous and polycrystalline growth, with the atomic H flux dictating the transition between the two microstructures. A two-dimensional Direct Simulation Monte Carlo (DSMC) code was applied for the first time to modeling a HWCVD reactor, examining the issue of film growth uniformity. Continuum simulations were used to predict the maximum growth rates achievable under non-agglomerate forming conditions. For dilute (1%) silane conditions, a maximum growth rate of 10 nm/s was predicted, while under pure silane conditions, 50 nm/s was predicted.

Chapter 5 focuses on the growth of silicon nitride films using HWCVD. Specifically, the reactor conditions needed to produce high hydrogen content films (up to 18 atomic %) with a high refractive index (up to 2.5) were identified. The hydrogen release kinetics for nitrogen-rich and silicon-rich nitride films were studied. Also, bulk and interface defect passivation by atomic hydrogen was examined using the technique of Multiple Internal Reflectance Fourier-Transform Infrared Spectroscopy (MIR-FTIR). Bulk passivation (of platinum

impurities in Si) by atomic H released from a nitride capping layer was demonstrated for the first time; the bulk concentration of these platinum-hydrogen complexes was determined to be $\sim 10^{14} \text{ cm}^{-3}$. Silicon nitride films were deposited onto commercial ribbon silicon diffused-emitter substrates, and the electrical properties of the resulting cells compare favorably with plasma CVD-nitride cells. Chapter 6 describes a technique being used to grow silicon films by atomic hydrogen etching of a cooled, solid silicon source. Negligible etching of a crystalline silicon source was observed, while an amorphous silicon source was found to etch at rates of up to 14 nm/min, allowing for growth onto a heated substrate at a rate of 0.6 nm/min. Finally, Chapter 7 summarizes the preceding chapters, with proposals for future work.

References

1. A. Shah, P. Torres, R. Tscharnner, N. Wyrsh, and H. Keppner, *Science* **285**, 692-698 (1999).
2. J. Turner, *Science* **285**, 687-689 (1999).
3. K. Knapp and T. Jester, in *An Empirical Perspective on the Energy Payback Time for Photovoltaic Modules*, Solar 2000 Conference, Madison, Wisconsin.
4. J. Werner, R. Bergmann, and R. Brendel, *Festkor A* **34**, 115-146 (1995).
5. M. Green, *Progress in Photovoltaics: Research and Applications* **8**, 127-139 (2000).
6. K. Yamamoto, M. Yoshimi, T. Suzuki, Y. Okamoto, Y. Tawada, and A. Nakajima, in *Below 5um thin Film poly-Si solar cell on glass substrate fabricated at low temperature*, 2nd World Conference and Exhibition on Photovoltaic Solar Energy Conversion, Vienna, Austria, 1998.
7. J. Pankove, *Optical Processes in Semiconductors* (Dover Publications, New York) 1971.
8. C. Chen, Ph.D. Thesis, California Institute of Technology, 2001.
9. H. Wiesmann, A. K. Gosh, T. McMahon, and M. Strongin, *J. Appl. Phys.* **50**, 3752 (1979).
10. H. Matsumura and H. Tachibana, *Appl. Phys. Lett.* **47**, 833-835 (1985).
11. H. Matsumura, *Jap. J. Appl. Phys., Part 2-Letters* **25**, L949-L951 (1986).

12. J. Doyle, R. Robertson, G. Lin, M. He, and A. Gallagher, *J. Appl. Phys.* **64**, 3215-3223 (1988).
13. A. Mahan, J. Carapella, B. Nelson, R. Crandall, and I. Balberg, *J. Appl. Phys.* **69**, 6728-6730 (1991).
14. R. Schropp, K. Feenstra, E. Molenbroek, H. Meiling, and J. Rath, *Phil. Mag. B* **76**, 309-321 (1997).
15. W. Jackson and J. Kakalios, *Phys. Rev. B* **37**, 1020-1023 (1988).
16. D. L. Staebler and C. R. Wronski, *Appl. Phys. Lett.* **31**, 292 (1977).
17. Microcrystalline silicon is typically defined as a two-phase amorphous and crystalline material, with grain sizes under 20 nm, while polycrystalline silicon consists of a single phase with grain boundaries and grain sizes up to 100 nm; see Reference 14.
18. H. Matsumura, *Jap. J. Appl. Phys.* **30**, L1522-L1524 (1991).
19. M. Heintze, R. Zedlitz, H. Wanka, and M. Schubert, *J. Appl. Phys.* **79**, 2699 (1996).
20. E. Molenbroek, A. Mahan, E. Johnson, and A. Gallagher, *J. Appl. Phys.* **79**, 7278-7292 (1996).
21. E. Molenbroek, A. Mahan, and A. Gallagher, *J. Appl. Phys.* **82**, 1909-1917 (1997).
22. J. Thiesen, E. Iwaniczko, K. Jones, A. Mahan, and R. Crandall, *Appl. Phys. Lett.* **75**, 992-994 (1999).

23. B. Stannowski, M. van Veen, and R. Schropp, *Mat. Res. Soc. Symp. Proc.* **664**, A17.3.1 (2001).
24. M. Sakai, T. Tsutsumi, T. Yoshioka, A. Masuda, and H. Matsumura, *Thin Solid Films* **395**, 330-334 (2001).
25. E. Hamers, A. Morral, C. Niikura, R. Brenot, and P. Cabarrocas, *J. Appl. Phys.* **88**, 3674-3688 (2000).
26. F. Jansen, I. Chen, and M. Machonkin, *J. Appl. Phys.* **66**, 5749-5755 (1989).
27. Y. Nozaki, K. Kongo, T. Miyazaki, M. Kitazoe, K. Horii, H. Umemoto, A. Masuda, and H. Matsumura, *J. Appl. Phys.* **88**, 5437-5443 (2000).
28. S. Tange, K. Inoue, K. Tonokura, and M. Koshi, *Thin Solid Films* **395**, 42-46 (2001).
29. H. Duan, G. Zaharias, and S. Bent, *Thin Solid Films* **395**, 36-41 (2001).
30. J. Holt, M. Swiatek, D. Goodwin, and H. Atwater, *Mat. Res. Soc. Symp. Proc.*, Vol. 664, A3.2, San Francisco, 2001.
31. C. Boehme and G. Lucovsky, *J. Appl. Phys.* **88**, 6055-6059 (2000).
32. M. McCann, K. Catchpole, K. Weber, and A. Blakers, *Sol. Ener. Matl. Sol. Cells* **68**, 135-171 (2001).
33. J. Maurits, 8th NREL Workshop on Crystalline Silicon Solar Cell Materials and Processes, Copper Mountain, Colorado, 1998, p. 10-17.
34. J. Abrefah and D. Olander, *Surface Science* **209**, 291-313 (1989).

35. A. Masuda, K. Kamesaki, A. Izumi, and H. Matsumura, *Mat. Res. Soc. Symp. Proc.* **664**, A4.5 (2001).

Chapter 2 Wire Surface Kinetics

Abstract

Wire-desorbed radicals present during hot-wire chemical vapor deposition growth have been measured by quadrupole mass spectrometry. New wires produce Si as the predominant radical for temperatures above 1500 K, with a minor contribution from SiH_3 , consistent with previous measurements; the activation energy for the SiH_3 signal suggests its formation is catalyzed. Aged wires also produce Si as the predominant radical (above 2100 K), but show profoundly different radical desorption kinetics. In particular, the Si signal exhibits a high temperature activation energy consistent with evaporation from liquid silicon. The relative abundance of the other SiH_x species suggests that heterogeneous pyrolysis of SiH_4 on the wire may be occurring to some extent. Chemical analysis of aged wires by Auger Electron Spectroscopy suggests that the aging process is related to the formation of a silicide at the surface, with silicon surface concentrations as high as 15 atomic %. A limited amount (2 atomic %) of silicon is observed in the interior as well, suggesting that diffusion into the wire occurs. Calculation of the relative rates for the various wire kinetic processes, coupled with experimental observations, reveals that silicon diffusion

through the silicide is the slowest process, followed by Si evaporation, with SiH_4 decomposition being the fastest.

2.1 Introduction

A knowledge of the primary radicals produced on the wire in a hot-wire chemical vapor deposition (HWCVD) reactor is critical to optimization of film microstructure and quality, as well as for modeling gas-phase chemistry. In the low pressure, collisionless regime, these wire-desorbed radicals may act as the primary film deposition precursors, while at higher pressure, they may react with other species in the gas phase to produce the precursors. In particular, the study by Molenbroek *et al.*¹ suggested a direct correlation between amorphous film quality and the degree of reaction of wire-generated Si in the gas-phase.

Recently, it has been demonstrated that wire age has an effect on the resulting electronic properties of the grown film,² thought to be related to differences in radical chemistries associated with aged versus new wires. No studies have examined, however, what these differences in radical chemistry might be, if they exist

Prior Work

There have been a number of recent reports³⁻⁶ of the distribution of wire-desorbed radicals, following the early report by Doyle *et al.*⁷ Experiments conducted using similar detection schemes, such as vacuum ultraviolet (VUV) photo-ionization mass spectrometry, have shown quite different results in some cases.^{4,5} Whether these differences are due to the different histories of the wire used or differences in the reactor condition (e.g., walls coated with amorphous silicon) is unclear.

One point that most of these studies agree on is that Si is the dominant radical observed at high wire temperatures (above 1800 K). However, the distributions of the minor species found at lower temperatures are in discrepancy among the various studies. In the report of Doyle *et al.*,⁷ SiH₃ was the next most abundant radical to Si. Duan *et al.*⁵ report disilicon species (Si₂H_x) as the next most abundant, followed by SiH₃; the presence of Si₂H_x was thought to be related to wall reactions, however, and not a result of wire processes. Tange *et al.*⁴ report SiH₂ as the next most abundant radical, followed by SiH₃. In contrast to the other studies, the SiH₂ and SiH₃ radicals show a precipitous drop above 1700 K. These discrepancies have motivated a detailed study of radical desorption kinetics under conditions where the wire history (as well as that of the reactor) is well known. Also, a detailed chemical and surface analysis of aged wires has been made to better understand the aging mechanism.

2.2 Experiment

Measurements were performed in an ultra-high vacuum chamber with a base pressure of order 10^{-9} Torr. Background gases consist mostly of residual H_2 and He. Operating pressures were approximately 5×10^{-6} Torr, using a dilute (1%) mixture of SiH_4 in He (i.e., SiH_4 partial pressures of 5×10^{-8} Torr), at flow rates of less than 1 sccm; gases were introduced through an inlet on the side of the chamber. Low pressures were chosen in order to eliminate the effects of gas-phase reactions and focus exclusively on wire processes. A straight tungsten wire of 0.5 mm diameter and 12 cm length was used, located 1-5 cm from the substrate heater or mass spectrometer (the latter being used for these studies). Although other studies⁴ have examined alternate wire materials (tantalum and molybdenum), tungsten was chosen due to its low vapor pressure across the temperature range of interest. Tungsten is also the most widely used wire material in HWCVD. Figure 1 provides a diagram of this hot-wire reactor. Illustrative photos of the chamber along with a discussion of design considerations can be found in Appendix A.

The wire temperature was determined by using a single wavelength, disappearing filament optical pyrometer (Leeds and Northrup, Model 8622-C), with corrections made for effective emissivity. The emissivity of elemental

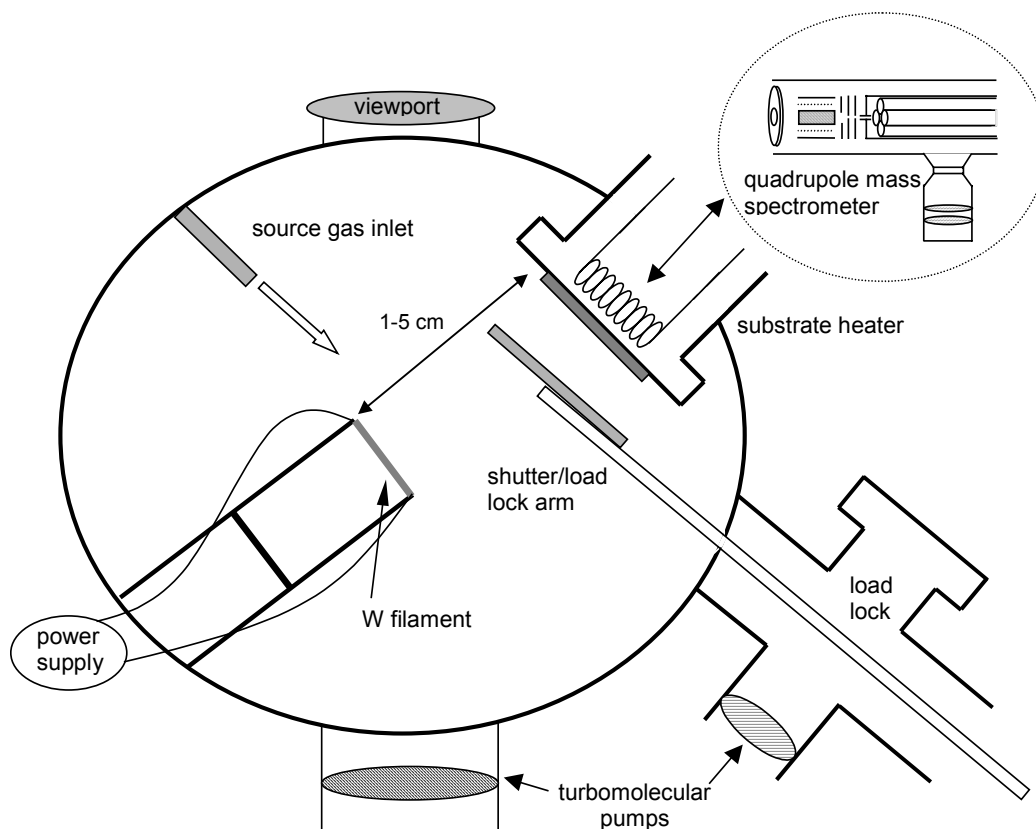


Figure 1. Diagram of the hot-wire reactor.

tungsten was taken as 0.44 (Ref. 8), along with a quartz transmission factor of 0.93, to give an effective value of 0.41. For the temperature dependent radical measurements of the present study, the largest source of error comes from the wire temperature determination (limited by the visual acuity of the user) and is estimated to be approximately ± 50 K over the entire temperature range investigated.

Radical measurements were made with the use of a quadrupole mass spectrometer (Hiden Analytical Ltd., HAL RC201), with the capability of tunable electron energy to enable radical detection. The spectrometer is placed at the

same location as the substrate heater during film growth, as Figure 1 shows. To enable the sensitivity to radical detection necessary at these low pressures, the spectrometer was operated in a so-called “open-source” mode. In this mode of operation, the 100 μm sampling orifice that usually lies in front of the ionizer is removed so that a larger fraction of radicals may reach the ionizer. The radical detection technique used here relies on the lower electron energy for direct radical ionization ($e^- + A \rightarrow A^+ + 2e^-$) versus ion production by dissociation of a parent molecule ($e^- + AB \rightarrow A^+ + B + 2e^-$).⁹ Measurements are made at a fixed electron energy over a range of masses.¹⁰ The electron energy chosen for these measurements was 10.5 eV, as it was found to result in preferential ionization of radical species, limiting the extent of dissociative ionization of SiH_4 to produce SiH_x ($x = 0-3$). The choice of energy is critical, as interference from SiH_4 dissociation at high energies can reduce the radical detection sensitivity. In addition, a characteristic of electron impact ionization, in contrast to a process such as photoionization, is the spread in the energy distribution (estimated to be 0.5 eV full-width half-maximum for our instrument). This spread allows for dissociative ionization of SiH_4 at energies that are nominally below the appearance potential of a particular radical, an effect similar to that previously noted by Hsu *et al.*⁹ We find this effect to be most important for the SiH_3 radical, given that SiH and SiH_2 are only trace in abundance, and that the gap between ionization and appearance potentials is slightly smaller for SiH_3 (3.9 eV) than for

Si (4.3 eV).¹¹ A related effect that could potentially bias the measurement of radicals is ion production from vibrationally excited SiH₄, at energies below the nominal appearance potential of the particular ion.¹² As a result of these effects, the data to be presented have been corrected for trace dissociative ionization by a method to be discussed in the next section.

Since the chamber used in this study is also used during high-pressure film growth, a thin layer of amorphous silicon is often observed on the walls. In order to eliminate the contribution of etching of this silicon from the walls to the measured radical signals, the chamber was cleaned by introducing H₂ at total pressures in the range of 100 mTorr (10-20 sccm), at a wire temperature of approximately 2200 K. Under these conditions, a large flux of atomic H can be generated, and this species can effectively clean the chamber by etching amorphous silicon at rates up to 200 nm/min, as reported by Uchida *et al.*¹³

2.2.1 Data Acquisition

The raw data obtained by this technique consists of a scan in masses (28-32 amu) at a fixed electron energy of 10.5 eV. To obtain the raw signal intensity for each species, the spectrum was integrated across a 1 amu interval (e.g., 27.5 to 28.5 m/z for Si). A background scan was made with no SiH₄ present and the wire on, and this was subtracted from the raw data. Next, a scan was made with

the gas present, but the wire off in order to assess the extent of dissociative ionization of SiH₄ at 10.5 eV, due to the finite electron energy distribution. In order to subtract this additional background contribution, a gas temperature correction was necessary as these data were acquired with the wire off. Comparing the signal intensity of Ar, with and without the wire on (and applying a mass correction factor since intensity \sim mass^{-1/2}), enabled the wire off data to be normalized and then subtracted from the raw data. Also, since the raw data at masses 29 and 30 includes not only the contribution from the SiH and SiH₂ radicals, but contributions from Si isotopes (²⁹Si: 4.7% abundance, ³⁰Si: 3.1% abundance), a correction was necessary to extract the radical contribution. Given the differing efficiencies with which the various radicals can be ionized (electron ionization cross sections), normalization of the background-corrected data is necessary to determine their relative abundance. The cross section for Si comes from the measurements by Freund *et al.*¹⁴ For the other SiH_x, cross section measurements by Tarnovsky *et al.*¹⁵ were used. After subtracting the background contributions to the raw data, the cross section normalization was applied. The sensitivity attainable with this technique is estimated to be better than 1 ppm, taking the ratio of the minimum distinguishable radical signal (of order 10⁻¹² Torr) to the total pressure (of order 10⁻⁶ Torr).

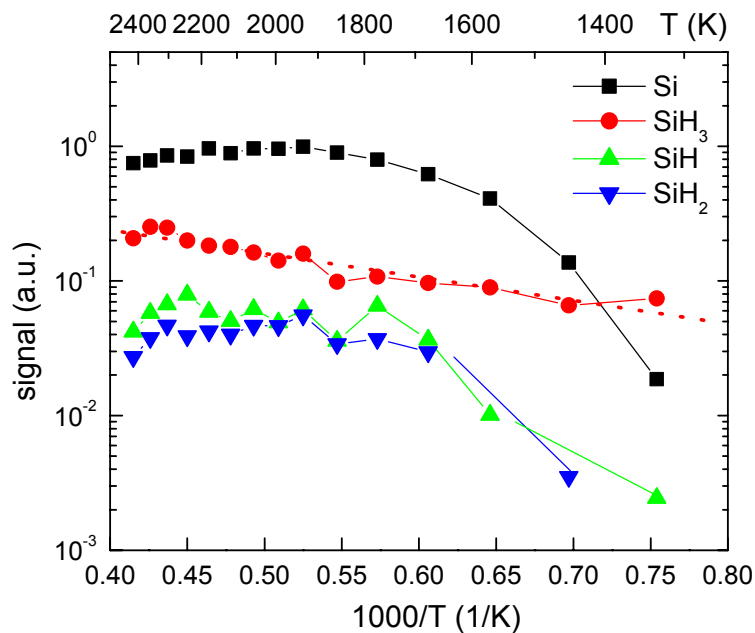


Figure 2. Low pressure (5×10^{-6} Torr) radical species measurements obtained using a new W wire. Activation energy accurate to within $\pm 10\%$, due to wire temperature uncertainties (± 50 K); error bars are not shown.

2.3 Results

2.3.1 Radical Detection - new wire

The distribution of monosilicon radical species as a function of wire temperature (1300-2500 K), at a total pressure of 5×10^{-6} Torr, is shown in Figure 2. These results were obtained with a new wire having had no previous SiH_4 exposure. In order to be able to measure results for a bare wire without silicide formation, the highest temperature measurements were made first, and then the wire temperature was decreased in steps to 1300 K. Starting at the lowest

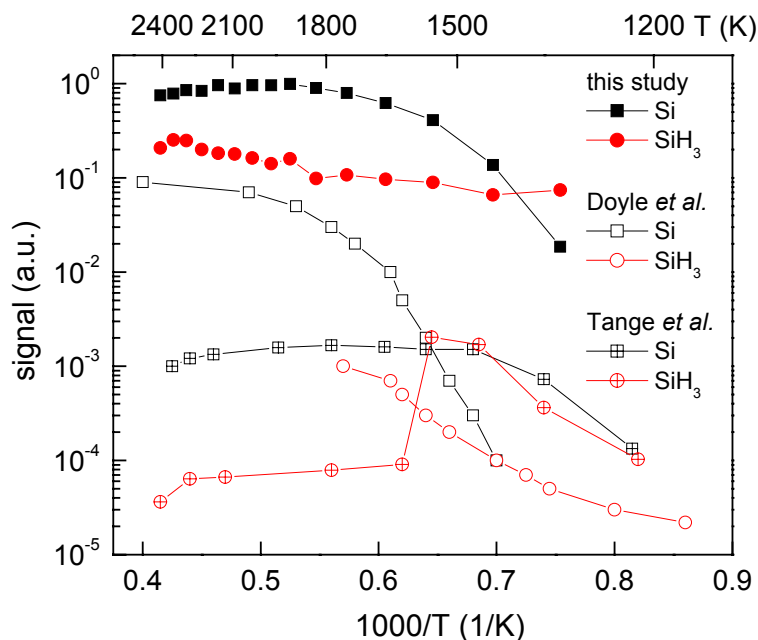


Figure 3. Summary of experimental studies on W wire surface kinetics.

temperatures, at which point a silicide or Si film forms,⁷ revealed a hysteresis in the Si signal, likely related to the desorption of this silicide or Si film from the wire.

Figure 3 compares the results of this study to those of similar low pressure studies (also utilizing W wires).^{4,7} The only species shown in Figure 3 are Si and SiH₃, as they were the predominant species in the present study, as well as in that of Doyle *et al.*⁷ In the study of Tange *et al.*,⁴ the SiH₂ signal exhibited very similar characteristics as SiH₃ and thus is omitted for clarity. Similar to the other studies,^{4,5,7} we find that Si is the predominant radical desorbed from the wire for wire temperatures above 1500 K. Above 1800 K, a saturation in the Si signal is noted, with a slight decrease above 2300 K, an effect also observed in these

studies. This phenomenon has been attributed to competition between desorption and decomposition;¹⁶ it should be pointed out that diffusion of Si through the wire may also be important at these high temperatures. The observation of primarily Si desorption at high temperatures indicates that surface decomposition of SiH₄ is faster than evaporation of SiH_x at these temperatures. It is important to note that the condition of the wire in the studies of Tange *et al.*⁴ and Doyle *et al.*⁷ was not specified, and thus quantitative comparisons of the apparent activation energies (which will be shown to depend on filament age in the next section) were not made.

The second most abundant radical evident from Figure 2 is SiH₃, in agreement with the report by Doyle *et al.*⁷ Over the entire temperature range investigated (1300-2500 K), this radical signal shows a small activation energy of 8 kcal/mole. As the formation of this species is believed to involve just an H atom exchange at the surface, such a small, constant activation energy is reasonable.⁷ Also suggested by this result is that SiH₃ formation is catalyzed as this activation energy is much smaller than the bond dissociation energy of SiH₄ (90 kcal/mole, Ref. 17). The radicals SiH and SiH₂ were detected in small quantities (< 8% of Si), only slightly larger than the isotopic contributions from ²⁹Si (4.7%) and ³⁰Si (3.1%).

2.3.2 Radical Detection – aged wire

A recent study by Mahan *et al.*² focused on the effect of wire alloying on the electronic properties of hydrogenated amorphous silicon films. They suggested that the differences in film electronic properties observed were most likely related to differences in radical chemistries associated with a “virgin” wire versus an alloyed wire. As a means of investigating whether there are discernable differences in radical chemistry depending on the condition of the wire, we have made low pressure radical measurements on aged wires to complement those performed on new wires. The temperature dependence of the SiH_x radical signals with the use of an aged wire (one used on several previous deposition runs, with SiH₄ partial pressures of order 10 mTorr and temperatures of 2000°C) is shown in Figure 4. The primary differences in surface kinetics with the use of the aged wire are the observation of high temperature (> 2100 K) activation energies for all radicals detected, as compared with the signals detected for a new wire, shown in Figure 2. In particular, the SiH₃ signal exhibits an activation energy of 106 kcal/mole, substantially higher than the 8 kcal/mole observed with a new wire, and close to the Si-H bond dissociation energy of SiH₄. This suggests that the aging of the wire has led to a reduction, if not an elimination, of its catalytic activity. It is also noteworthy that the high temperature activation energy measured for Si (117 kcal/mole) is close to the

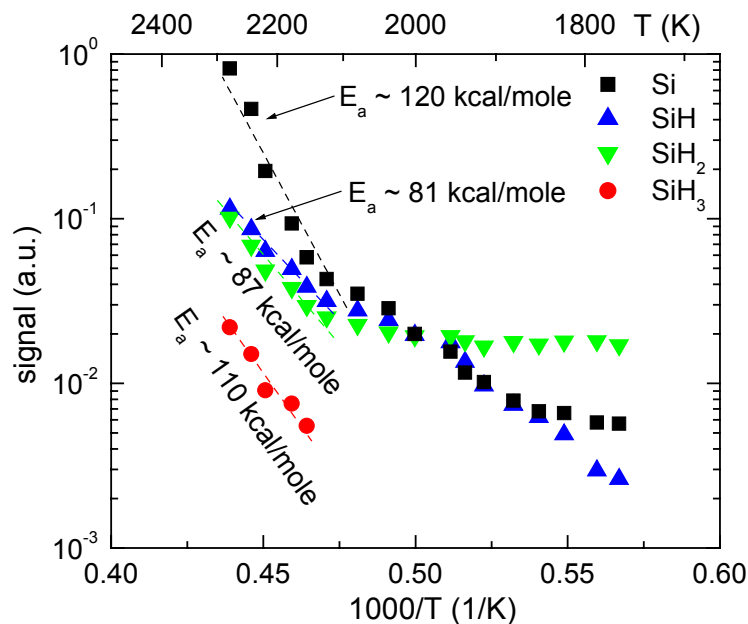


Figure 4. SiH_x radical signals measured from an aged W wire at a total pressure of 5×10^{-6} Torr. Activation energies quoted are accurate to within $\pm 10\%$, due to uncertainties ($\pm 50\text{K}$) in wire temperature; error bars are not shown.

known heat of vaporization of liquid Si (92 kcal/mole), within experimental uncertainties. Also, in contrast to the results obtained with the new filament, SiH and SiH_2 are both in greater abundance than SiH_3 . The cause for this might be the contribution of heterogeneous pyrolysis to SiH_4 decomposition. At low pressures, surface-initiated SiH_4 pyrolysis (on the wire) should produce SiH_2 predominantly, while SiH_3 can be ruled out as a primary product, based on the enthalpy of its formation reaction.¹⁷ The lower formation enthalpy for SiH relative to SiH_3 , as determined by thermodynamic calculations,¹⁸ may also explain its greater relative abundance. However, it is clear that the amount of liquid Si remaining

on the wire is large enough under these conditions that its evaporation dominates over pyrolysis of SiH_4 to other SiH_x .

2.3.3 Wire Characterization

Scanning Electron Microscopy

To complement radical measurements and gain insight into the nature of the changes occurring at the wire surface, *ex situ* diagnostics were performed on portions of wires, including the aged wire referred to above. Field emission scanning electron microscopy (SEM), operating at 30.0 kV with 1.5 nm point resolution, was used to characterize the surface morphology of three different wires. Figure 5 depicts the SEM images of a new wire (with no previous SiH_4 or high temperature exposure), a heat-treated wire (having minimal SiH_4 exposure at the operating temperature of 2000°C for approximately 10 hours), and an aged wire (having had exposure to a partial pressure of 10 mTorr SiH_4 at 2000°C for approximately 10 hours). Evident with the new wire are striations caused by the wire extrusion process, while the heat-treated wire appears to have a much smoother, glassy surface (it should be noted that the heat-treated wire also appears to have a much higher reflectivity). The properties of the heat-treated wire could be a result self-diffusion of W along the wire surface that takes place at these high temperatures. The latter image of the aged wire reveals a much

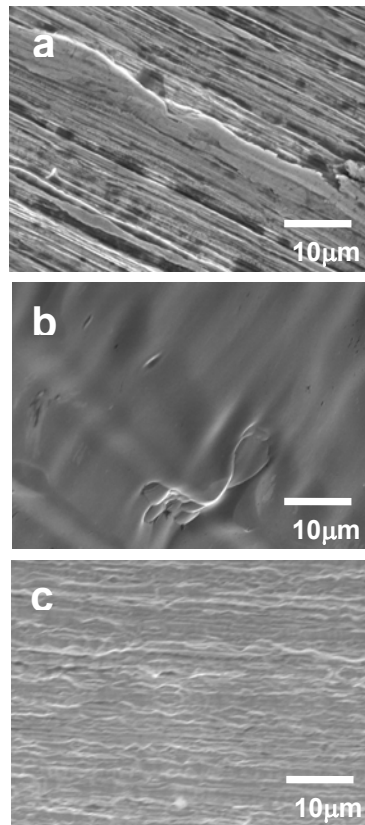


Figure 5. Surface morphology of (a) new, (b) heat-treated, and (c) aged wires.

rougher, irregular surface with striation lines absent, similar to observations of Mahan *et al.*² for a comparably aged wire. Since the wires used during deposition go through the high temperature treatment before the introduction of SiH_4 , the surface morphology observed with the aged wire is attributed to deposition of Si (present as elemental Si and/or a silicide phase). Given the profound differences in surface morphology of the heat-treated and aged wire, it

is not surprising that large differences in activation energies for radical desorption are observed.

Auger Electron Spectroscopy

To provide insight into the changes in chemical composition that occur during wire aging, Auger Electron Spectroscopy (AES) was used to probe discrete points at the wire surface and interior (having a spatial resolution of order $0.1\ \mu\text{m}$ and sampling depth of order $10\ \text{nm}$). Figure 6 is a low magnification SEM image of the aforementioned aged wire, revealing the locations at which AES measurements were made; the measured composition is given in Table 1. The ratio $\text{Si}/(\text{Si}+\text{W})$ is quoted as the other impurities detected (carbon, oxygen) were thought to be a result of *ex situ* contamination. As a result, the ratio $\text{Si}/(\text{Si}+\text{W})$ should be representative of the overall fraction of Si in the wire during the high temperature exposure to SiH_4 in the chamber. As evident from Table 1, the Si concentration at the surface reaches as high as 15% and drops off precipitously to approximately 2% in the interior of the wire; surface concentrations at other locations ranged from that given by points "a" and "b" (11.6-15.1%). The two interior points "c" and "d" (5% and 2% Si, respectively) were estimated to be approximately $25\ \mu\text{m}$ and $50\ \mu\text{m}$ in depth. It is noteworthy that these concentrations are comparable to the equilibrium solid solubility of Si in W at the respective wire temperatures.

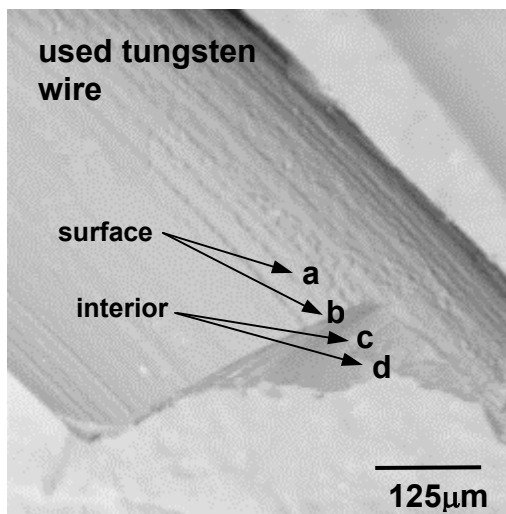


Figure 6. Scanning electron microscopy (SEM) image of aged tungsten wire.

Table 1. Composition of used tungsten wire, as determined by Auger Electron Spectroscopy (AES).

Location	Si/(Si+W)
Surface (a)	11.6%
Surface (b)	15.1%
Interior (c) – 25 μm deep	4.9%
Interior (d) – 50 μm deep	1.9%

2.4 Discussion

Examining the Si-W phase diagram in Figure 7 (generated with TAPP¹⁹), in light of these measured concentrations, shows that silicon concentrations of 15% at a typical wire temperature of 2000°C corresponds to a two-phase equilibrium between the silicide W_5Si_3 (33% abundance) and tungsten (67% abundance) at a silicon solubility of 4%. The Auger measurements support the idea that the nature of the wire alloying or aging process involves the growth of a silicide layer. Given that, at a depth of 10% of the wire radius (25 μm), silicon is present

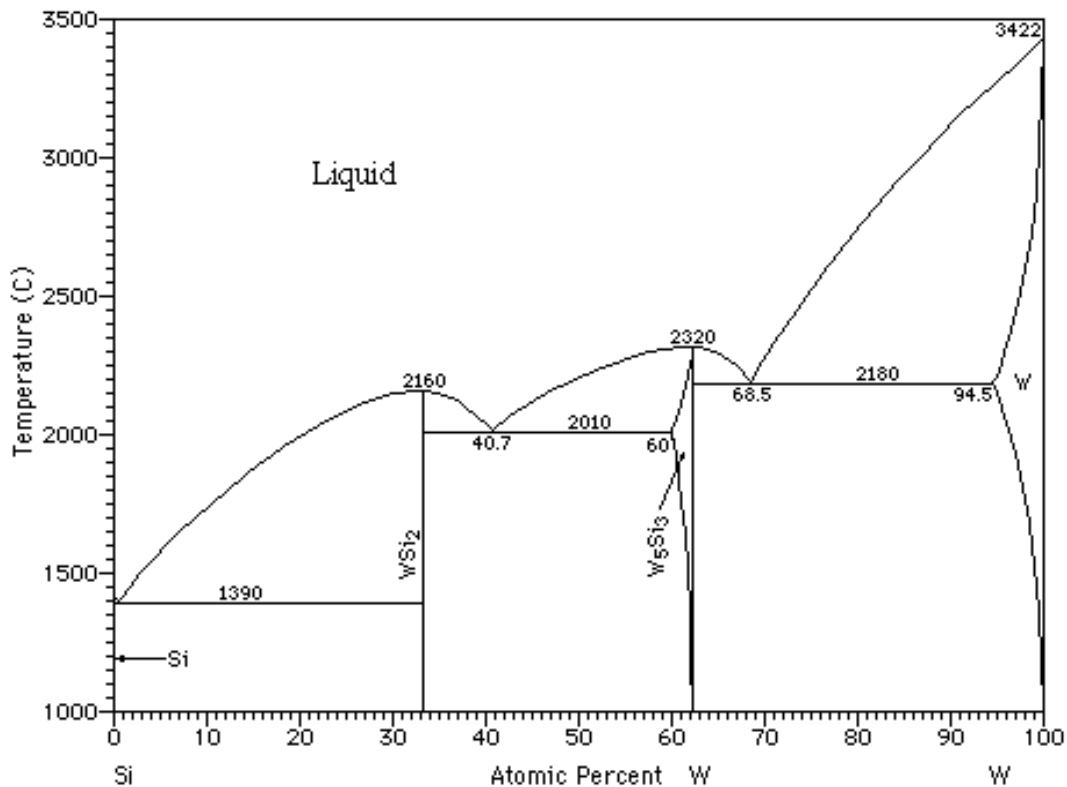


Figure 7. Si-W phase diagram, created with TAPP v2.1 (Thermochemical and Physical Properties), ES Microware, 1991.

only up to its solubility limit, the silicide layer is likely to be thin. Under more severe conditions (larger Si concentrations at lower temperatures), the silicide constitutes a large fraction of the wire, as Figure 7 reveals. As the silicide is more brittle than elemental tungsten, this leads to the wire breakage so commonly observed in HWCVD reactors.

To provide some insight into the kinetics of Si diffusion into W, additional radical measurements were made. A standard aging treatment was adopted for these measurements, consisting of a 15 minute bake at $\sim 1000^{\circ}\text{C}$ in an ambient of SiH_4 at a partial pressure of 0.2 mTorr (20 mTorr total, balance He). A mass spectrum was then acquired at a higher wire temperature (1470°C), at a SiH_4 partial pressure of 4.4×10^{-8} Torr, followed by a scan in the absence of SiH_4 . Figure 8 reveals contributions from Si and SiH_3 (produced by H abstraction from SiH_4) for the case of the SiH_4 background. In the absence of SiH_4 , Si is the predominant radical observed, and this signal is attributed to Si (in excess of the thermodynamic solubility) diffusing from the interior of the wire; this signal was observed to persist for more than 1 hour, with no decrease in intensity. Comparing the relative magnitudes of the two signals, one estimates that the diffusion signal corresponds to a SiH_4 partial pressure of $\sim 2 \times 10^{-8}$ Torr (it should be noted that this contribution is relatively small compared to the SiH_4 partial pressures of > 1 mTorr, typical of growth conditions). For an assumed average

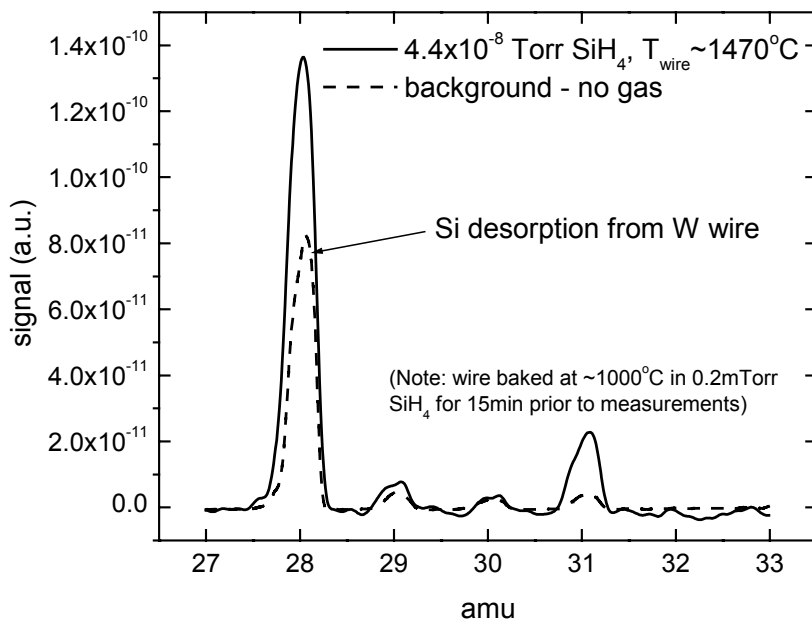


Figure 8. Mass spectrometry evidence for Si incorporation by W wire.

concentration of 1% Si throughout the entire wire, a simple calculation shows that the corresponding pressure would be ~ 30 mTorr, at a typical wire temperature of 1800°C . This result suggests that the timescale to completely deplete the wire of its Si is extremely long, consistent with the mass spectrometry observations suggesting Si diffusion.

2.4.1 Rates for Surface Kinetic Processes

A comparison of the relative rates for the various surface kinetic processes, namely, diffusion, evaporation, and decomposition allows further insight into the nature of the wire aging process. At the highest temperatures investigated in this study (~ 2400 K), the solid solubility of Si in W is a few atomic percent,

dropping to less than 1 at.% at the lowest temperature (1273 K). To our knowledge, there have been no studies that examined the diffusion of Si into elemental W. A study by Kharatyan *et al.*,²⁰ however, investigated the diffusion of Si into various silicides of tungsten and molybdenum. For the diffusion of Si into W_5Si_3 (the only silicide for which data were available), a diffusion coefficient of

$$D_{W_5Si_3}^{Si} = 6.9 \exp(-69000 \pm 5000 / RT), \text{cm}^2/\text{s} \quad (1)$$

was obtained.²⁰ Using this diffusion coefficient, the rate for diffusion (using the wire radius as a lower limit for the characteristic length) as a function of wire temperature is given in Figure 9.

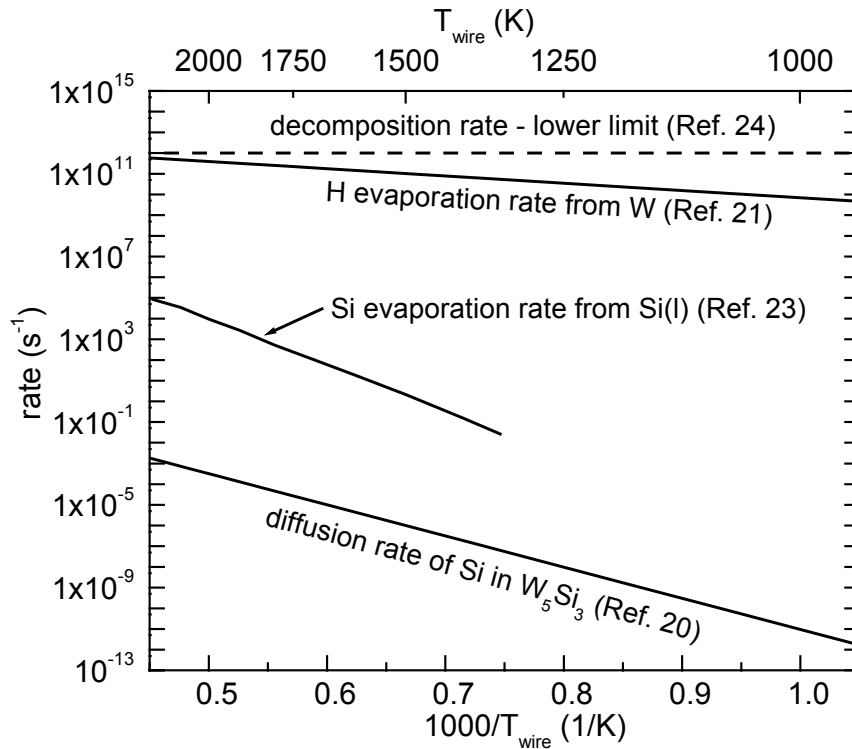


Figure 9. Rates of interest for wire surface kinetic processes.

Data on the evaporation rate of Si from W were unavailable, but the study by Ehrlich²¹ does provide an evaporation rate for H from W,²² which is relevant to the SiH₄ decomposition process; this rate is plotted in Figure 9. The evaporation rate of Si from liquid Si could be determined from the vapor pressure data of Margrave.²³ As liquid Si can form at some point during the aging process (Figure 7, T = 2000°C, W<33%/Si>66%), this rate has relevance to the aged wires of this study. This rate of evaporation, as a function of wire temperature, is also plotted in Figure 9. Finally, rates of SiH₄ decomposition on W were not directly available, but a study by Yang *et al.*²⁴ suggests the timescale for Si-H bond breaking is of order a few picoseconds (in a liquid environment), establishing a lower bound to the decomposition rate for the significantly higher temperatures in the present study; this rate is included for comparison in Figure 9.

Examining these rates in Figure 9, bulk diffusion of Si through the silicide is clearly the slowest process, followed by Si evaporation, and then decomposition. These rates, coupled with experimental observations, give a picture of the relative rates of surface kinetic processes on the wire. First, the high rate of decomposition compared with evaporation and diffusion suggests that for the vast majority of wire temperatures, Si (as opposed to other SiH_x) is the predominant evaporating/diffusing species; radical measurements in particular support the idea that it is the dominant evaporating species. At sufficiently low temperatures, however, this process becomes decomposition-limited, and a

spectrum of other species is observed (see Fig. 4). The Auger and radical measurements described earlier provide clear evidence that diffusion through the wire is occurring, and at rates faster than would be predicted by bulk diffusion (through a silicide) alone. This suggests that the majority of Si that diffuses into the wire does so before a thick silicide has formed. Whether this higher *effective* diffusivity is due to a higher intrinsic rate of Si diffusion into W (rather than W_5Si_3) or diffusion occurring primarily through cracks that develop on the surface of the wire is unclear.

Finally, it appears that the rate of evaporation of Si from Si(l) is several orders of magnitude below that of decomposition, even at the highest wire temperatures. It was previously observed, however, that for wire temperatures in excess of 2000 K, a saturation in the Si signal occurs with the use of a new wire that does not occur with an aged wire (see Fig. 2). This observation is consistent with a competition between evaporation (of Si and/or SiH_4) and decomposition. This, in turn, may suggest that the mechanism of Si desorption from a new wire does not consist of Si evaporation from Si(l), but a different mechanism, namely, the direct desorption of Si from a W surface. The rate for this process is likely to be of a similar magnitude as H evaporation from W, depicted in Figure 9. It is also possible that the rate of SiH_4 evaporation becomes comparable to its rate of decomposition at high temperatures, explaining the Si saturation.

A picture then emerges of the hot-wire CVD decomposition process. First, SiH_4 is adsorbed and then rapidly decomposed to Si and H on the surface of a new wire. This surface Si will then either evaporate or, if the surface concentration is high enough, diffuse to the interior of the wire up to its solubility limit. Once the thermodynamic solubility has been reached, excess Si can contribute to the formation of the W_5Si_3 phase, or at higher concentrations, WSi_2 . At the highest Si concentrations ($> 67\%$), liquid Si can form at the surface and then Si evaporation from $\text{Si}(l)$ becomes the dominant mechanism of Si production. The observation that a new wire readily absorbs Si, but retains it for a long period of time can be explained as a silicide diffusion-limited process. The silicide that forms at the surface acts as a diffusion barrier to Si in the interior of the wire (as well as to further diffusion of surface Si into the wire), and Figure 9 shows that the characteristic diffusion time at the wire temperature used (~ 1750 K in Fig. 8) is, at minimum, several hours.

2.5 Conclusions

With the use of a new wire, Si is found to be the predominant radical produced in a HWCVD reactor for wire temperatures in excess of 1500 K. For temperatures below 1500 K, the SiH_3 radical becomes predominant. The small activation energy (8 kcal/mole) observed for SiH_3 formation suggests the process

is catalyzed with the use of these wires. These results are in qualitative agreement with previous studies of radical chemistry at the wire. Radical measurements performed on aged wires show high temperature activation energies for all SiH_x species, suggesting a non-catalyzed process for radical formation.

Scanning electron microscopy of aged wires revealed a surface both rougher and more irregular than seen with new or heat-treated wires; this morphology is thought to be characteristic of Si deposition (either as free Si or a silicide). Auger electron spectroscopy revealed surface Si concentrations as high as 15%, suggesting a two-phase equilibrium between W_5Si_3 and W (at a Si solubility of 4%). Concentrations of Si in the interior of the wire (2-5%) are of order the solubility limit and reveal that Si diffusion into the wire is significant. Radical measurements added further evidence of Si diffusion, as Si was detected in a silane-free ambient following an aging treatment.

Examining rates for various surface kinetic processes reveals that bulk diffusion of Si through a silicide is the slowest, followed by Si evaporation and then surface decomposition. The high rate of surface decomposition supports the idea that Si is in fact the predominant evaporating and diffusing species. In light of the low rate of diffusion through the silicide, the diffusion mechanism in the initial stages of SiH_4 exposure must either consist of bulk diffusion through elemental W or large cracks that develop on the wire surface and propagate to

the interior. Finally, experimentally observed evaporation kinetics suggest that Si desorption from a new wire comes from direct Si-W bond breakage, as opposed to evaporation from Si(l).

References

1. E. Molenbroek, A. Mahan, E. Johnson, and A. Gallagher, *J. Appl. Phys.* **79**, 7278-7292 (1996).
2. A. Mahan, A. Mason, B. Nelson, and A. Gallagher, *Mat. Res. Soc. Symp. Proc.*, Vol. 609, A6.6, San Francisco, 2000.
3. Y. Nozaki, K. Kongo, T. Miyazaki, M. Kitazoe, K. Horii, H. Umemoto, A. Masuda, and H. Matsumura, *J. Appl. Phys.* **88**, 5437-5443 (2000).
4. S. Tange, K. Inoue, K. Tonokura, and M. Koshi, *Thin Solid Films* **395**, 42-46 (2001).
5. H. Duan, G. Zaharias, and S. Bent, *Thin Solid Films* **395**, 36-41 (2001).
6. J. Holt, M. Swiatek, D. Goodwin, and H. Atwater, *Mat. Res. Soc. Symp. Proc.*, Vol. 664, A3.2, San Francisco, 2001.
7. J. Doyle, R. Robertson, G. Lin, M. He, and A. Gallagher, *J. Appl. Phys.* **64**, 3215-3223 (1988).
8. *CRC Handbook of Chemistry and Physics*, 61st edition (CRC Press, Cleveland, 1980) p. E-400.
9. W. Hsu and D. Tung, *Rev. Sci. Inst.* **63**, 4138-4148 (1992).
10. This rapid method of acquiring data was chosen over that used in threshold ionization mass spectrometry (TIMS), where scans in electron energy are made at specific masses. The length of time needed for a TIMS experiment measuring all four species and acquiring reasonable statistics would have

been at least a factor of 4 longer (approximately 12 h). Over such a time period it was believed that drift, associated with a number of factors such as wire aging, could have biased the resulting data.

11. R. Robertson, D. Hils, H. Chatham, and A. Gallagher, *Appl. Phys. Lett.* **43**, 544 (1983).
12. R. Robertson and A. Gallagher, *J. Appl. Phys.* **59**, 3402 (1986).
13. K. Uchida, A. Izumi, and H. Matsumura, *Thin Solid Films* **395**, 75-77 (2001).
14. R. Freund, R. Wetzell, R. Shul, T. Hayes, *Phys. Rev. A* **41**, 3575 (1990).
15. V. Tarnovsky, H. Deutsch, and K. Becker, *J. Chem. Phys.* **105**, 6315 (1996).
16. H. Matsumura, A. Masuda, and A. Izumi, *Mat. Res. Soc. Symp. Proc., San Francisco, 1999, Vol. 557*, 67.
17. J. H. Purnell and R. Walsh, *Chem. Phys. Lett.* **110**, 330 (1984).
18. R. Kee, F. Rupley, and J. Miller, "Chemkin-II: A Fortran Chemical Kinetics Package for the Analysis of Gas-Phase Chemical Kinetics," Technical Report No. SAND89-8009 (1989).
19. TAPP - Thermochemical and Physical Properties, Version 2.1, ES Microware (1991).
20. S. Kharatyan and H. Chatilyan, *J. Prikladnoy Khimii Armenii* (1-2), 22-30 (1999).
21. G. Ehrlich, *Adv. Catal. Rel. Subj.* **14**, 271-273 (1963).

22. The Ehrlich study involved flash desorption measurements of N₂, CO, H₂, and H below room temperature, up to 2200 K. Molecules were allowed to adsorb at lowered temperatures for a period of 3 minutes, and then the filament was heated at a constant rate, allowing desorption to be monitored by an ion gauge.
23. J. Margrave, *The Characterization of High-Temperature Vapors*, John Wiley and Sons, Inc. (New York) 1967.
24. H. Yang, M. Asplund, K. Kotz, M. Wilkens, H. Frei, and C. Harris, *J. Amer. Chem. Soc.* **120**, 10154-10165 (1998).

Chapter 3 Gas-Phase Experiments

Abstract

The motivation for studying the gas-phase chemistry of CVD growth, in terms of its effect on film microstructure and electronic properties, is presented. Residence time distribution measurements are made to characterize the flow behavior of the hot-wire reactor, which can have a significant effect on the gas species distributions. Thermochemical calculations reveal the onset of agglomerate formation as a function of pressure and residence time. Mass spectrometry is used to measure the ion contribution during film growth, determine the radical distribution under specific deposition conditions, and detect disilicon or larger species present at high pressures.

3.1 Introduction

A knowledge of the primary species present during silicon CVD growth is critical to optimization of film microstructure and electronic properties. In plasma CVD processes, the discussion centers around the SiH_2 and SiH_3 radicals. The SiH_2 radical is produced by electron impact dissociation of SiH_4 ,¹ while SiH_3 is typically produced via the reaction, $\text{H} + \text{SiH}_4 = \text{SiH}_3 + \text{H}_2$.² In hot-wire CVD,

atomic Si (produced by decomposition of SiH_4 on the wire³) and SiH_3 (produced by H abstraction from SiH_4) are believed to be the important radical species.

These species all have different gas-phase and surface reactivities that can ultimately impact film properties.

For example, SiH_2 has been found to readily insert into Si-H bonds,⁴ producing Si_2H_6 in the case of its reaction with SiH_4 . This species may dissociate, due to internal energy carried from the reaction, or participate in further insertion reactions with SiH_2 (provided pressures are high enough to collisionally stabilize the species), ultimately resulting in the formation of silicon powders.⁵ By contrast, SiH_3 is unreactive with SiH_4 and is most likely to undergo recombination (if its concentration is high enough), briefly producing Si_2H_6 (carrying an even larger amount of internal energy) before rapidly dissociating.² Like SiH_2 , atomic Si can insert into the Si-H bond of SiH_4 , producing H_3SiSiH^* , which can isomerize to H_2SiSiH_2 (provided dissociation does not take place).^{6,7} Similar to their different gas-phase reactivities, these species all have different surface reaction probabilities. Atomic Si as well as SiH are the most reactive, with probabilities near unity,⁸ while SiH_2 is believed to be near 0.6.⁹ The SiH_3 radical is believed to have a reaction probability between 0.1-0.4,^{10,11} dependent largely on the hydrogen coverage of the surface, and thus the surface temperature.

The different gas-phase and surface reactivities of these species can have important consequences for film growth. In particular, the study by Roth *et al.*² concluded that a-Si:H films are deposited if secondary reactions, namely those producing Si₂H₆, take place. This suggests that methods that reduce the relative abundance of SiH₂ may suppress Si₂H₆ formation. The study of Hamers *et al.*¹² suggests that the key to producing low defect density a-Si:H at low temperature is to avoid gas-phase polymerization, a condition favored by the presence of SiH₂. Thiesen *et al.*¹³ explain the observation of low temperature epitaxial growth by HWCVD on the basis of the abundance of SiH₃, a species with high mobility and relatively low reactivity on a H-terminated Si surface. A principal conclusion of the study by Molenbroek *et al.*¹⁴ was that highly reactive Si atoms must react with SiH₄ en route to the substrate, likely forming H₂SiSiH₂,¹⁵ in order to produce high-quality a-Si:H films (e.g., large light-to-dark conductivity ratio, $\sigma_{\text{ph}}/\sigma_{\text{d}}$).

3.2 Residence Time Distribution (RTD)

The flow characteristics of the hot-wire reactor, specifically the residence time of gas species, can have a large impact on the resulting gas species distribution. For stable molecules (e.g., SiH₄) or low surface reactivity radicals (e.g., SiH₃), the residence time can determine whether reaction routes with other

radical species (e.g., Si and/or SiH₃) take place. As some of these reactions may or may not be desirable, it can be challenging to determine the residence time that is optimal. In this regard, kinetics calculations that include the relevant reactions are helpful.

3.2.1 RTD Measurements

The residence time distribution was determined by applying a pulse input (i.e., quickly opening and closing a leak valve) of a mixture of argon diluted in helium (1%) to the hot-wire reactor and monitoring the decay of the Ar signal over time with a quadrupole mass spectrometer (Hiden Analytical Ltd., HAL RC201). Short dwell (time to acquire a single data point) and settle (time between data point acquisition) times of 1 ms were chosen for the mass spectrometer in order to adequately capture the features of the pulse input. Argon was chosen as the tracer gas for this experiment due to its similarity in mass to SiH₄ (40 amu versus 32 amu), resulting in a difference in diffusivity of just a factor of 1.1. The residence time of SiH₄ is of greatest interest here, due to its participation in the primary gas-phase reactions with Si and H.

Figure 1a shows the response to a pulse input of the Ar mixture at a peak pressure of 187 mTorr and 47.1 sccm flow rate, with the wire maintained at a temperature of 2000°C, conditions representative of those during film growth.

The cause of the “glitch” that appears at 20 sec in the data is uncertain, but possibly related to the chosen settle/dwell times. Data of this variety is typically represented as a residence time distribution function $F(t)$, which specifies the fraction of gas with an age less than t .¹⁶ This function can be determined by integration of the response curve, normalized by the total integrated area under the curve:

$$F(t) = \frac{\int_0^t I(t)dt}{\int_0^{\infty} I(t)dt} \quad (1)$$

where $I(t)$ is the raw signal. By similar procedures, the average residence time τ can be obtained by:¹⁶

$$\tau = \frac{\int_0^{\infty} tI(t)dt}{\int_0^{\infty} I(t)dt} \quad (2)$$

Under the aforementioned conditions, the average residence time was determined to be 11 seconds (after the initial spike at time = 15 sec).

Figure 1b displays the normalized response function and residence time distribution functions for the experiment and for an idealized continuous stirred tank reactor (CSTR) with an average residence time of 11 seconds as well. The CSTR model assumes perfect mixing of all fluid elements and as can be seen

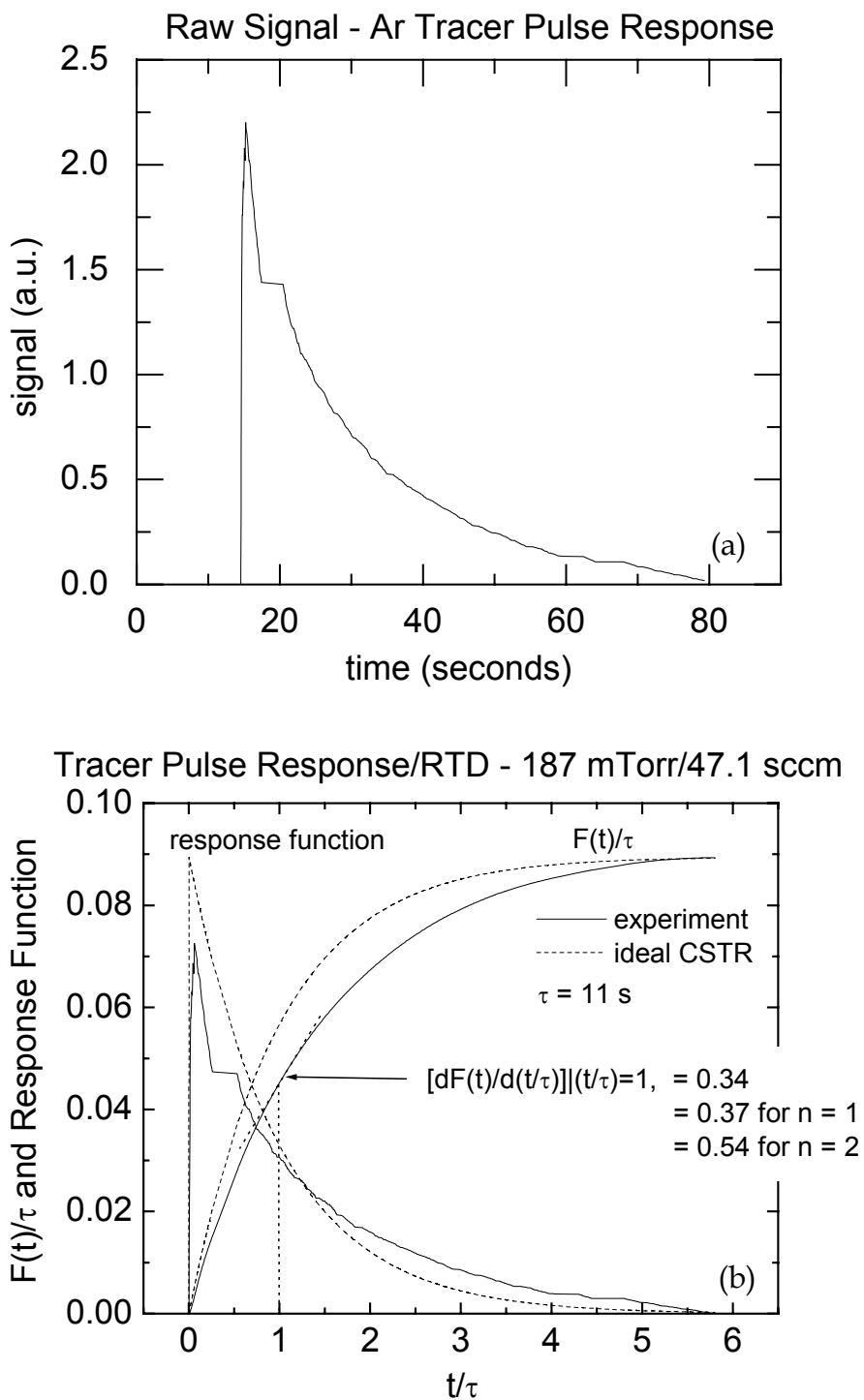


Figure 1. (a) Response of reactor to a pulse input of gas - 187 mTorr/47.1 sccm of 1% Ar in He mixture; (b) Normalized response function and residence time distribution (RTD) function for Ar tracer experiment and for an ideal CSTR.

from the figure, both the response function and RTD function for the experiment match that of the CSTR well. Deviations from ideality can often be simulated by a cascade of ideal CSTRs in series.¹⁶ It has been shown¹⁶ that the slope of the RTD can be related to the number of such CSTRs in series. A value of 0.37 is obtained for a single CSTR (0.54 for two in series), while the experiment gives a value of 0.34, showing that under these conditions, the hot-wire reactor can be modeled as a single CSTR.

The pressure of 187 mTorr was found to be the minimum achievable for this pulse input tracer experiment, due to the slow response of the mass flow controller to its set point. Subsequent experiments were carried out at higher pressure to evaluate the effect on average residence time. The residence time reached as high as 24 seconds for pressures of 400 mTorr. Pressures any higher than this were not explored as they are unrepresentative of those during film growth and place a strain on the turbomolecular pumps of the reactor.

3.2.2 Stirred Tank Reactor Calculations

Given the knowledge that the hot-wire reactor behaves as an idealized CSTR, estimates of species abundance can be obtained by simple calculations. The tool used for this purpose was the Thermo Chemical Calculator (TCC), developed by David Goodwin.¹⁷ To approximate the gas-phase chemistry relevant to the hot-

wire reactor, the silane reaction mechanism of Ho *et al.*¹⁸ was used, which includes 10 reactions and 9 species (from silane up to trisilane); H and Si₂H₂ were not available with this mechanism, species that are included in later simulation mechanisms in this thesis. As this is only a gas-phase calculation, the surface reactivities of the various species (e.g., Si versus SiH₃), which will reduce their relative gas-phase abundance and residence times, have not been taken into account. It is also assumed in the calculation that all species have identical residence times, which is not strictly true due to their different pumping speeds (e.g., H₂ and SiH₄). These calculations can, however, provide a lower bound to the pressure at which the onset of Si particle formation may occur.

A well-stirred reactor calculation was performed that provided the effluent composition as a function of reactor residence time. To model conditions relevant to hot-wire growth, a gas mixture of SiH₄ diluted in He (1%) was chosen, with an average gas temperature of 750 K (a value intermediate between that of the substrate - 600 K, and the wire - 2300 K) and fixed pressures of 0.1 and 1 Torr. To account for the decomposition that occurs on the wire, the initial conditions were specified assuming 50% of the SiH₄ is decomposed into Si and H₂.

Figure 2 shows the species distributions obtained at pressures of (a) 0.1 Torr and (b) 1 Torr for the above specified system. For residence times of 1 second and less, no significant reaction occurs and H₂, Si, and SiH₄ remain the

predominant species. At a residence time of 10 seconds (comparable to the experimentally determined value for Ar), gas-phase reactions start to become significant, with H_2SiSiH_2 (produced by the reaction of Si and SiH_4) comparable to Si in abundance. For residence times of 100 seconds and higher, the equilibrium distribution of species is approached, which consists mostly of the radical H_2SiSiH_2 and the mono-, di-, and tri-silane molecules, along with H_2 . For the higher pressure of 1 Torr, the onset of gas-phase reactions occurs at a shorter residence time (1 second). In contrast to the lower pressure distribution, Si_2H_6 and Si_3H_8 exceed the concentrations of the radicals for residence times greater than 10 seconds at 1 Torr. Again, it should be emphasized that these seemingly long residence times are more characteristic of the stable gas species (e.g., Ar and He), and the radical species have actual residence times orders of magnitude smaller than these, due to their high sticking probabilities at the reactor walls; for illustrating qualitative trends, however, the results obtained here are useful and have implications for silicon film growth.

As mentioned, gas-phase polymerization to form species like Si_2H_6 , Si_3H_8 , and larger is thought to be deleterious to amorphous film quality.¹² This clearly indicates that the reactor should be operated as far from thermodynamic equilibrium as possible to suppress the formation of these species. At higher

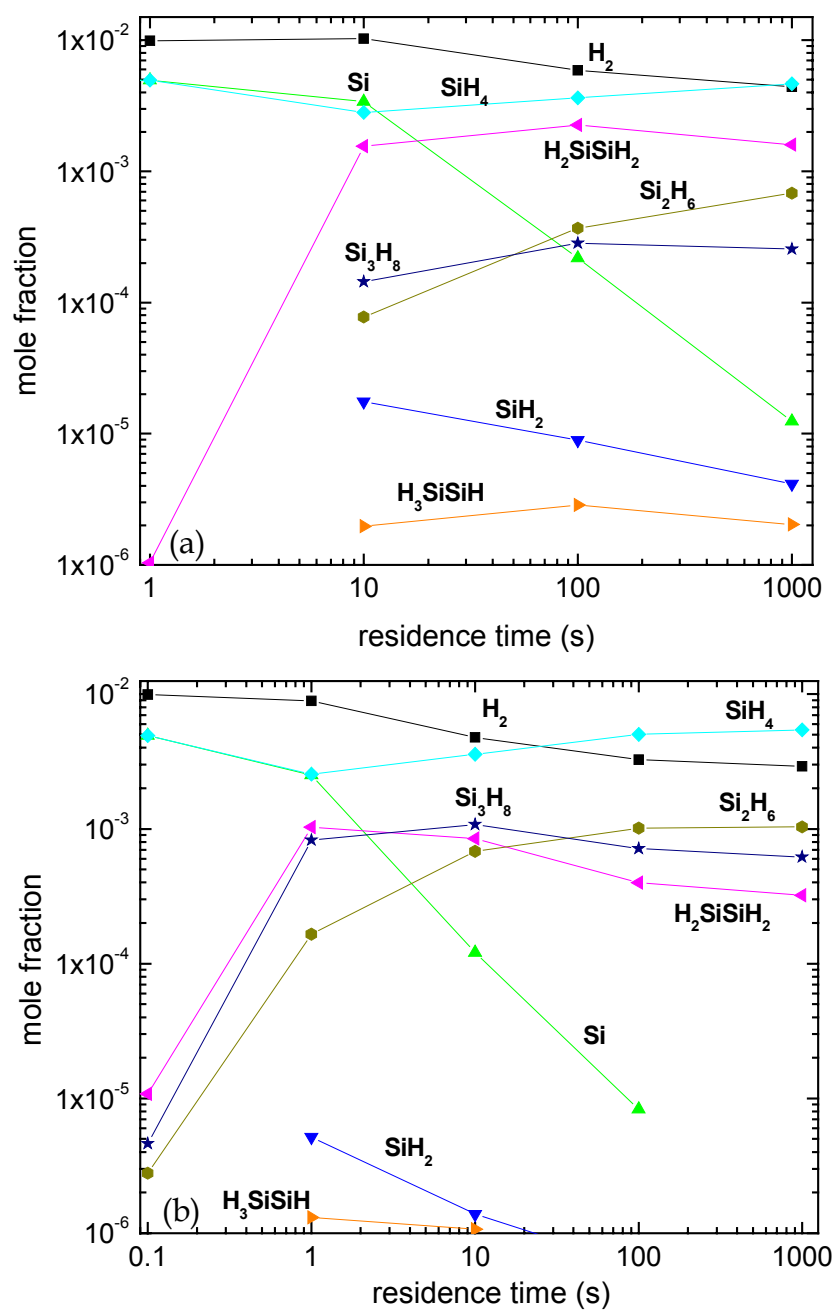


Figure 2. Simulated species distributions as a function of reactor residence time for total pressures of (a) 0.1 Torr and (b) 1 Torr, for a 1% SiH_4 in He mixture.

pressures, it becomes more difficult to suppress these reactions, so an upper bound of several Torr for these conditions should be imposed. If H_2SiSiH_2 is indeed a beneficial precursor to high-quality a-Si film growth, as suggested by Molenbroek *et al.*,¹⁵ then both the pressure and residence time (in effect, the mass flow rate) must be carefully tuned to produce a modest amount of gas-phase reactions and maximize the production of this species, while suppressing the formation of the larger species.

3.3 Detection of Radical Species

3.3.1 Introduction

It has been established thus far that knowledge of the radical species present during hot-wire film growth is important for film quality optimization. There are a number of techniques available for the detection of radical species that have inherent advantages and limitations. The technique of mass spectrometry offers the unique ability to simultaneously measure the relative abundance of numerous species of interest in CVD processes. For silicon film deposition, the species of interest are primarily H, H_2 , SiH_x , and higher silanes such as Si_2H_x .

In particular, the technique of threshold ionization mass spectrometry (TIMS) offers a sensitivity and discrimination that is typically better than that provided

by optical techniques, such as laser induced fluorescence.¹⁹ There have been recent successes using LIF to detect Si and SiH present during hot-wire growth,²⁰ but the difference in absorption bands of each radical makes it practically impossible to measure all radicals of interest simultaneously. Other problems associated with optical techniques include overlapping bands and interference from background radiation (particularly problematic in plasma CVD systems), but these techniques do offer the advantage of measuring radical density variations within a reactor.¹⁹ By contrast, mass spectrometry techniques measure the flux of radicals, typically at a fixed location. Quantification of mass spectrometry signals can be difficult at high pressures ($P > 5$ Torr), where the sampling orifice diameter is significantly larger than the collision mean free path. Under these conditions, the flow transitions from effusive to continuum, and the mass spectrometer signal (I) no longer exhibits simple relations to gas properties:

$$I \propto [n v_{th}] \propto [P/T] \quad (3)$$

(where n is the local gas density, v_{th} is the mean thermal speed of the gas, and P and T are the process pressure and temperature).²¹

3.3.2 Radical-to-Ion Flux in HWCVD

Although it has been established that radicals constitute the main growth precursor in HWCVD, while ions contribute up to 70% of the deposited film for

polymorphous and microcrystalline silicon by plasma CVD,¹² there have been few attempts, if any, to measure the ion flux present in HWCVD growth.

Considering the higher gas-phase reactivity of ions compared to radicals (due to induced dipole effects between ions and neutrals),¹² quantification of this ion flux is crucial to an understanding of the gas-phase kinetics. Due to the high filament temperatures encountered in HWCVD (up to 2000°C), thermionic emission of electrons can occur, resulting in a flux of up to 10^{17} electrons/cm²-sec.²² It has been further shown²² that these electrons can have a modest effect on the dark conductivity of the resulting a-Si:H films, depending on the substrate bias. It is largely unknown, however, whether these electrons can cause ionization of the gas between the filament and substrate.

To test whether electron impact ionization can occur in the hot-wire reactor, a coiled filament (~ 30 cm long, 0.5 mm diameter, 5 mm diameter coils) was used, for which the voltage drop was 34 V at the operating temperature of 1700°C (9.3A). This suggests that electrons, on average, reach the substrate (which is grounded) with an energy of 17 eV. This energy is well above reported dissociation and ionization energies for SiH_x (x=0-4) species.^{23,24} As a result, the potential for electron impact ionization of SiH_x occurring in the reactor exists with such an experimental arrangement.

Figure 3 shows a mass spectrum collected of the SiH_x species at a pressure of 382 mTorr (1% SiH₄ in He), with the ionizer of the mass spectrometer both on

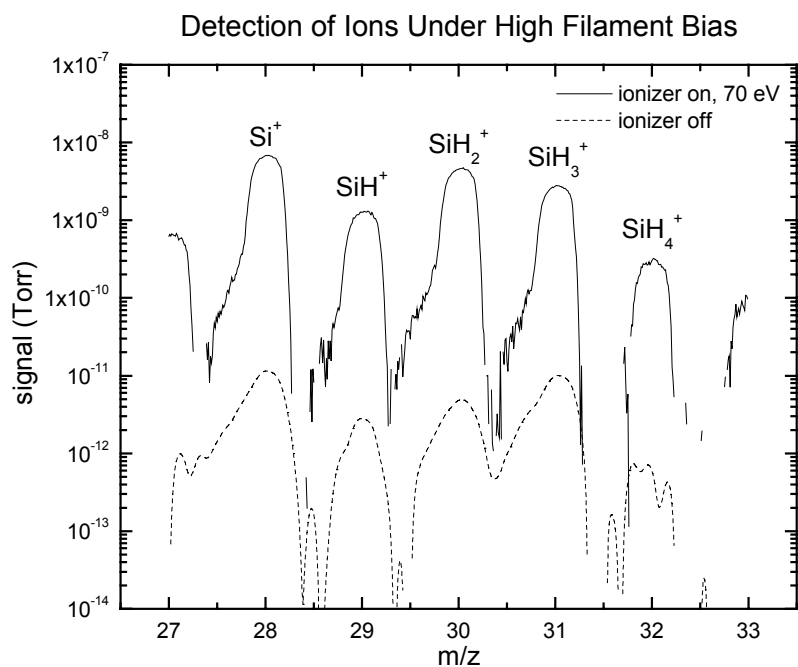


Figure 3: Detection of ions under conditions of 382 mTorr (1% SiH₄ in He), filament temperature of 1700°C, and filament bias of 34 V. Both spectra were background corrected. Discontinuities are caused by negative baseline values, the absolute values of which are much less than the peak signal intensities.

(electron impact ionizer, operating at 70 eV) and off; the spectra were plotted on a logarithmic intensity scale in order to compare their magnitudes. With the ionizer turned off, the signal is derived exclusively from ions produced in the chamber by thermionic electron impact ionization. With the ionizer on, the signal is derived from both ion production in the chamber and dissociative ionization of SiH₄ (to other SiH_x) that occurs at the 70 eV electron energies present in the ionizer (the latter being the predominant contribution).

Comparing signal intensities obtained with the *wire* on and off (not depicted) and the ionizer on revealed that the contribution of wire-produced atomic Si to the

observed signal is at least as great as the contribution from SiH_4 dissociation in the ionizer (i.e., the SiH_4 depletion caused by the wire is about 50%). Comparing the two signals in Figure 3, it can be seen that a measurable amount of ions is produced, although they are approximately 3 orders of magnitude lower in abundance when compared with the radical and SiH_4 signal. This would suggest that ion production would not significantly impact the gas-phase chemistry under these conditions, despite the higher gas-phase reactivity of these species.

The ion production that occurs here is clearly a result of the large voltage drop encountered across the long filament. If ion production was to become problematic, simple measures could be implemented to reduce their contribution to the film growth process. This would involve dividing up the same total length of filament into separate strands wired in parallel, with a voltage drop across each that is below that which would cause ionization by the aforementioned process.

3.3.3 Threshold Ionization Mass Spectrometry

The technique of threshold ionization mass spectrometry (TIMS) has been widely used for the detection of radical species present in silane-argon dc discharges,^{19,25} silane-methane RF discharges,²⁶ and methane-hydrogen discharges or hot filament-assisted processes.^{3,21} Not since the early study of

Doyle *et al.*,³ however, has it been applied to the detection of species present during hot-wire CVD growth in silane ambients. Furthermore, such measurements have not been made under the dilute (1%) silane conditions and higher pressures (up to 0.5 Torr) of the present study. It is important to note that with the higher pressures used here, the mass spectrometer must be operated with the differential pumping orifice (of $\sim 100 \mu\text{m}$ diameter) in front of it; this differs from the “open-source” mode of operation described in section 2.2, and results in lowered radical sensitivity due to reactions of radicals at the surface of the orifice.

TIMS relies on the lower energies typically required for direct radical ionization (e.g., $A + e^- = A^+ + 2e^-$, ionization potential) versus their production from a parent molecule (e.g., $AB + e^- = A^+ + B + 2e^-$, appearance potential). The ionizer of the mass spectrometer is typically operated at an electron energy between that of these two processes. For the silane system, the separation between these thresholds are 2-4 eV, making possible the discrimination of SiH_x radicals from SiH_4 , provided electron beam broadening effects are not significant.¹⁹ A listing of the ionization and appearance potentials for the silane system, derived from measurements of Robertson *et al.*,²⁵ can be found in Table 1.

Table 1. Threshold energies (eV) for direct radical and dissociative ionization. From Robertson *et al.*²⁵

Neutral	Si ⁺	SiH ⁺	SiH ₂ ⁺	SiH ₃ ⁺
Si	8.2			
SiH	11.2	9.5		
SiH ₂	10.4	13.1	9.7	
SiH ₃	13.1	11.3	12.5	8.4
SiH ₄	12.5	15.3	11.9	12.3

Data Normalization

Due to offsets between the voltage applied to the filament emitting electrons in the ionizer and the actual electron energy (caused by, for example, the voltage drop across the filament), an offset correction is often necessary.²¹ Using He as a reference, an apparent threshold of 25.5 eV was obtained, as compared with the known threshold of 24.6 eV.²⁷ Using Ar as a reference, an apparent threshold of 16.8 eV was obtained, as compared with the known threshold of 15.8 eV.²⁷ As a result, a correction of 0.95 eV (the average of the two offsets) was applied to all of the data that follow.

Another correction is necessary to account for the depletion of SiH₄ at the filament, in order to facilitate comparison of spectra obtained with the filament

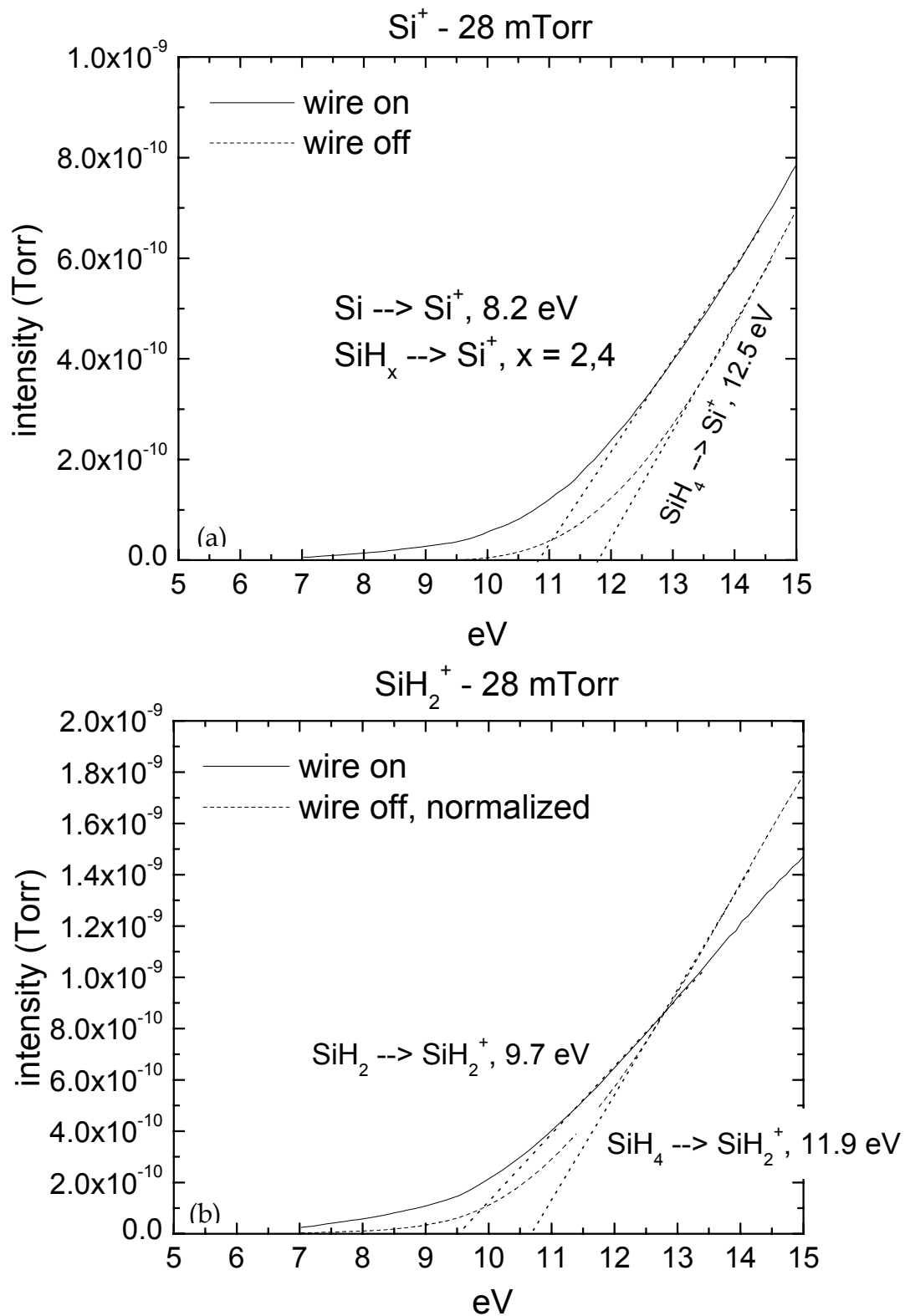
on and off. At electron energies well above the ionization and dissociation thresholds (~ 30 eV), the predominant contribution to the SiH_x^+ signal in the mass spectrometer is that resulting from SiH_4 dissociation.²⁵ This is due to the high sticking probability of SiH_x compared with SiH_4 , resulting in a reduction in the $\text{SiH}_x/\text{SiH}_4$ ratio within the mass spectrometer. As a result, species like SiH_2^+ or SiH_3^+ , which are the primary products of electron impact ionization, will show a decrease in intensity proportional to the depletion of SiH_4 for spectra acquired with the hot-wire on (compared to the wire off spectra). The magnitude of this decrease at an electron energy of 30 eV can be used to normalize all of the “wire off” spectra. Once the spectra are normalized, the net radical signal is obtained as the difference between the “wire on” and “wire off” signals.

Threshold ionization measurements were performed under conditions of relevance to hot-wire CVD film growth, namely, total pressures of 28 and 200 mTorr (1% SiH_4 in He). A coiled tungsten filament (0.5 mm diameter) was used, having a total length of 30 cm, operating at a temperature of 1900°C, at a distance of 2.5 cm from the mass spectrometer orifice. For the low electron energies (8-30 eV) used in these measurements, lower ionizer filament currents ($< 100 \mu\text{A}$ versus 1000 μA) were necessary to reduce its operating temperature to a level at which filament evaporation does not occur. These lower currents impose a limitation, however, on the sensitivity of the instrument that should be kept in mind.

Results

Figure 4 shows the threshold ionization spectra for Si^+ , SiH_2^+ , SiH_3^+ , and H^+ obtained at 28 mTorr. A spectrum acquired at mass 29 suggested only trace amounts of the SiH species, within the detection limits of this technique. Based on the extent of SiH_4 atomization on the filament at these temperatures²⁸ and the low pressures involved, it is unlikely that SiH is produced either on the wire or via gas-phase processes. Spectra are acquired with the wire both on and off in order to assess the extent of radical production on the wire. The apparent threshold energies for each species were determined by extrapolating the linear portions of each signal down to zero intensity, a procedure adopted by Hsu *et al.*²¹ for simple ionization processes such as $\text{A} \rightarrow \text{A}^+$, and believed to be accurate to within 0.5 eV. The energies for representative ionization processes are listed as a reference.

The Si^+ “wire on” spectrum provides some evidence for the presence of the Si radical, but interference from dissociative ionization of SiH_4 (and perhaps SiH_2 as well) results in an apparent threshold of 10.8 eV. It is notable that the “wire off” spectrum reveals a threshold 0.8 eV lower than expected from dissociative ionization of SiH_4 . The “wire on” spectrum of SiH_2^+ shows a threshold that



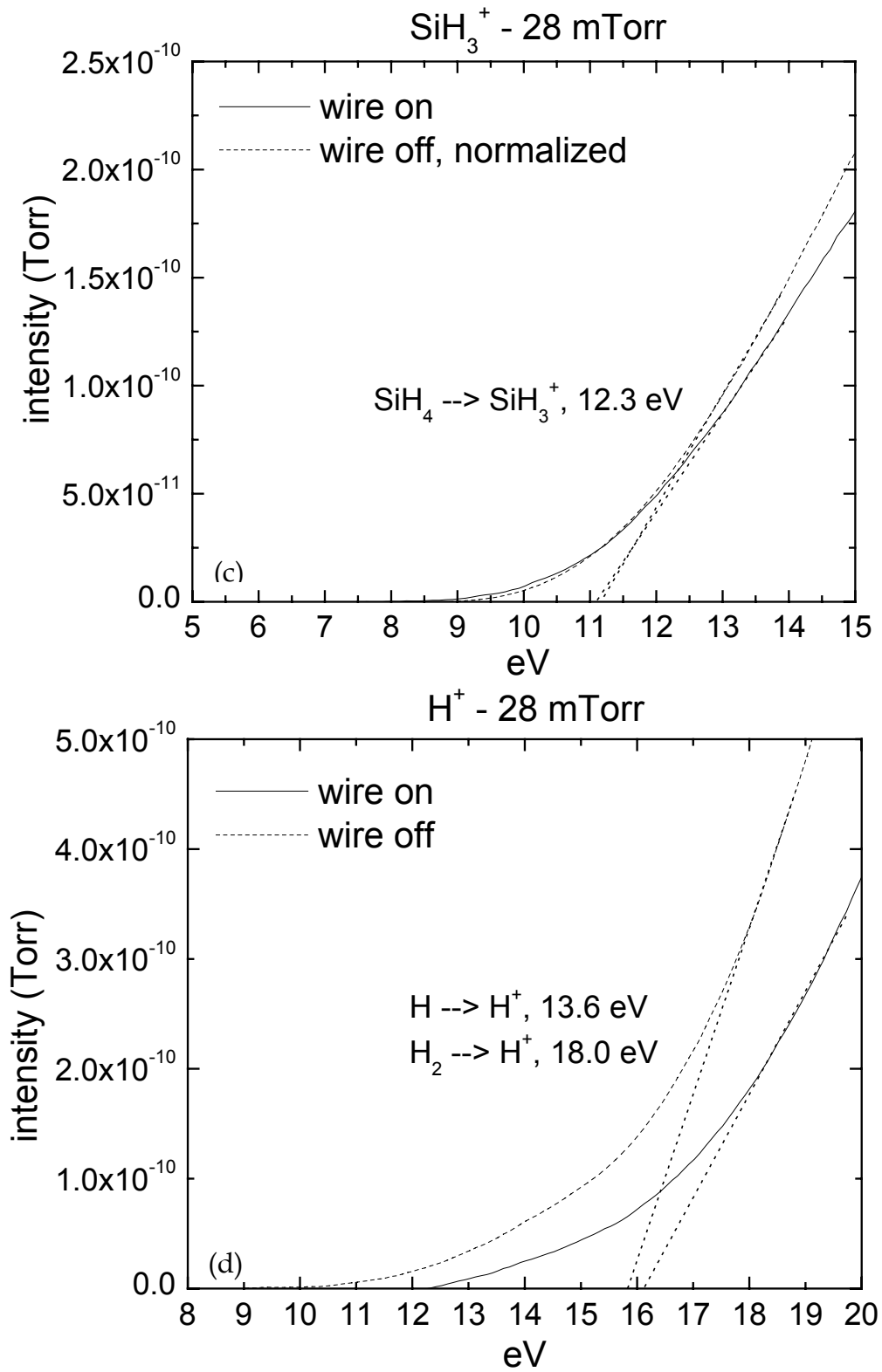


Figure 4c, d. Threshold ionization spectra of (c) SiH_3 and (d) H acquired at 28 mTorr (1% SiH_4 in He).

agrees well with that expected from direct ionization of the SiH₂ radical and the higher signal intensities as compared with that of Si suggest larger amounts of the SiH₂ radical. As with Si⁺, the “wire off” spectrum for SiH₂⁺ shows an apparent threshold lower (1.2 eV) than expected from the dissociative ionization route. For SiH₃⁺, both the “wire on” and “wire off” spectra have the same apparent threshold, suggesting no SiH₃ is produced in the chamber. Again, this energy is lower (1.1 eV) than that for dissociative ionization. Both H⁺ spectra show identical thresholds that are between that expected for direct ionization versus production from H₂; unlike with SiH_x⁺, the “wire off” H⁺ spectrum was not normalized. The similarity in threshold might suggest that the predominant contribution to H⁺ is from dissociative ionization of background H₂ in the chamber. This is certainly the case for the “wire off” spectrum, and again there is a lower than expected threshold (16 eV versus 18 eV).

The lower than expected thresholds for dissociative ionization of SiH₄ to SiH_x⁺ and H₂ to H⁺ could be rationalized as resulting from vibrational excitation of SiH₄ and H₂. The study of Robertson *et al.*¹⁹ comments that vibrational excitation could be expected to yield lower dissociative ionization thresholds. This, in turn, might contribute to an apparent “radical” signal. Although SiH₄ molecules are likely to undergo some wall collisions en route to the sampling orifice, these may be insufficient in the absence of gas collisions (at 28 mTorr) to de-excite the molecule. Yet another means for dissociative ionization below the

nominal threshold relates to the spread in the electron energy distribution from the ionizer (estimated as 0.5 eV full-width half maximum). With a distribution of electron energies, the net effect should be to make the threshold less distinct, increasing the error in its determination.

Figure 5 shows the threshold ionization spectra for the same species at a total pressure of 220 mTorr (1% SiH₄ in He). The Si⁺ “wire on” spectrum shows a threshold near 12.5 eV, expected for dissociative ionization from SiH₄, suggesting few Si radicals (within detection limits) are present. The “wire off” spectrum shows an apparent threshold of approximately 13.5 eV, above that expected for Si⁺ production by this route. One explanation that can account for this *higher* than normal threshold is non-linearity in the ionization cross section near the threshold region. This is believed to explain slight non-linearities in the threshold in cases even as simple as $\text{H} + \text{e}^- = \text{H}^+ + 2\text{e}^-$,²⁹ and thus it is reasonable that for the more complicated process of Si⁺ formation, non-linearities would be observed. The SiH₂⁺ “wire on” signal shows a threshold between that expected for direct ionization versus dissociative ionization, suggesting some radical contribution. The corresponding “wire off” spectrum shows the threshold expected for dissociative ionization from SiH₄. The higher pressures under which these measurements were made (and the consequent larger number of collisions) might be the reason that vibrational excitation of SiH₄ did not cause a lowering of the threshold, as

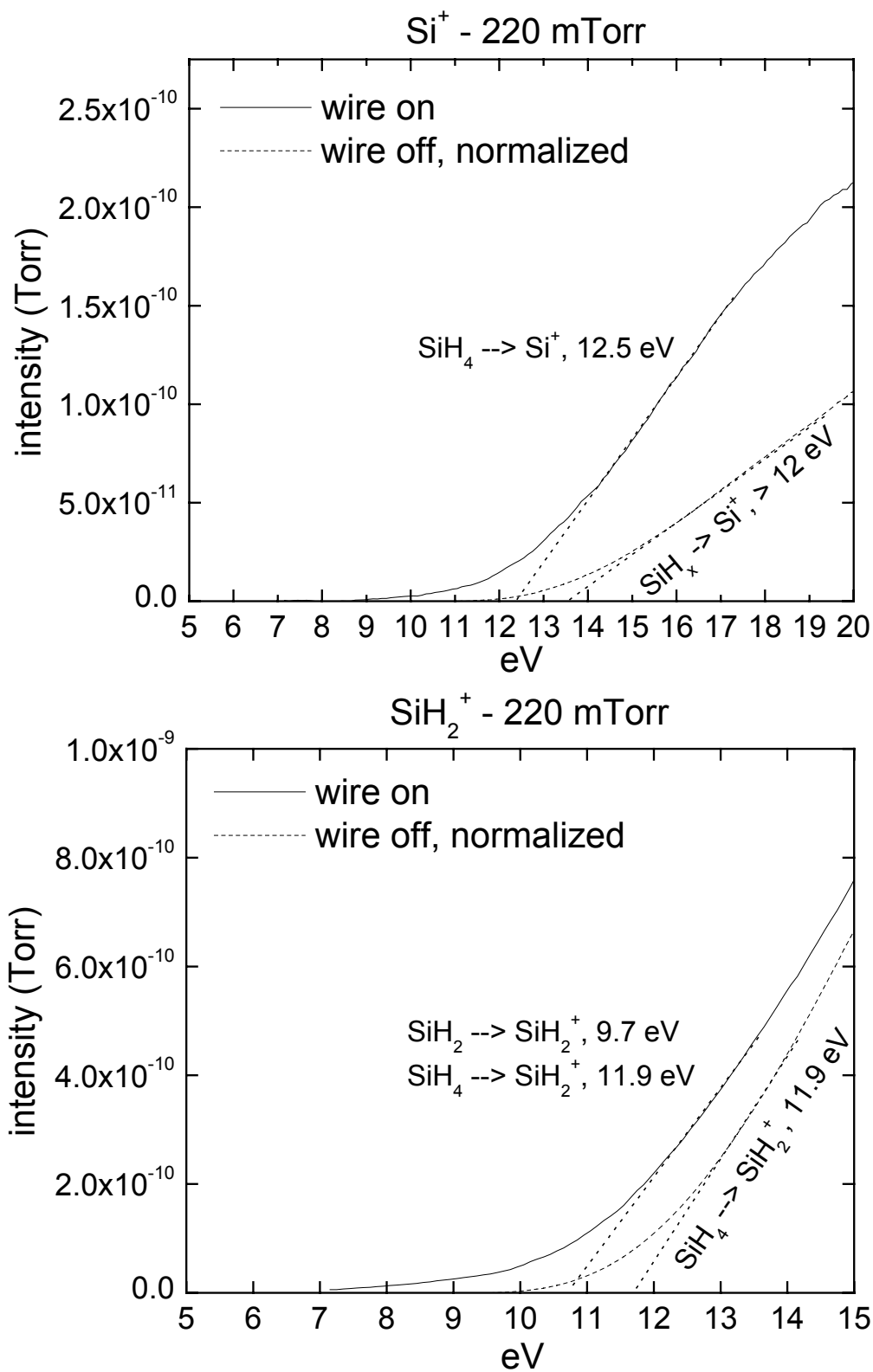


Figure 5a, b. Threshold ionization spectra of (a) Si and (b) SiH_2 , obtained at 220 mTorr (1% SiH_4 in He).

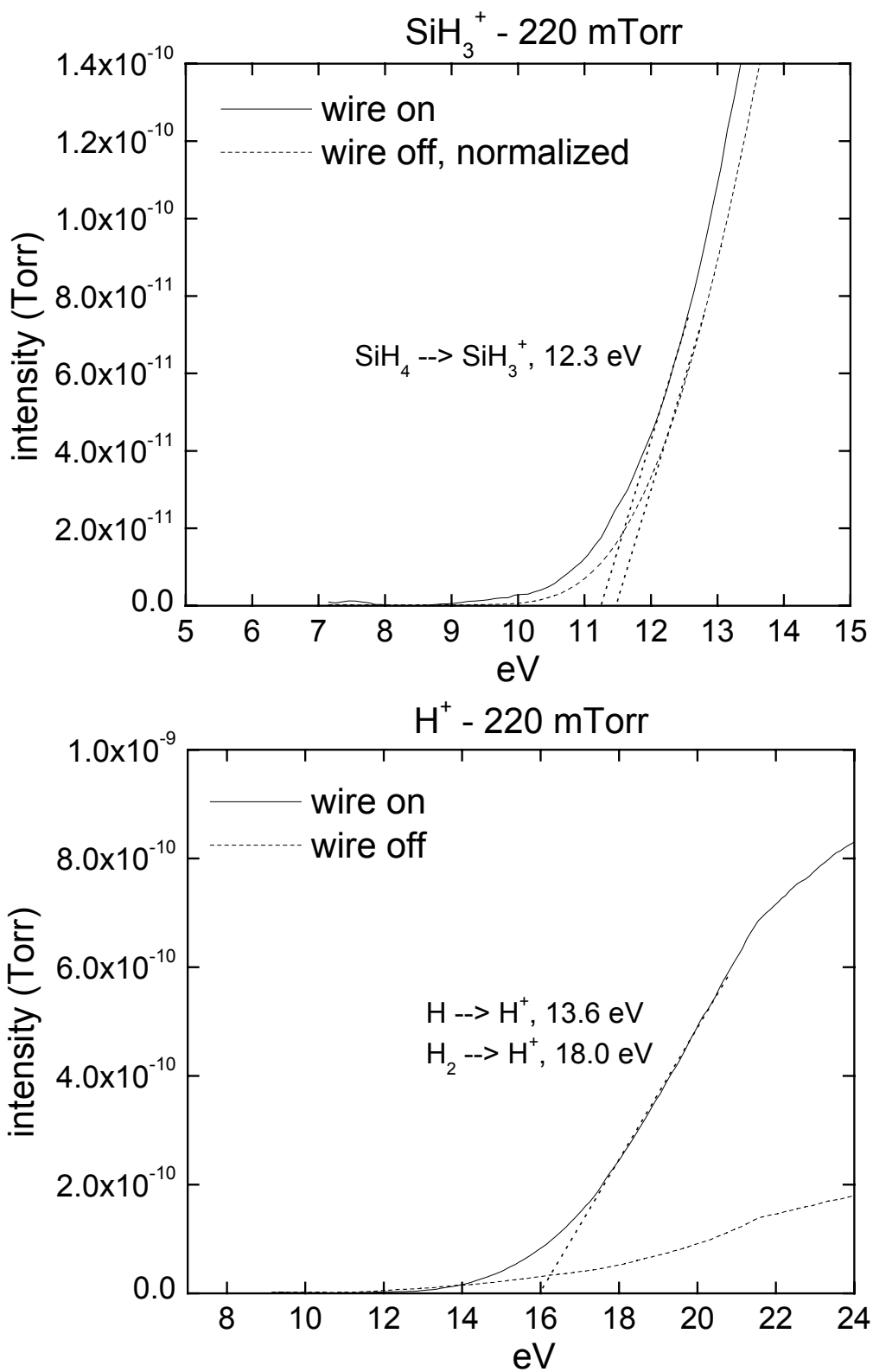


Figure 5c, d. Threshold ionization spectra of (c) SiH_3 and (d) H obtained at 220 mTorr (1% SiH_4 in He).

observed for SiH_2^+ production at 28 mTorr. The SiH_2^+ signal intensity is again larger than that of Si.

As before, the SiH_3^+ thresholds in each case are similar, suggesting only trace amounts of this radical. The thresholds are identical, however, to those obtained at the lower pressure, suggesting that vibrational excitation may not be the explanation for the lowered threshold for SiH_3^+ production at the two pressures investigated; it may, instead, be related to the electron energy distribution. This explanation is not necessarily inconsistent with the results for SiH_2^+ , as the two species are produced by different mechanisms. The H^+ “wire on” spectrum shows a similar threshold as observed previously (~ 16 eV), suggesting again a significant contribution of H_2 to the signal; the signal intensities in the “wire off” spectrum were near the detection limits for the instrument, so definitive statements regarding this data cannot be made.

Subsequent measurements were made at lower pressures (in the range of 2 mTorr), but the signal-to-noise ratio was unacceptable for threshold analysis. Higher pressure measurements (including the use of H_2 -dilution) were also made in an attempt to preferentially produce the SiH_3 radical and potentially higher silicon species (Si_2H_x). For pressures of up to 500 mTorr, similar results to those obtained at 220 mTorr were seen.

Summary

For the range of pressures investigated with the threshold ionization technique, SiH_2 was the predominant radical species detected. At a pressure of 28 mTorr, there was a trace amount of Si, while SiH_3 was not detected at either pressure. The data at higher pressure was difficult to interpret, as threshold energies were at higher- and lower-than-expected values. It should be pointed out that the higher surface reactivity of Si relative to SiH_2 may reduce its apparent abundance, given the number of collisions radicals may undergo en route to the sampling orifice. There was evidence for the presence of H_2 , but H could not be unambiguously detected, due perhaps to the large contribution from vibrationally excited H_2 . It also appears that vibrational excitation of SiH_4 can account for some of the lowered dissociation thresholds observed. However, the number of different mechanisms that may interfere with the desired signal (some of which are radical dependent) make unambiguous radical measurements difficult with this technique; this was particularly true for the high pressure measurements here, where threshold energies were at higher and lower than expected values.

The large amounts of SiH_2 observed at low pressure were unexpected as previous SiH_4 decomposition measurements²⁸ revealed that Si and H should be the predominant species produced at the wire and thus observed in the gas

phase. However, another route for SiH₂ production could have been heterogeneous pyrolysis of SiH₄ on hot surfaces other than the wire. In particular, the amorphous silicon-coated walls nearest the wire (~1-2 cm away) can reach temperatures in excess of 400°C, considering the high wire temperatures used (1900°C) and the larger surface area of the wire used for these studies (4.7 cm² versus 1.9 cm²). Also, the production of SiH₂ by reaction of SiH₄ on amorphous silicon surfaces at these temperatures has been previously suggested.³⁰ The production of SiH₂ at high pressures is also believed to result from the above described process. Primary gas-phase reactions of radicals to produce SiH₂ (e.g., Si + SiH₄ = 2 SiH₂) are believed to be too endothermic to occur to a significant extent.¹⁵

Given what is known about the high surface reactivity of SiH₂⁹ and its participation in the formation of Si₂H₆,⁴ measures to suppress this pyrolysis reaction are desirable. These measures should include a combination of limiting the SiH₄ residence time in the reactor (e.g., operating at higher SiH₄ flow rates), along with substrate thermal management. In this case, the environment seen by the film will be dominated SiH₄ dissociation on the wire, rather than thermal CVD at the substrate.

3.3.4 Detection of Higher Silicon Species

The identification of the pressure regime in which disilicon (and larger) species are formed is critical, as these species are a potential precursor to the formation of particulates. As mentioned, the earlier threshold ionization measurements required ionizer filament currents to be lowered, at the expense of instrument sensitivity. For the detection of disilicon species, standard operating conditions of 70 eV and 1000 μA were used to maximize sensitivity. With such a high electron energy, individual Si_2H_x radicals could not be distinguished (due to dissociative ionization), but the detection of a fragmentation pattern in the mass range of 56-62 would provide evidence for the formation of these radicals or the stable Si_2H_6 .

Sampling of Si_2H_x and Si_3H_x species was carried out at pressures of 500 mTorr (1% SiH_4 in He) and higher, at a wire temperature of 1700°C. No Si_xH_y ($x \geq 2$) species were detected for pressures less than 2000 mTorr. At a pressure of 2050 mTorr, a distribution of species in the mass range from 58-62 was observed, as shown in Figure 6a. These species are believed to be consistent with Si_2H_x ($x = 0-6$). Species in the mass range 84-92 (Si_3H_x) were not observed under these conditions. Experiments at pressures higher than 2050 mTorr were not possible due to operating pressure restrictions ($< 5 \times 10^{-6}$ Torr) of the electron multiplier of the mass spectrometer.

For purposes of comparison with the Si_2H_x distribution in Figure 6a, a cracking pattern of Si_2H_6 was obtained. The cracking pattern was obtained by flowing a mixture of Si_2H_6 in He (~1%) into the chamber, while the mass spectrometer was operated under conditions identical to those during radical sampling (70 eV, 1000 μA). Figure 6b shows the Si_2H_6 cracking pattern, revealing that the distribution of species is similar. The Si_2^+ and Si_2H^+ species are somewhat higher in abundance in the high pressure distribution. A comparison of these distributions suggests that Si_2 , Si_2H , and Si_2H_6 are comparable in abundance (assuming similar electron impact ionization cross sections³¹) at

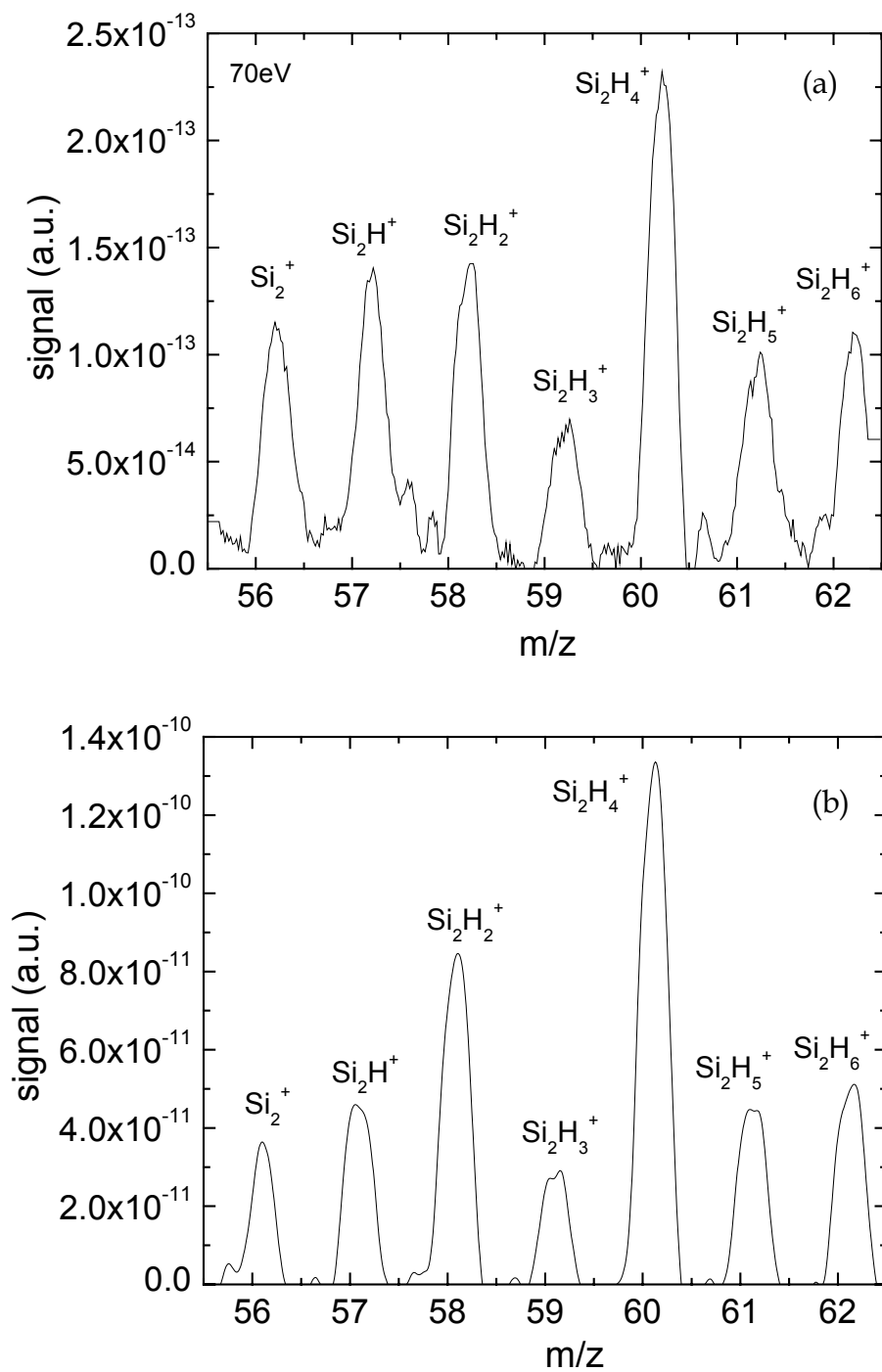


Figure 6. (a) Distribution of Si_2H_x species observed at 2050 mTorr, (b) Cracking pattern of Si_2H_6 within the mass spectrometer.

pressures of 2050 mTorr. The signal intensities for these species are less than 1% that of monosilicon species, suggesting that their formation has little impact on film growth. The detection of these species is a useful indicator, however, for the onset of gas-phase chemistry.

In consideration of the relative energies and kinetics of various reaction paths, it is possible that the Si_2H_6 observed comes from the reaction of SiH_2 and SiH_4 . It was demonstrated by threshold ionization measurements (section 3.3.3) that SiH_2 is created in significant quantities under particular conditions where heterogeneous pyrolysis can occur. This radical can also be generated directly on the wire (section 2.3.1), at an abundance of a few percent relative to Si. The SiH_2 created can react with SiH_4 at sufficiently high pressures to produce Si_2H_6^* (* = internal energy),² which has been estimated to have a metastable lifetime of 0.1 μs by means of this reaction path.⁵

The mean collision time (t_{colln}) under these conditions can be estimated from the mean free path (λ) and the mean thermal speed of the gas (v_{th}):^{32,33}

$$\lambda = \frac{1}{\pi n d_{\text{eff}}^2} \sqrt{\frac{m_{\text{buffer}}}{m_{\text{probe}}}}, \quad m_{\text{probe}} \gg m_{\text{buffer}} \quad (4)$$

$$v_{\text{th}} = \sqrt{\frac{8kT}{\pi m_{\text{probe}}}} \quad (5)$$

$$t_{\text{colln}} = \frac{\lambda}{v_{\text{th}}} \quad (6)$$

where n is the buffer gas (He) number density, d_{eff} is the sum of the radii of the two colliding species, m_{buffer} is the mass of the buffer gas, m_{probe} is the mass of the probing molecule of interest (Si_2H_6), k is Boltzmann's constant, and T is the gas temperature (estimated to be ~ 750 K). The mean free path under these conditions (2050 mTorr) is calculated to be $16 \mu\text{m}$, while the mean thermal speed is 5×10^4 cm/s, resulting in a mean collision time of approximately 30 ns. This suggests that an excited Si_2H_6 molecule will have at least 3 collisions with He within its calculated metastable lifetime⁵ to carry away this excess energy and stabilize the molecule. Thus, the route of Si_2H_6 formation through reaction of SiH_2 and SiH_4 seems plausible.

The formation of Si_2 and Si_2H can occur first through the insertion of Si into SiH_2 :³⁴



which is believed to proceed at gas-kinetic rates, without a barrier. This is followed by



which has a pressure-dependent rate coefficient and a modest barrier of 20 kcal/mole.³⁴ As all three disilicon formation reactions can occur through the reaction of SiH_2 , it is perhaps not surprising that they are comparable in abundance.

3.4 Conclusions

Residence time distribution measurements suggest the hot-wire system behaves as a well-stirred reactor. For conditions representative of film growth, the average residence time (for Ar and, approximately, SiH₄) was determined to be 11 seconds. Equilibrium calculations show that Si agglomerates (Si₂H₆, Si₃H₈) will form under these conditions. Thus, an adequate flow rate to limit the residence time is necessary to prevent their formation.

Electron impact ionization of SiH_x was observed in the reactor, but the yield of ions was approximately 3 orders of magnitude less than the radical signal, suggesting ions play little or no role in film growth; this is in stark contrast to the typical conditions for plasma enhanced CVD. Threshold ionization mass spectrometry measurements revealed primarily SiH₂ production, attributed to heterogeneous pyrolysis on the hot walls of the reactor. At high pressures, Si₂, Si₂H, and Si₂H₆ were detected, but they are less than 1% in abundance relative to monosilicon species. As a result, Si₂H_x do not contribute substantially to film growth or participate in further reactions, but provide an indicator for the onset of gas-phase chemistry (~ 2 Torr for 1% SiH₄ in He).

References

1. J. Doyle, D. Doughty, and A. Gallagher, *J. Appl. Phys.* **68**, 4375 (1990).
2. A. Roth, F. Comes, and W. Beyer, *Thin Solid Films* **293**, 83-86 (1997).
3. J. Doyle, R. Robertson, G. Lin, M. He, and A. Gallagher, *J. Appl. Phys.* **64**, 3215-3223 (1988).
4. J. Jasinski, B. Meyerson, and B. Scott, *Ann. Rev. Phys. Chem.* **38**, 109 (1987).
5. T. Dietrich, S. Chiussi, M. Marek, A. Roth, and F. Comes, *J. Phys. Chem.* **95**, 9302 (1991).
6. P. Skell and P. Owen, *J. Am. Chem. Soc.* **94**, 5434 (1972).
7. P. Gaspar, B. Boo, and D. Svoboda, *J. Phys. Chem.* **91**, 5011 (1987).
8. P. Ho, W. Breiland, and R. Buss, *J. Chem. Phys.* **91**, 2627 (1989).
9. M. Hertl and J. Jolly, *J. Appl. Phys. D* **33**, 381 (2000).
10. J. Perrin and T. Broekhuizen, *Appl. Phys. Lett.* **50**, 433 (1987).
11. D. Doughty, J. Doyle, G. Lin, and A. Gallagher, *J. Appl. Phys.* **67**, 6220 (1990).
12. E. Hamers, A. Morral, C. Niikura, R. Brenot, and P. Cabarrocas, *J. Appl. Phys.* **88**, 3674-3688 (2000).
13. J. Thiesen, E. Iwaniczko, K. Jones, A. Mahan, and R. Crandall, *Appl. Phys. Lett.* **75**, 992-994 (1999).
14. E. Molenbroek, A. Mahan, and A. Gallagher, *J. Appl. Phys.* **82**, 1909-1917 (1997).

15. E. Molenbroek, A. Mahan, E. Johnson, and A. Gallagher, *J. Appl. Phys.* **79**, 7278-7292 (1996).
16. C. Hill, *Chemical Engineering Kinetics and Reactor Design* (John Wiley and Sons, New York), 1977, Chapter 11.
17. D. Goodwin, *Thermo Chemical Calculator*, v.1.01b (Pasadena, California) 2002.
18. P. Ho, M. Coltrin, and W. Breiland, *J. Phys. Chem.* **98**, 10138 (1994).
19. R. Robertson and A. Gallagher, *J. Appl. Phys.* **59**, 3402-3411 (1986).
20. Y. Nozaki, K. Kongo, T. Miyazaki, M. Kitazoe, K. Horii, H. Umemoto, A. Masuda, and H. Matsumura, *J. Appl. Phys.* **88**, 5437-5443 (2000).
21. W. Hsu and D. Tung, *Rev. Sci. Instr.* **63**, 4138-4148 (1992).
22. Q. Wang, B. Nelson, E. Iwaniczko, E. Mahan, R. Crandall, and J. Benner, in *The Influence of Charge Effect on the Growth of Hydrogenated Amorphous Silicon by the Hot-Wire Chemical Vapor Deposition Technique*, 2nd World Conference and Exhibition on Photovoltaic Solar Energy Conversion, Vienna, Austria, 1998.
23. J. Berkowitz, J. Greene, H. Cho, and B. Ruscic, *J. Chem. Phys.* **86**, 1235 (1987).
24. H. Chatham, D. Hils, R. Robertson, and A. Gallagher, *J. Chem. Phys.* **81**, 1770 (1984).
25. R. Robertson, D. Hils, H. Chatham, and A. Gallagher, *Appl. Phys. Lett.* **43**, 544-546 (1983).

26. P. Kae-Nune, J. Perrin, J. Guillon, and J. Jolly, *Jpn. J. Appl. Phys.* **33**, 4303 (1994).
27. D. Lide, in *CRC Handbook of Chemistry and Physics*, p. 10-211, 1992 edition.
28. J. Holt, M. Swiatek, D. Goodwin, and H. Atwater, *J. Appl. Phys.*, in press (2002).
29. J. McGowan and E. Clarke, *Phys. Rev.* **167**, 43 (1968).
30. R. Robertson, D. Hils, and A. Gallagher, *Chem. Phys. Lett.* **103**, 397-404 (1984).
31. H. Chatham, D. Hils, R. Robertson, and A. Gallagher, *J. Chem. Phys.* **81**, 1770-1777 (1984).
32. C. Kittel and H. Kroemer, *Thermal Physics*, second edition (W. H. Freeman and Co., New York) 1980.
33. R. Bird, W. Stewart, and E. Lightfoot, *Transport Phenomena* (John Wiley and Sons, New York) 1960.
34. D. Woiki, L. Catoire, and P. Roth, *AIChE Journal* **43**, 2670-2678 (1997).

Chapter 4 Computations and Simulations of Gas-Phase Processes

Abstract

The energetics and kinetics of the reaction of Si and SiH₄ are investigated by means of density functional theory and RRKM calculations. A two-dimensional Monte Carlo simulation was used to model gas processes and investigate such issues as hydrogen dilution and the use of wire arrays. To model higher pressure conditions, a continuum simulation was used. The effects of the choice of buffer gas and limitations to the growth rate were studied using this simulation.

4.1 Reaction of Si + SiH₄

4.1.1 Introduction

Given the perception that the reaction of Si and SiH₄ plays a crucial role in determining the electronic properties of a-Si films,¹ a more thorough

investigation of this reaction and its products was warranted. The conclusion that the principal product of this reaction is H_2SiSiH_2 (Ref 2) was based partly on energetic grounds, not taking into consideration the kinetics of the first step of the reaction, $\text{Si} + \text{SiH}_4 = \text{H}_3\text{SiSiH}^*$. Based on kinetic data in Ho *et al.*,³ this reaction has been estimated⁴ to have a rate coefficient of $10^7 \text{ cm}^3/\text{mole-s}$ at a representative pressure of 75 mTorr, well below the gas-kinetic limit of order $10^{14} \text{ cm}^3/\text{mole-s}$. The pressures encountered during film growth (10-1000 mTorr) are well below that needed for collisional stabilization of H_3SiSiH^* , implying that this species will dissociate back to reactants or perhaps into other species.

The other feasible dissociation route for the energetic intermediate H_3SiSiH^* is into $\text{Si}_2\text{H}_2 + \text{H}_2$. The overall reaction $\text{Si} + \text{SiH}_4 = \text{Si}_2\text{H}_2 + \text{H}_2$ is said to be exothermic by 82 kJ/mole, and was predicted to proceed at gas-kinetic rates ($4 \times 10^{14} \text{ cm}^3/\text{mole-s}$) without a barrier.¹ However, the kinetic data come from shock tube measurements carried out at near atmospheric pressure conditions. The species Si_2H_2 is closed-shell, with the lowest energy isomer having the hydrogen atoms in a bond centered position $[\text{Si}(\text{H}_2)\text{Si}]$,² rendering it less reactive than Si. In this regard, it could be a low reactivity film growth precursor like SiH_3 , but isomerization reactions to more highly reactive species (e.g., H_2SiSi) could make it a precursor to silicon agglomerates.³

4.1.2 Computational Chemistry Studies

First principles (i.e., *ab initio*) calculations were performed by Muller *et al.*⁴ using density functional theory (DFT) to investigate the possible reactions of Si with SiH₄. Specifically, the goal was to identify whether an energetically favorable pathway not requiring collisional stabilization exists, meaning the reaction could be very rapid, even at the low pressures characteristic of hot-wire CVD. The computational details (e.g., functional, basis set used) can be found in reference 4. A fixed temperature of 1200 K was used for the energy calculations, given that it is intermediate between the wire temperature (2300 K) and substrate temperature (600 K).

There are two possible bimolecular reactions between Si and SiH₄: 1) abstraction of H from SiH₄ to form SiH and SiH₃, and 2) insertion of Si into a Si-H bond of SiH₄ to form H₃SiSiH. The energetics for the abstraction of an H atom by Si from SiH₄ were found to be significantly uphill (by 21 kcal/mole in energy and 10 kcal/mole in free energy), thus making the insertion of Si the more likely process under HWCVD conditions. Fig. 1 shows the energy profile for the insertion of a Si atom into the Si-H bond of SiH₄. The ground spin

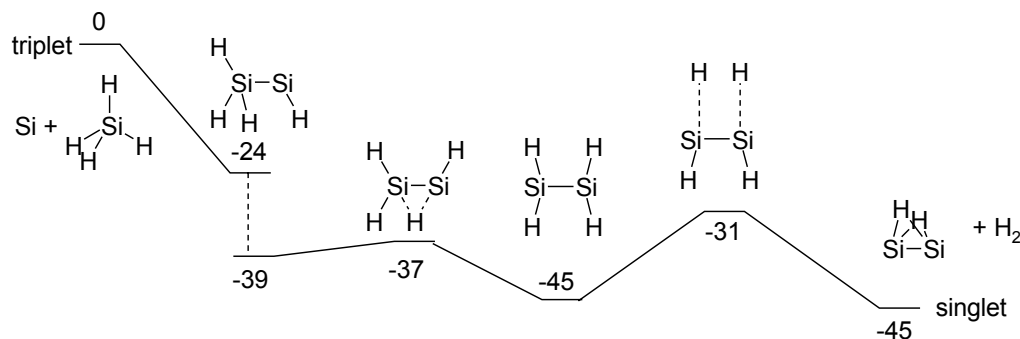


Figure 1. Energy profile (kcal/mole) for the insertion, rearrangement, and H₂ elimination process that leads to Si₂H₂.

state of the Si atom has triplet (t) multiplicity, while SiH₄ is a singlet (s) in its ground state, implying that the spin-conserved product will have triplet multiplicity. This process is predicted to occur without a significant barrier and is calculated to be downhill in energy by 24.3 kcal/mole, and is only slightly uphill in free energy by 1.0 kcal/mole (~ 0.5 kT) at 1200 K.

A singlet state for H₃SiSiH exists which is even more stable than the triplet. Calculations show that the singlet state is 39.0 kcal/mole in energy and 13.4 kcal/mole in free energy below the reactants at 1200 K. The rate at which the molecule may cross from the triplet to single state was not investigated in this study, but it is known that collisions can mix spin states,⁵ so the process is likely to be pressure dependent.

However, in either of the two states, the H₃SiSiH species carries a great deal of internal energy due to the exothermicity of the insertion process. Unless sufficient collisions are available to stabilize this species, it will likely dissociate in a few vibrational periods (on the order of picoseconds) back to reactants or to

other products. To confirm the expectation that this species dissociates back to reactants, calculations were performed to determine the steady-state rate coefficient as a function of temperature and pressure for the decomposition of $\text{H}_3\text{SiSiH (t)}$. From this rate and thermodynamic data (from the DFT calculations), the rate of the reverse reaction of Si and SiH_4 to form (collisionally stabilized) $\text{H}_3\text{SiSiH (t)}$ could be calculated. The calculations were carried out with the program ChemRate⁶ that seeks a solution to the so-called “master equation,” which captures the relevant energy-transfer effects pertaining to unimolecular decomposition reactions of this type. Further details regarding ChemRate and the theory on which it is based may be found in the article by Tsang *et al.*⁷

The characteristic time for the formation of collisionally stabilized H_3SiSiH (triplet) was calculated to be on the order of 10 seconds (rate $\sim 0.1 \text{ s}^{-1}$, or a rate coefficient of $1 \times 10^7 \text{ cc/mole-s}$) at a typical pressure of 100 mTorr (and a temperature of 1200 K), *significantly* longer than the 10 μs transit time of this species from the wire to the substrate in the reactor. Therefore, Si_2H_4 (either as H_3SiSiH or H_2SiSiH_2) is not expected to be a significant product of the reaction of Si and SiH_4 under typical HWCVD conditions.

The issue remaining is to determine if other (low pressure) dissociation pathways for excited H_3SiSiH exist. Calculations by DFT show that a significant barrier (30 kcal/mole) exists for $\text{H}_3\text{SiSiH (t)}$ to rearrange to $\text{H}_2\text{SiSiH}_2 \text{ (t)}$. However, $\text{H}_3\text{SiSiH (s)}$ shows only a small energy (2 kcal/mole) and free energy

(1 kcal/mole) barrier to rearrange to H_2SiSiH_2 (s), both of which are of order kT . At this step, the only energetically accessible dissociation pathway is H_2 elimination. Although uphill in energy from ground state H_2SiSiH_2 (see Fig. 1), it remains lower in energy than the initial reactants, thus allowing the reaction to proceed. The overall energetics of this entire process, Si insertion in SiH_4 , H_3SiSiH triplet to singlet conversion, rearrangement to H_2SiSiH_2 , and H_2 elimination to produce Si_2H_2 and H_2 are summarized in Fig. 1. No intermediate states with energies higher than the reactants were found, and no substantial free energy barriers ($> kT$) existed. The only unknown is the rate at which the triplet to singlet conversion for H_3SiSiH can take place.

4.1.3 Summary

The two possible outcomes of the reaction of Si with SiH_4 are 1) dissociation of the energetic intermediate Si_2H_4 back to $\text{Si} + \text{SiH}_4$ (on a time scale of picoseconds), or 2) dissociation to $\text{Si}_2\text{H}_2 + \text{H}_2$. The latter pathway will be significant if the triplet to singlet transition is sufficiently fast. If it is not, then it is unlikely that Si is sufficiently reactive with SiH_4 for this reaction to shield a growing film from Si atoms, as has been proposed by Molenbroek *et al.*^{8,9} In this event, other explanations would be required to account for the improvement

observed in a-Si:H quality under conditions in which Si atoms undergo a few collisions between the wire and substrate.

It is notable that the previously described radical measurements (section 3.3.4) provide evidence for the production of Si_2H_6 (under highly diluted silane conditions), and not Si_2H_2 or Si_2H_4 . The pressures at which this species was observed (~ 2 Torr) are into the regime that Molenbroek *et al.*⁸ described as leading to deteriorating film quality. The absence of other Si_2H_x species could suggest that the low pressure pathway proposed for Si_2H_2 generation is slow (specifically, the $\text{H}_3\text{SiSiH (t)} \rightarrow \text{H}_3\text{SiSiH (s)}$ transition) compared with the rate of $\text{H}_3\text{SiSiH (t)}$ decomposition. It should be noted that a high surface reaction probability for Si_2H_2 and Si_2H_4 could explain their absence, but the closed-shell structure for Si_2H_2 (in the ground state)² in particular, coupled with the low energies involved in the hot-wire process would suggest that it is of low reactivity. Thus, these results may suggest that other explanations besides the reaction of Si and SiH_4 must be invoked to explain the enhancement in a-Si:H quality at intermediate pressures (~ 0.3 Torr). It is conceivable that it is in fact the increased production of SiH_3 by reaction of H and SiH_4 at higher pressures that accounts for the improvement in a-Si:H quality. More direct, *in situ*, measurements of radical species during film growth could provide the definitive answer.

4.2 Gas-Phase Simulations

The simulation of the gas-phase environment of a CVD reactor can be a useful tool in the optimization of film growth and properties. Many “virtual experiments” can be carried out where a number of parameters (e.g., hydrogen dilution, wire temperature) can be varied and their effects on, for example, the predominant radical species can be determined. Provided that accurate gas-phase and surface reactions are implemented, these types of simulations may be the only way to determine the densities of the number of radicals typically of interest. Techniques like mass spectrometry can only determine the fluxes of radicals to the surface, and optical techniques (although able to probe densities) are limited in the scope of radicals they can measure within a fixed wavelength range.

4.2.1 Direct Simulation Monte Carlo (DSMC)

Modeling

For conventional hot-wire CVD deposition conditions, gas-phase modeling is difficult due to the transitional nature of the flow regime. Near the wire, the local mean free path is typically larger than the wire diameter, which prevents the use of continuum modeling. Far from the wire, however, species typically

undergo a number of gas collisions prior to hitting the substrate. If enough of these collisions occur (~ 10), then the far field region can be modeled by continuum equations. The most effective strategy for transitional flow regimes like this, however, is believed to be direct numerical particle-based simulations.³

Direct Simulation Monte Carlo (DSMC)¹⁰ is a technique that enables the modeling of gas systems like that described above. In DSMC, gas molecules are lumped together into simulation “particles” that are allowed to move, collide, and react with one another and with surfaces. Rules are implemented to result in collision and reaction rates that are statistically correct. The flow region is divided into cells and particle properties (e.g., momentum, energy) are sampled and averaged once steady-state has been reached to determine the mean flow properties for the system.³ The calculations are presumed unsteady with time as a principal variable in the simulation; if a flow becomes steady, it will be found as the large time state of an initially unsteady flow. Unlike continuum-based simulations, there is no need for initial approximations to the flow field or iterative procedures to arrive at a solution.

The details to follow come primarily from Bird’s text, *Molecular Gas Dynamics and the Direct Simulation of Gas Flows* (Clarendon Press, Oxford).¹⁰ The primary approximations involved in a DSMC computation are 1) the number of real molecules represented by each simulation particle, 2) the time step over which molecular motion and collisions are uncoupled, and 3) the finite cell and sub-cell

sizes. Regarding the first point, DSMC simulations generally involve the use of simulation particles that represent of order 10^{12} , or more, molecules. As a result, a simulation generally involves a level of statistical scatter that is much greater than the scatter present in the real gas. The standard deviation of this scatter is generally of order the inverse square root of the sample size. Thus, for a sufficiently large sample that is time averaged (for a steady flow) or ensemble averaged (for an unsteady flow), an acceptable level of scatter is obtained. The second point refers to the criterion that the time step be much less than the mean collision time. The use of a single, short time step for the entire flow region that satisfies this criterion is often computationally inefficient. The more recent implementations of DSMC¹¹ have a time variable associated with each molecule and cell that still remain consistent with the overall time variable for the simulation. The last point pertaining to finite cell sizes plays a critical role in determining collision partners, as these are calculated on a cell-by-cell basis. If cells are chosen to be too large, then collision partners can be chosen (randomly) that lie on opposite sides of the cell. This can have the effect, for example, of reversing gradients that would otherwise be present in the real gas. Again, the more recent DSMC code¹¹ uses sub-cells with dimensions such that collisions will be, effectively, nearest neighbor.

In the DSMC programs used, gas collisions are treated by means of the variable hard sphere (VHS) model. In this model, molecules are treated as hard

spheres with diameters (d) that are a function of the relative velocities (c_r) of the colliding species:

$$d = d_{\text{ref}} (c_{r,\text{ref}} / c_r)^{\nu} \quad (1)$$

with $_{\text{ref}}$ denoting reference values, and ν being the viscosity-temperature (μ - T) index:

$$\mu \propto T^{\nu+1/2} \quad (2)$$

A simple hard sphere model predicts a μ - T exponent of 0.5, while real gases are characteristically around 0.75. The index (ν) can be set separately for each species, resulting in a more realistic treatment of collision cross sections. This phenomenological approach to treating gas collisions has been found to result in agreement between experiment and simulation.

To treat inelastic collisions among the simulation molecules, it is first assumed that some fraction of the total number of collisions are completely inelastic. For those collisions that are treated as inelastic, the total energy contained in the rotational modes of the molecule is determined by sampling from the equilibrium distribution of modes particular to that total energy. Further details regarding this model (referred to as the classical Larsen-Borgnakke model) may be found in Bird.¹⁰ For cases in which vibrational excitation is important, a quantum model is used for the partitioning of energy. Because of the relative wide spacing of these levels, each can be treated as a distinct species, with cross sections assigned to the transitions that occur between

them during intermolecular collisions. However, for the simulations used in this thesis, vibrational excitation was generally ignored, as temperatures were low enough for these levels to be relatively unpopulated.

To treat chemical reactions, a model is used that calculates reactive cross sections to be consistent with specified rate constants. For a specified activation energy (E_a), a bimolecular reaction is assumed to occur between two species if the cumulative translational energy, along with internal energy in the molecules, exceeds E_a . In general, the reactive cross section may not be a constant (due to the internal modes of the molecules) and thus, the reaction model used takes this into account.

Gas-surface collisions can be treated in a number of ways, ranging from complete specular reflection to classical diffuse reflection with complete thermal accommodation to the surface. The latter case is the preferred way to model surfaces not exposed to high vacuum for long periods. For modeling surfaces of interest to CVD processes, however, only partial thermal accommodation may be appropriate, and this can be treated by specifying what fraction of collisions are specular.

The two-dimensional DSMC model used in this thesis takes both molecular properties and reaction data as inputs. Among the molecular properties specified are, diameter, mass, viscosity-temperature index, and rotational and vibrational degrees of freedom. For reaction data, the program takes the

activation energy, pre-exponential factor, temperature exponent (i.e., the “b” in $AT^b \exp(-E_a/RT)$), and enthalpy of reaction.

Model Details

Critical to a model of the hot-wire CVD process is the inclusion of relevant wire, surface, and gas-phase chemistry. For the wire, the primary reactions were assumed to be the decomposition of SiH_4 and H_2 into atomic Si and H.¹² Silane is assumed to decompose with a probability of 0.7,⁹ while H_2 is assumed to decompose with a probability of 0.14 at 2000°C, a value derived from the H/ H_2 equilibrium ratio. At the surface, reactions are treated by use of sticking probabilities taken from Perrin *et al.*¹³ The substrate is assumed to remain nearly fully hydrogenated during the deposition process¹³ (valid for low enough substrate temperatures, $\leq 300^\circ\text{C}$). Incident H is assumed to recombine to H_2 , while incident SiH_3 may abstract a surface hydrogen and leave as SiH_4 (probability 0.1), or be incorporated into the film with the evolution of 1.5 H_2 molecules (probability 0.18). Highly reactive species (e.g., Si) are assumed to be incorporated into the film with a probability of 0.7, unless otherwise indicated. An overall H balance is insured by making adjustments to the H_2 flux back into the gas for reactions involving surface hydrogen exchanges. Appendix B contains a summary of these wire and surface reactions.

Simulations were initially carried out with a one-dimensional model, developed by Goodwin,³ using a moderate-sized gas-phase reaction mechanism. The mechanism consisted of 19 reversible reactions among 13 total species. The silane pyrolysis mechanism of Ho *et al.*⁵ was used, with several reactions added involving atomic hydrogen, with rates from Woiki *et al.*¹ These initial results suggested that only direct reactions of Si and H from the wire with ambient silane were significant under most HWCVD conditions. The two gas-phase reactions identified as being the most important were



and



and these two reactions were chosen for use with the two-dimensional code developed by Bird.¹¹

The first reaction produces gas-phase silyl radicals, likely an important precursor for high-quality a-Si:H deposition due to its lower surface reaction probability,¹⁴ and possibly important for epitaxial silicon growth for this same reason.¹⁵ The rate coefficient was taken to be

$$k_1 \text{ (cm}^3\text{/mole-s)} = 7.8 \times 10^{14} \exp(-E/kT) \quad (5)$$

with $E = 4491 \text{ cal/mole}$.¹ The second reaction, which was investigated in section in 4.1, is believed to have a rate coefficient between $2.6\text{--}4.0 \times 10^{14} \text{ cm}^3\text{/mole-s}$, with a minimal barrier.^{1,16} These values were determined at relatively high pressures

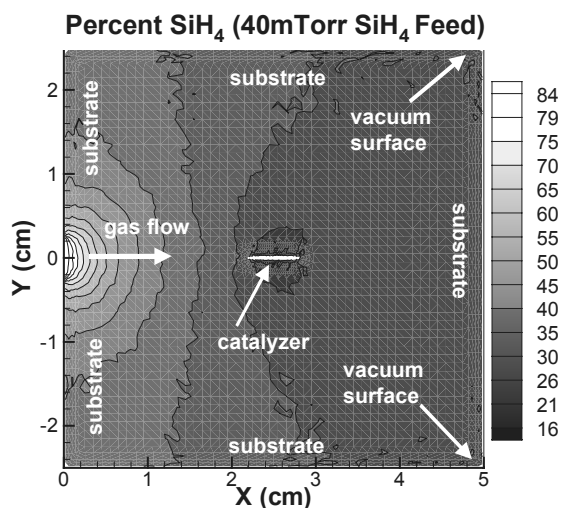


Figure 2. Simulation domain for two-dimensional DSMC model of the hot-wire reactor.

(>10 Torr), however, and indirectly from the decay of the Si concentration measured by laser induced fluorescence or absorption measurements. It was initially unclear whether these rate coefficients were appropriate for the significantly lower pressures involved in HWCVD. Initial simulations used the rate coefficient of Takahara *et al.*¹⁶ for reaction (2). Later simulations will make use of the results obtained in section 4.1, along with radical species measurements (section 3.3.4) that suggest reaction (2) does not occur to a significant extent under typical hot-wire conditions. A listing of all 19 gas-phase reactions in the original mechanism can be found in Appendix B.

Figure 2 shows a sample contour plot, illustrating the simulation domain in a two-dimensional DSMC model of the hot-wire reactor. This model makes use of the program DS2V (v2.0), developed by Bird.¹¹ The specific case modeled here is for a feed gas consisting of pure SiH₄ at a total pressure of 40 mTorr and a wire

temperature of 2000°C, with the contours indicating the percentage of SiH₄. The simulation domain consists of a long square channel, 5 cm on a side, with the catalyzer (wire or plate) in the center. Gas enters from an opening at the left, at flow rates of approximately 90 sccm, and is exhausted to vacuum through two small openings (of order 1 mm length, to match experimental pumping speeds) at the upper and lower right corners. Film growth occurs on all four surfaces (by use of reactive sticking probabilities provided earlier), maintained at a temperature of 300°C.

Initial Results

An initial simulation was run under experimentally relevant conditions, with a total silane pressure of 10 mTorr, a flow rate of 90 sccm, and a wire temperature of 2000°C (wire diameter 0.25 mm). Figure 3 shows the species profiles taken along the gas-inlet axis ($Y=0$), from the wire ($X=2.5$ cm) to the substrate ($X=5.0$ cm). Atomic silicon showed concentration near the wire where it is generated, and was depleted rapidly away from the wire, due both to reaction on the substrate and gas-phase reaction with SiH₄. The distribution of SiH₃ was broader, since it is produced in the gas by reaction of H from the wire with SiH₄. It is notable that the simulation predicts a buildup of Si₂H₂. This is a consequence of the assumption that it is produced by rapid reaction of Si and SiH₄, but there are no equally rapid reactions included to remove it, either in the

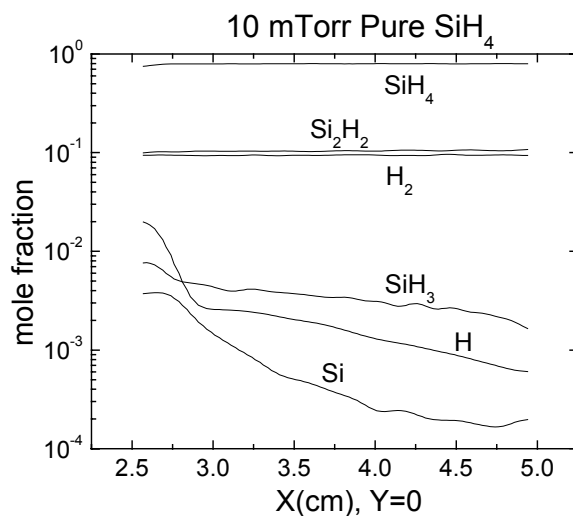


Figure 3. 1-D species profiles along the gas-inlet axis ($Y=0$) for conditions of 10 mTorr pure SiH_4 , $T_{\text{wire}} = 2000^\circ\text{C}$.

gas-phase or on the surface. These concentrations of Si_2H_2 are far in excess of the experimentally observed disilicon abundance, and would result in growth rates (even for a small reactive sticking probability of 0.03) several orders of magnitude beyond experimentally reasonable levels (i.e., ~ 1 nm/s). As a result, subsequent simulations of typical hot-wire conditions (pressures < 1 Torr) use the rate coefficient of 1×10^7 cc/mole-s, determined in section 4.1.2 for the reaction of Si and SiH_4 .

Effect of H₂ Dilution

The amorphous to microcrystalline or polycrystalline transition that occurs upon H₂-dilution (for H₂ dilutions $> 80\%$) has been well documented, with one of

Table 1. Conditions leading to amorphous or polycrystalline silicon growth from Schropp *et al.*,²² and corresponding radical flux ratios to the surface from DSMC simulations. Also listed are experimental conditions from a recent study²³ by the present author.

film microstructure	%SiH ₄ (in feed gas)	%H ₂ (in feed gas)	P (Pa)	SiH ₃ /Si flux	H/SiH _x flux
a-Si:H ^a	100	0	5	2.3	0.4
poly-Si:H ^a	10	90	11	3.8	1.4
poly-Si:H ^b	1	0	22	0.3	2.0

^afrom Schropp, ^bpresent author; buffer gas He

the first systematic studies carried out by Conde *et al.*¹⁷ This transition has been largely attributed to preferred etching of silicon from disordered sites on the growing film surface by H.¹⁸ Other proposals have included enhancement in growth precursor mobility on the surface and bulk changes in the material caused by diffusing H.^{19,20} Hamers *et al.*¹⁴ have further shown a decrease in the average surface reaction probability (β) of the radicals responsible for growth in going from amorphous to polymorphous[†] and microcrystalline silicon. Unclear, however, is whether this reduction in β is due to a change in the surface reactivity (i.e., the hydrogen coverage), the precursor identity (e.g., Si versus SiH₃), or both.¹⁴

Simulations were performed in an attempt to address this question of surface reactivity versus precursor identity. The conditions were chosen to approximate

those of Schropp *et al.*²² for amorphous and polycrystalline silicon growth, as shown in Table 1. As discussed in section 4.2.1, the model assumes a fully hydrogenated surface (valid for $T_{\text{substr}} \leq 300^\circ\text{C}$), with incident H recombining to H_2 and no H etching reactions included. A comparison of the relative radical fluxes (SiH_3/Si and H/SiH_x) can allow for inferences about whether the changes in surface reaction probability (and microstructure) are related to the SiH_x precursor or H.

Figure 4 shows the species profiles under each of these conditions (the same wire diameter of 0.25 mm was used). For these simulations, the rate coefficient determined in section 4.1.2 for the reaction of Si and SiH_4 was used. The approximate value of 1×10^7 cc/mole-s for these pressures, which is several orders of magnitude below the gas-kinetic limit, suggests that Si does not react appreciably with SiH_4 under these conditions. The simulated profiles bear this out, as no Si_2H_2 is generated under either condition. The predominant gas species in each case is seen to be SiH_3 , with the relative concentration of SiH_3 and H increasing upon H_2 -dilution. The abundance of SiH_3 (relative to Si) is consistent with measured surface reaction probabilities by Hamers *et al.*¹⁴ for a-Si:H deposition by hot-wire CVD.

[†] Polymorphous silicon results when deposition occurs near the point of powder formation, where silicon

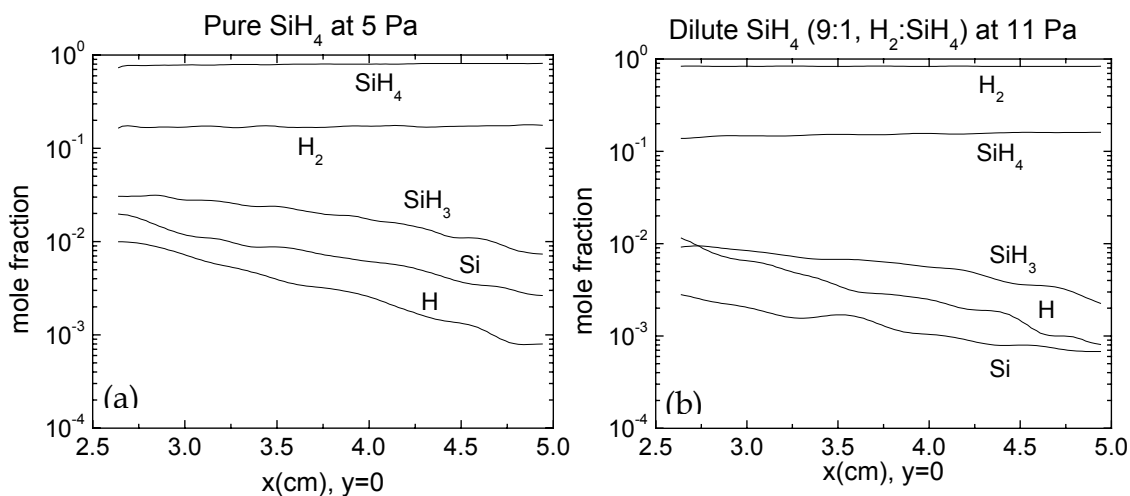


Figure 4. Species profiles obtained along the gas-inlet axis ($y=0$) for feed gas conditions of (a) 35 mTorr SiH_4 , and (b) 80 mTorr dilute SiH_4 (9:1, H_2 : SiH_4).

The reactive flux (namely, the flux times the reactive sticking probability) of SiH_3/Si and $\text{H}/(\text{Si}+\text{SiH}_3)$ is provided in Table 1. These numbers suggest that the relative contribution of SiH_3 to film growth also increases measurably under H_2 -dilution. An increase in the relative abundance of SiH_3 is consistent with the observed drop in average surface reaction probability going from a-Si:H to $\mu\text{c-Si:H}$.¹⁴ Also significant is that the H/SiH_x flux increases by a factor of 3 upon H_2 -dilution. These results would suggest that both the precursor and H flux are contributing factors to the structural transition.

Table 1 also lists the computed radical flux ratios for conditions used in a film growth experiment²³ by the present author. For this experiment, a dilute mixture (1%) of SiH_4 in He was used with no further H_2 -dilution. In this case, Si

clusters can form; see reference²¹.

was the predominant growth species (by a factor of 3), but the H/SiH_x ratio was even larger (2.0) than in the H₂-dilution case; this may be due to the predominance of He collisions and the consequent lower production rate of SiH₃. Despite the predominance of a radical with a much higher surface reaction probability¹⁴ (1 versus 0.1-0.4 for SiH₃), polycrystalline silicon was obtained. To reconcile this result with the known reduction in β for the a \rightarrow μ c-Si transition requires using the H flux as the explanation. Thus, although H₂ dilution may result in changes in the SiH_x radical distribution in the gas-phase, the consequent larger H flux (which may result in surface and/or bulk modifications to the material) is likely to be the dominant factor governing the microstructure transition.

Use of Wire Arrays

The two-dimensional model is useful in examining such issues as film growth rate and uniformity and the methods that can be used to improve it. The most straightforward method for improving film uniformity (and potentially growth rate) involves increasing the number of filaments used. To examine this effect, simulations were run under feed gas conditions of 84 mTorr SiH₄ (90 sccm) and

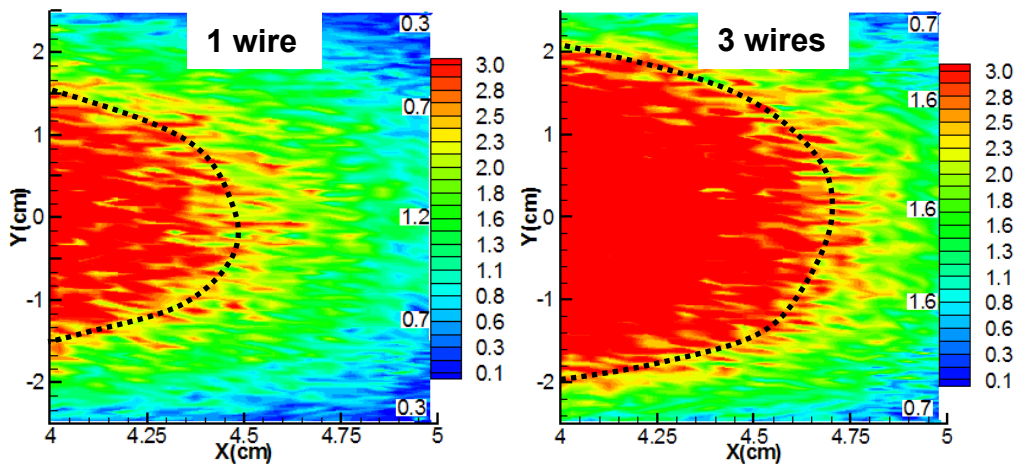


Figure 5 (color). Contour plots of the SiH₃ concentration (atomic %) for feed gas conditions of 84 mTorr SiH₄ with (a) one wire and (b) three wires (0.25 mm diameter). The near-substrate region is shown here (X = 4-5 cm) to enhance contrast.

a wire temperature of 2000°C (diameter 0.25 mm). Figures 5a/b are contour plots of the SiH₃ concentration (atomic %) obtained with one filament (located at X = 2.5 cm, Y = 0 cm) and three filaments (located at X = 2.5 cm, Y = 0, 1.0, -1.0 cm), respectively; the near-substrate region is shown here to enhance contrast. With the use of three filaments, the average concentration of SiH₃ (produced by reaction of H and SiH₄) is higher, due to the greater production of atomic H from the filaments. This overall larger concentration of SiH₃, which is the predominant growth species under these conditions, results in a higher growth rate. The boundaries of the flow region also have a more uniform concentration of SiH₃, which results in a more uniform flux and growth rate across the substrate.

There is a practical limit to the number of filaments that can be used, imposed by (a) excessive substrate heating and (b) SiH_4 depletion. For growth on low temperature substrates like soda-lime glass, the surface temperature must be maintained below 600°C . For a large enough number of filaments, it is conceivable that the surface temperature could approach this value by radiative heating. The second practical issue concerns the decrease in SiH_4 concentration (increased depletion) as the number of filaments increase. For a large enough number of filaments, this depletion could be severe enough to significantly reduce the SiH_3/Si ratio. For situations where it is desirable to maximize this ratio, a balance must be struck between providing enough H by SiH_4 dissociation at the filament, while not excessively depleting the SiH_4 with which it must react.

4.2.2 Continuum Simulations

For gas pressures in excess of 1 Torr, where the Knudsen number (Kn) is less than 0.01 ($\text{Kn} = \text{mean free path}/\text{characteristic length}$), DSMC methods become computationally intensive, requiring more than 20 hours to achieve an acceptably low level of statistical scatter.³ In such cases, a model employing the continuum equations of fluid mechanics is not only appropriate ($\text{Kn} < 0.1$), but is the preferred method of gas simulation. Because of the reduced computational demands, the full 19 gas-phase reaction mechanism (discussed in section 4.2.1)

could be used for these simulations (with the same wire/substrate chemistry), and it is likely that many of these additional reactions are important under these higher pressure conditions. Below is a description of the continuum simulation, developed by Goodwin.²⁴ It should be pointed out that the continuum approximation breaks down in the near-wire region (a few mean free paths from the wire), and the methods to handle this are also described below.

The continuum model solves the species and energy balance equations for a cylindrical geometry (one-dimensional, with axial and angular variations ignored), with the wire assumed to be in the center and the substrate at the perimeter. The equations are solved by a finite difference technique. For a differential element dr , the species equation (for species k) takes the following form for this geometry:

$$\frac{1}{r} \frac{\partial}{\partial r} (r \rho U_k Y_{k,r+dr}) - W_k \dot{\omega}_k + \frac{\rho(Y_{k,r+dr} - Y_{k,r})}{\tau} = 0 \quad (6)$$

where ρ is the mass density (kg/m³), U_k is the diffusion velocity (m/s), Y_k is the mass fraction, W_k is the molecular weight of species k (kg/mole), $\dot{\omega}_k$ is the destruction rate of species k by chemical reaction (mole/m³-sec), and τ is the fixed gas residence time.

Near the wire (one mean free path - λ - away), a jump boundary condition is used to handle the effects of gas rarefaction. This boundary condition relates the net flux by diffusion of species k to the surface creation/destruction rate at the wire (derived from the user-specified wire reaction probabilities). At the

substrate, a flux boundary condition is used that equates the flux by diffusion of species k to its destruction rate (also derived from user-specified surface reaction probabilities).

The fixed residence time employed in the continuum simulations is determined by the characteristic diffusion time (τ) for the species of interest (e.g., Si):

$$\tau = L^2/D \quad (7)$$

where L is the characteristic length – the distance between the wire and the substrate (of order cm), and D is the molecular diffusivity:

$$D = (1/3)v_{th}\lambda \quad (8)$$

where v_{th} is the mean thermal speed of the gas, and λ is the mean free path. For conditions of 5 Torr total pressure of dilute (1%) SiH_4 in He, a diffusion time of approximately 2 ms is calculated. It should be pointed out that this residence time is significantly less than the experimentally determined residence time (section 3.2), given that a highly reactive species such as Si will typically stick upon traveling the distance from the wire to the substrate.

The energy balance used for the continuum model consists of a solution of the steady-state heat conduction equation, which for cylindrical geometry takes the following form:

$$\frac{\partial}{\partial r} \left(kr \frac{\partial T}{\partial r} \right) = 0 \quad (9)$$

where k is the thermal conductivity (J/m-sec-K), and T is the temperature (K). A temperature jump boundary condition²⁵ is used at the wire to handle rarefaction.

This boundary condition takes the form:

$$T_{r=0} - T_{\text{wire}} = \frac{2-a}{a} \lambda \frac{\partial T_{r=0}}{\partial r} \quad (10)$$

where $T_{r=0}$ is the gas temperature at $r = 0$, T_{wire} is the wire temperature, a is the thermal accommodation coefficient (extent to which reflected molecules assume the temperature of the surface; the wire in this case), and λ is the mean free path. The temperature at the substrate is user specified and acts as the other boundary condition.

The continuum model interfaces with Chemkin²⁶ for the determination of kinetic, thermodynamic, and transport properties. For further details, the interested reader may consult reference of Goodwin.²⁴

Choice of Buffer Gas

Simulations were carried out to determine the effect, if any, of the choice of buffer gas (Ar versus He) on the resulting gas species distributions. Differences were noted only for pressures above 5 Torr. Figure 6 shows the species profiles for conditions of 5 Torr pressure (1% SiH₄) with He (a) and Ar (b) as the buffer gas, for gas residence times of 2 ms in each case. The reaction of Si and SiH₄ to produce Si₂H₂ was included, as the study by Takahara *et al.*¹⁶ indicates this reaction is near gas-kinetic in this pressure regime. The most significant

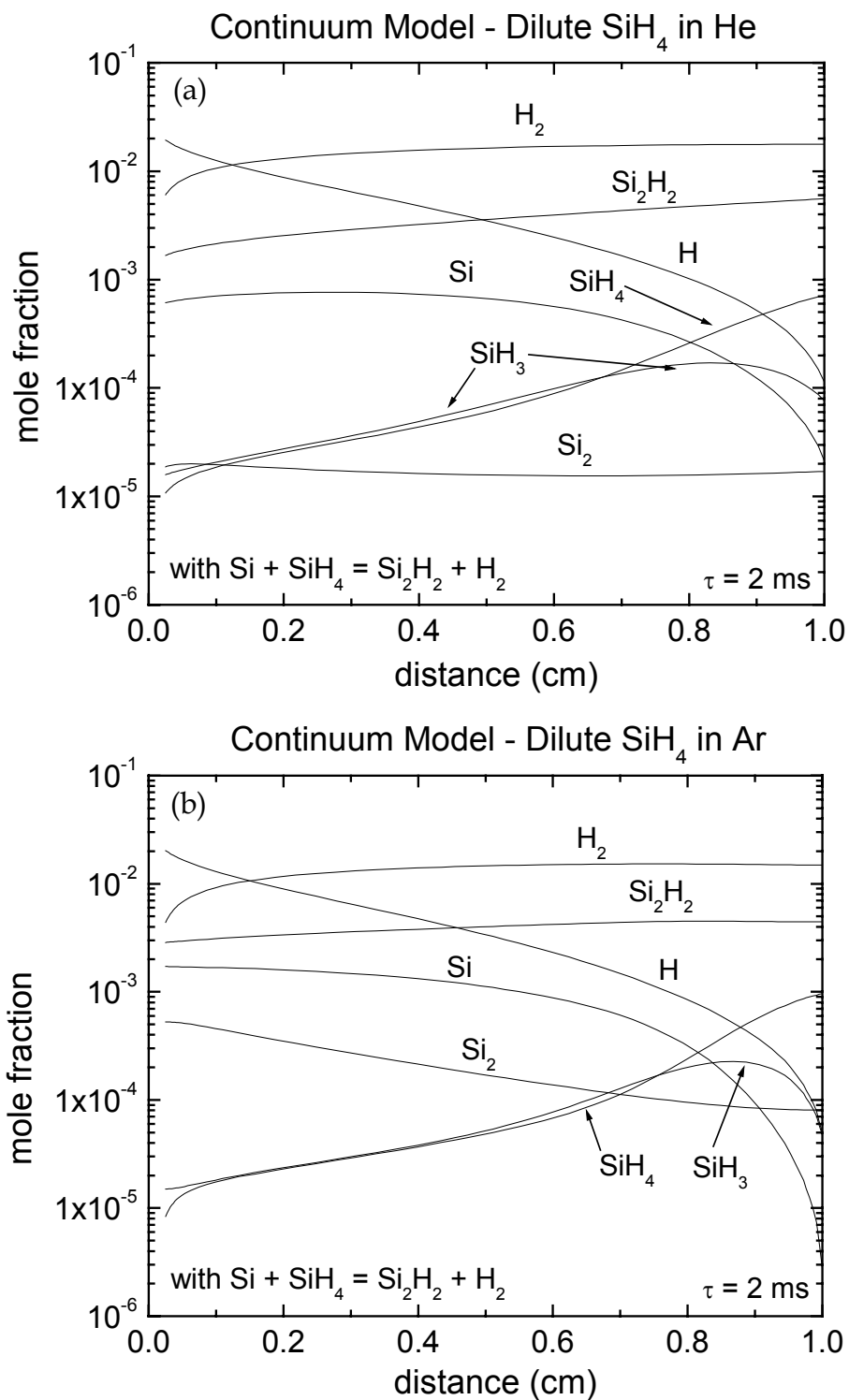


Figure 6. Gas species profiles obtained with the continuum simulation for dilute (1%) SiH_4 at 5 Torr pressure in (a) He and (b) Ar for a residence time of 2 ms in each case.

difference between these profiles lies in the relative abundance of Si₂, which increases by more than an order of magnitude in abundance when Ar is used rather than He. The Si₂ species is produced by a three-body reaction between two Si atoms and a third body collision partner to carry away the excess energy for this highly exothermic reaction:



Si₂ may also be produced by the unimolecular decomposition of Si₂H₂:



Such a substantial increase in Si₂ upon switching to Ar suggests that it acts as a better collision partner for this reaction, primarily because of the larger cross section for Si-Ar versus Si-He collisions.

This increase in Si₂ concentration is significant as this species is an indicator for the onset of gas-phase polymerization and particulate formation, which is believed to be deleterious to film properties. Although potentially even more reactive than Si, with a surface reaction probability greater than 0.7, Si₂ was not included as a growth species for these simulations, given the lack of literature data. Given that no further reactions of Si₂ with monosilicon species were included in the reaction mechanism, this omission would not affect their relative abundances. It is worth noting that the relative abundance of Si₂ (1%) compared with Si agrees well with the high-pressure radical measurements described in section 3.3.4. If the reactivity of Si₂ is comparable to Si, the Ar-dilution case

indicates Si_2 could be a major growth species. These results would then suggest that for high-pressure growth in a diluted SiH_4 ambient, a lighter buffer gas is preferable.

Limits to the Growth Rate

For purposes of maximizing throughput in an industrial application of HWCVD, it is desirable to know the limitations imposed on the film growth rate. The most straightforward method for increasing the growth rate is to increase the total gas pressure. At some pressure, however, gas-phase polymerization will start to become significant, as described in the previous section. The goal of the following simulations is to identify the pressure regime in which the growth rate starts to saturate with respect to pressure, due to polymerization.

Figure 7 shows the film growth rate as a function of pressure (from 0.1-100 Torr) for dilute and pure SiH_4 conditions. As it is the high pressure limit to the growth rate that is of interest here, the formation reaction of Si_2H_2 was included (i.e., $\text{Si} + \text{SiH}_4 = \text{Si}_2\text{H}_2 + \text{H}_2$), using the high pressure gas-kinetic rate constant (10^{14} cc/mole-s). The lowest pressure was bounded by the validity of the continuum approximation. The pressure spans the region from where Si_2H_2 is not believed to form in appreciable amounts ($P < 1$ Torr, section 3.3.4) to that at which the reaction is believed to be gas-kinetic¹⁶ ($P > 10$ Torr). Selected experimental data for dilute⁸ and pure^{9,22} SiH_4 conditions were also included in

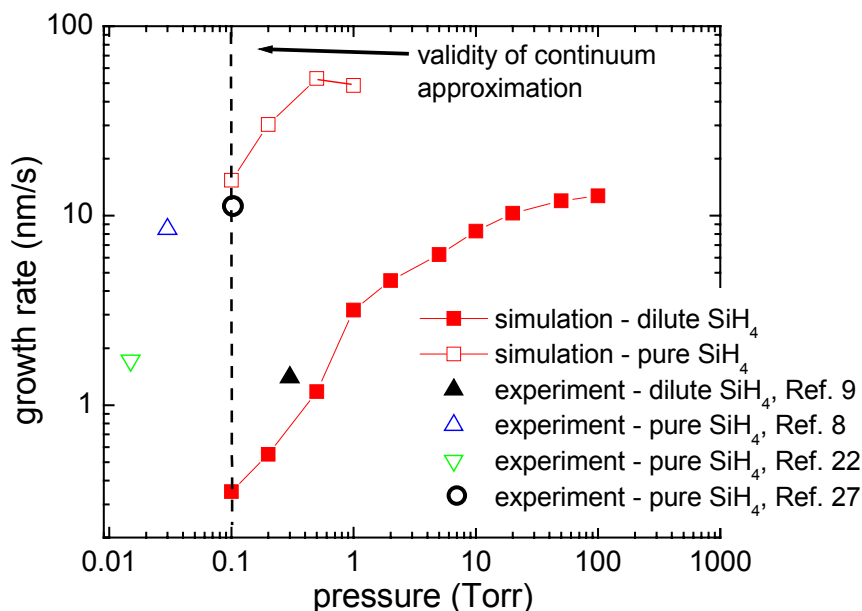


Figure 7. Growth rate as a function of pressure, determined from the continuum model. Conditions of dilute (1%) and pure SiH₄ are simulated. Selected experimental growth rates from the literature are included as a reference; Ref. [9] Molenbroek *et al.* (1997), Ref. [8] Molenbroek *et al.* (1996), Ref. [22] Schropp *et al.* (1997), Ref. [27] B.P. Nelson *et al.* (2002).

Figure 7 as a reference. For these simulations, the reactor residence time (τ) was increased in proportion with the pressure to reflect the increase in the characteristic diffusion time (from the wire to the substrate) with pressure. Also, the disilicon species (Si₂H₂ and Si₂) were not included as film growth species for the reasons cited previously. Thus, a saturation in film growth rate with respect to pressure is an indication that these species are becoming significant in abundance relative to SiH_x.

Such a saturation is apparent for the dilute SiH_4 simulation case illustrated in Figure 7, with an onset of approximately 20 Torr, attributed to a buildup in Si_2 concentration (most of the Si is already bound in Si_2H_2). It is noteworthy that the simulation underpredicts the growth rate at low pressures, as is seen by comparison with the experimental data point. This is attributed to the assumption that Si_2H_2 is not a film growth species.

Under pure SiH_4 conditions, a saturation is observed at 0.5 Torr, with a drop in growth rate above this pressure. This behavior is attributed to the buildup in Si_2H_2 , which eventually exceeds the concentrations of the growth species Si and SiH_3 ; at these lower *total* pressures, the formation of Si_2 , requiring a third-body, is unlikely. The simulation shows agreement in growth rate with an experiment conducted at a SiH_4 pressure of 0.1 Torr. Finally, these simulations suggest that the limits in growth rate (where disilicon formation is to be avoided) are approximately 10 nm/s for dilute SiH_4 conditions, and 50 nm/s for pure SiH_4 conditions.

4.3 Conclusions

The most energetically accessible pathway for the reaction of Si and SiH_4 was proposed, involving the formation of Si_2H_2 and H_2 . This reaction could proceed at the low pressures characteristic of hot-wire CVD, but only if an intermediate

spin state transition is sufficiently fast. Experimental mass spectrometry measurements suggest this transition may be too slow to proceed, as there was no clear evidence for the presence of Si_2H_2 .

DSMC simulations predicted that the predominant growth species produced under conditions leading to amorphous and polycrystalline growth was SiH_3 , with the flux ratios SiH_3/Si and H/SiH_x increasing upon H_2 dilution. Of the two ratios, the H/SiH_x flux appears to be the more likely in accounting for the amorphous-to-microcrystalline transition that occurs upon H_2 dilution. The two-dimensional DSMC simulation revealed an increase in SiH_3 concentration and improvement in flux uniformity by increasing the number of filaments from 1 to 3.

Continuum simulations predict a buildup of Si_2 for total pressures of order 1 Torr, at levels comparable to those observed by mass spectrometry. With the use of a larger buffer gas such as Ar, the concentration of this species increases significantly. Finally, simulations also predict that if disilicon species formation is to be suppressed, the maximum attainable growth rate for dilute (1%) silane conditions is 10 nm/s, while for pure SiH_4 it is 50 nm/s.

References

1. D. Woiki, L. Catoire, and P. Roth, AICHE JOURNAL **43**, 2670-2678 (1997).
2. B. Colegrove and H. Schaefer, J. Phys. Chem. **94**, 5593 (1990).
3. D. Goodwin, Mat. Res. Soc. Symp. Proc., Vol. **557**, p. 79-84 (1999).
4. R. Muller, J. Holt, D. Goodwin, and W. Goddard III, Mat. Res. Soc. Symp. Proc. Vol. **609**, A6.1.1 (2000).
5. P. Ho, M. Coltrin, and W. Breiland, J. Phys. Chem. **98**, 10138 (1994).
6. V. Mokrushin, V. Bedanov, W. Tsang, M. Zachariah, and V. Knyazev, Chem Rate v.1.10, Gaithersburg, Maryland (1999).
7. W. Tsang, V. Bedanov, and M. Zachariah, J. Phys. Chem. **100**, 4011-4018 (1996).
8. E. Molenbroek, A. Mahan, E. Johnson, and A. Gallagher, J. Appl. Phys. **79**, 7278-7292 (1996).
9. E. Molenbroek, A. Mahan, and A. Gallagher, J. Appl. Phys. **82**, 1909-1917 (1997).
10. G. Bird, *Molecular Gas Dynamics and the Direct Simulation of Gas Flows* (Clarendon Press, Oxford) 1994.
11. G. Bird, DS2V v2.0, General 2D/Axi Visual DSMC Program, GAB Consulting, Sydney, Australia (2002).

12. J. Doyle, R. Robertson, G. Lin, M. He, and A. Gallagher, *J. Appl. Phys.* **64**, 3215-3223 (1988).
13. J. Perrin, M. Shiratani, P. Kae-Nune, H. Videlot, J. Jolly, and J. Guillon, *J. Vac. Sci. A* **16**, 278-289 (1998).
14. E. Hamers, A. Morral, C. Niikura, R. Brenot, and P. Cabarrocas, *J. Appl. Phys.* **88**, 3674-3688 (2000).
15. J. Thiesen, E. Iwaniczko, K. Jones, A. Mahan, and R. Crandall, *Appl. Phys. Lett.* **75**, 992-994 (1999).
16. A. Takahara, A. Tezaki, and H. Matsui, *J. Phys. Chem.* **103**, 11315-11320 (1999).
17. J. Conde, P. Brogueira, and V. Chu, *Phil. Mag. B* **76**, 299-308 (1997).
18. M. Heintze, R. Zedlitz, H. Wanka, and M. Schubert, *J. Appl. Phys.* **79**, 2699 (1996).
19. A. Matsuda, *Thin Solid Films* **337**, 1 (1999).
20. N. Layadi, P. Roca i Cabarrocas, B. Drevillon, and I. Solomon, *Phys. Rev. B* **52**, 5136 (1995).
21. P. Cabarrocas, S. Hamma, S. Sharma, J. Costa, and E. Bertran, *J. Non-Cryst. Solids* **227-230**, 871 (1998).
22. R. Schropp, K. Feenstra, E. Molenbroek, H. Meiling, and J. Rath, *Phil. Mag. B* **76**, 309-321 (1997).

23. J. Holt, M. Swiatek, D. Goodwin, R. Muller, W. Goddard III, and H. Atwater, *Thin Solid Films* **395**, 29-35 (2001).
24. D. Goodwin, *Proc. Electrochem. Soc. (San Diego, California)* p. 227, 1998.
25. E. Kennard, *Kinetic Theory of Gases* (McGraw-Hill, New York), Chapter 8, 1938).
26. R. Kee, F. Rupley, and J. Miller, "Chemkin-II: A Fortran Chemical Kinetics Package for the Analysis of Gas-Phase Chemical Kinetics," Technical Report SAND89-8009 (1989).
27. B. Nelson and D. Levi, *Mat. Res. Soc. Symp. Proc.*, Vol. 715, A17.3.1 (2002).

Chapter 5 HWCVD of Silicon Nitride

Abstract

The stoichiometry and hydrogen content of hot-wire-grown silicon nitride was examined as a function of SiH_4/NH_3 flow ratio. The effect of post-deposition hydrogenation treatment on overall film hydrogen content was determined. The hydrogen release properties in Si-rich and N-rich nitride layers were examined under various annealing treatments. Defect hydrogenation was then studied using attenuated total reflectance FTIR spectroscopy on platinum-diffused silicon substrates. Hot-wire nitride layers were deposited onto diffused emitter String Ribbon silicon substrates, producing cells with comparable J_{SC} , V_{OC} , FF, and efficiency to those fabricated using plasma CVD nitride layers.

5.1 Introduction

Silicon nitride (SiN_x) has been widely used in the semiconductor industry as a lithographic mask and gate dielectric. The low deposition temperature possible for SiN_x is particularly advantageous for gate dielectric applications, avoiding the problems of impurity diffusion that can occur at conventional processing

temperatures.¹ For photovoltaic applications, silicon nitride acts as an effective anti-reflection (AR) coating due to its high refractive index (2.0-2.5). These films may also serve as passivation coatings for surface and bulk defects in the underlying silicon, due to the large fraction of hydrogen that may be incorporated (up to 25 atomic %)² and subsequently released during annealing treatments. It is noteworthy that for gate dielectric applications, completely different requirements for the SiN_x layer are necessary. In particular, a low hydrogen content (a few atomic %) is desirable due to the requirements of high resistivity and high breakdown field strength.¹

The conventional means for depositing silicon nitride films uses plasma enhanced chemical vapor deposition (PECVD). As compared with other methods, such as atmospheric pressure CVD (APCVD) or low pressure CVD (LPCVD) that involve substrate temperatures in the range of 700-1000°C, PECVD allows for low temperature (<500°C) growth.³ Such low temperatures have enabled SiN_x growth to occur after the metallization step in conventional solar cell processing.⁴

Another promising technique for low temperature SiN_x growth is hot-wire CVD (HWCVD), also known as catalytic CVD (Cat-CVD).⁵ As compared with PECVD, HWCVD offers the advantages of high deposition rate,⁶ due in part to its higher gas utilization.⁷ In addition, it has been demonstrated that the process is compatible with large area deposition by careful design of gas delivery and

filament geometry.⁸ Recent work on SiN_x growth by HWCVD has focused on gate dielectric applications,¹ with one group fabricating a thin-film transistor made entirely by this technique.⁹ The work to be described aims to use HWCVD of SiN_x for photovoltaic applications, with particular attention paid to the refractive index and hydrogen content of the films.

5.2 Experiment

The system used in the deposition of SiN_x is a high vacuum chamber with a 10⁻⁹ Torr base pressure, as illustrated in Figure 1 from section 2.2. Source gases consisted of SiH₄ (diluted to 1% in He), NH₃, and H₂ (used for post-deposition treatments). The gases are introduced through an inlet and decomposed on a W wire (0.5 mm diameter, 12 cm length, 1800°C temperature). Gas flow rates range from 4-48 sccm, SiH₄/NH₃ ratios vary from 0.01-0.08, and pressures were between 20-100 mTorr. The substrate holder is located approximately 5 cm from the wire, and a shutter is used to protect substrates from the evaporation of impurities from the wire during its initial heating; growth temperatures were approximately 300°C for this study. The substrates used were lightly doped p-type (350 Ω-cm), double-side polished, float-zone Si. Substrates went through a standard preparation treatment consisting of 1) sonication in acetone/methanol for 10 minutes each to degrease the substrates, 2) UV-ozone treatment for 10

minutes to remove residual hydrocarbons, and 3) dip in 5% hydrofluoric acid (in H₂O) to remove the thermally grown oxide and to H-terminate the surface. The substrate heater was replaced by a quadrupole mass spectrometer for experiments aimed at measuring the abundance of radicals desorbed from the W filament at the substrate position.

5.3 Results

5.3.1 NH₃ Decomposition

As a means to probe the kinetics of NH₃ decomposition on the wire, low pressure radical species measurements were made using a quadrupole mass spectrometer with the capability of tunable electron energy for selective radical ionization. This method is detailed in another study by these authors¹⁰ and in section 2.2 of this thesis. An electron energy of 13 eV was chosen for these measurements, as it lies 2-3 eV above the ionization potentials of NH_x (x = 0-3) species, but is 2-3 eV below the appearance potentials of NH_x⁺ (x = 0-2) from NH₃.¹¹ Under these conditions, selective ionization of wire-produced NH_x (x = 0-2) radicals can be achieved. Figure 1 shows a mass spectrum of the NH_x species measured from the wire under conditions of 3 x 10⁻⁶ Torr NH₃, at a wire

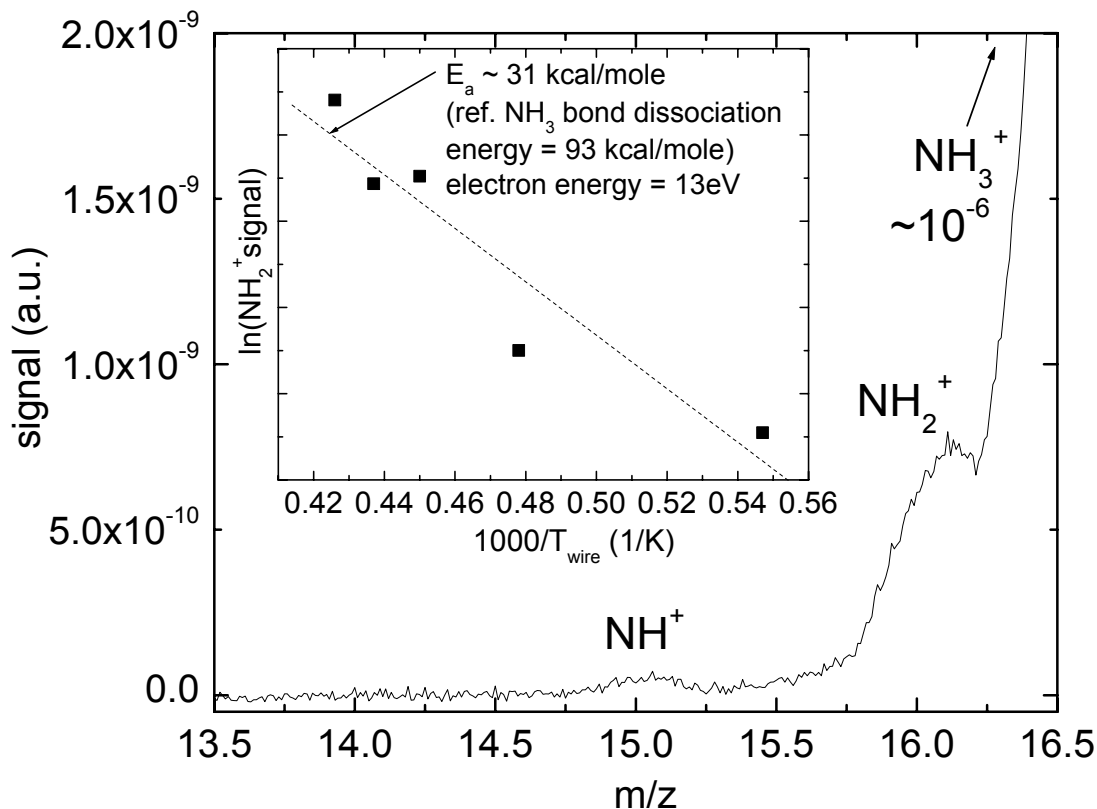


Figure 1. Low pressure radical measurements probing NH₃ decomposition.

temperature of 2100°C. Even at such a high temperature, there is an extremely small yield of NH₂ from NH₃ decomposition. Relative to the decomposition probability of SiH₄ at a similar temperature, NH₃ is almost a factor of 100 less. This suggests that to produce stoichiometric (Si₃N₄) films, the feed gas must contain SiH₄ in a large dilution of NH₃, a common observation in the growth of these films.¹⁹ The intensity of the NH₂ yield was also measured as a function of wire temperature, from 1550-2100°C, and is illustrated as an Arrhenius plot in the inset of Figure 1. These data yield an approximate activation energy of 31 kcal/mole for the NH₃ decomposition reaction:



where “W” represents a bare surface site on the tungsten wire, and “W-H” is a hydrogenated surface site on the wire. This measured activation energy is significantly smaller than the known N-H bond dissociation energy of 93 kcal/mole,¹² indicating that like the hot-wire decomposition of SiH₄ to SiH₃,¹⁰ the decomposition reaction of NH₃ to NH₂ is catalyzed by the tungsten filament.

5.3.2 Initial Film Growth Results

SiN_x films were initially prepared at a SiH₄/NH₃ flow ratio of 0.018 (16 sccm 1% SiH₄ mixture, 8.7 sccm NH₃), 20 mTorr total pressure, and a substrate temperature of 280°C, with a growth time of 60 minutes. Resulting films were analyzed with a single wavelength (633 nm) ellipsometer, yielding a thickness of 185 nm and refractive index of 1.8. Subsequent analysis was performed using X-ray Photoelectron Spectroscopy (XPS) to gain insight into the bonding structure of the film. Figure 2 shows the XPS N 1s spectra for the above described film grown by HWCVD and a standard (stoichiometric nitride) grown by conventional PECVD (50 nm Si₃N₄ on Si substrate). Evident from this figure is a 0.8 eV core level shift for the hot-wire film, relative to the plasma-grown film. These shifts to higher binding energy are consistent with a change from the stoichiometric N-Si₃ structure to a N-Si₂ bond structure, with the remaining bond

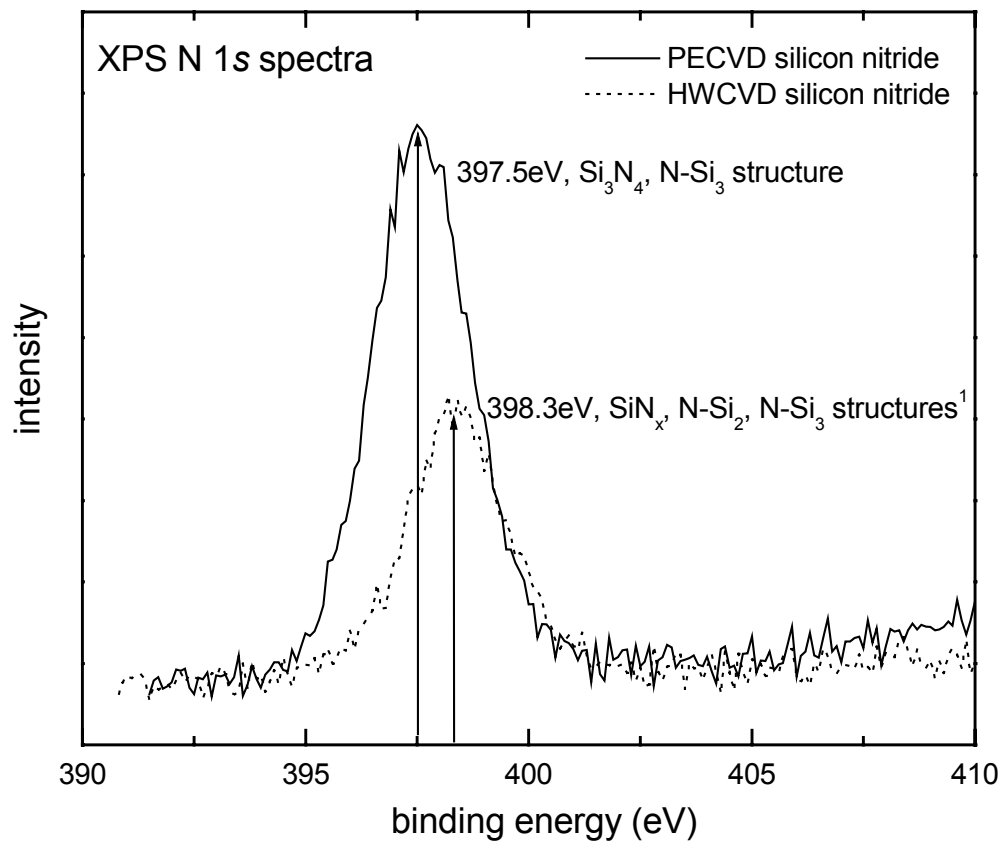


Figure 2. XPS N 1s spectra for films grown via hot-wire and plasma CVD.

either dangling or to hydrogen.¹³ The relative percentage of oxygen was larger in the HWCVD film versus the PECVD film, suggestive of SiO₂, and an examination of the Si signal yielded a Si/N ratio of approximately 1.3. These results suggest that the film was a combination of SiO₂ and SiN_x, possibly a silicon oxynitride (Si_xO_yN_z).

5.3.3 Variation of SiH₄/NH₃ Flow Ratio

Prompted by the results indicating that the initial growth conditions led to a film of low index (1.8), a series of different SiH₄/NH₃ flow ratios were used to examine the effects on film properties. The films to be described were grown at a substrate temperature of 300°C for a period of 40 min, with a wire temperature of 1800°C and a total pressure of 100 mTorr. Figure 3 provides the Fourier Transform Infrared (FTIR) transmission spectra for a series of four SiN_x films grown under different SiH₄/NH₃ flow ratios: 0.01, 0.02, 0.04, and 0.08. Figure 4 shows the thickness-normalized spectra for the same films, focusing on the hydrogen-containing features. Table 1 provides the flow rates used for film growth (Q_S = SiH₄ mixture flow rate, Q_N = NH₃ flow rate), as well as the resulting film thickness (t) and refractive index (n). The most prominent feature in the transmission spectra of Figure 3 is the Si-N absorption around 860 cm⁻¹; the breadth of this feature suggests that the SiN_x films are amorphous. Evident from Figure 4 is that the majority of H is bound to N for the 0.01, 0.02, and 0.04 flow ratios, however the H is mostly bound to Si at a flow ratio of 0.08. For the 0.01, 0.02, and 0.04 cases, it is likely that the H observed comes from NH₂ species produced at the wire. For the 0.08 case, the H of the film likely results from atomic H (produced by SiH₄ decomposition) passivating Si dangling bonds present in the growing film.

Using absorption cross sections provided by Lanford and Rand,² an estimate

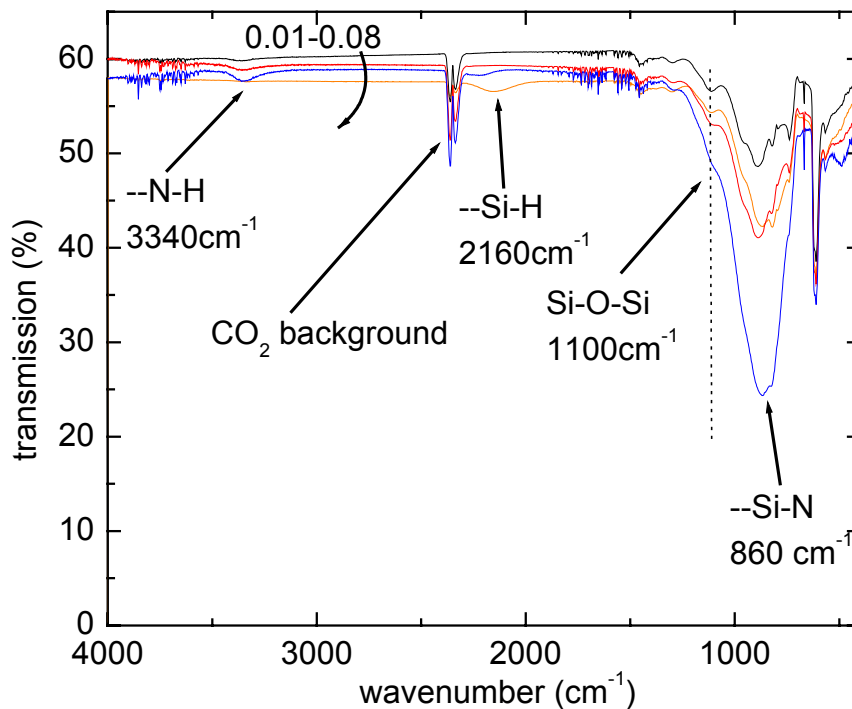


Figure 3. FTIR spectra for films grown under different SiH_4/NH_3 flow ratios.

of the hydrogen concentration in the various films could be obtained. The range of values obtained by this method was $0.9\text{-}1.5 \times 10^{22} \text{ cm}^{-3}$ ($\sim 10\text{-}18 \text{ at. } \%$), although the degree of uncertainty associated with these measurements (due to the baseline determination) prevents the determination of whether there is a trend in hydrogen content with respect to flow ratio. Other trends are noticeable from Table 1. The growth rate is proportional to the product of the SiH_4 and NH_3 flow rates. Also, the refractive index increases from 1.8 up to 2.5 as the flow ratio increases from 0.01 to 0.08, with the 0.04 flow ratio being closest to stoichiometric silicon nitride (2.0). Finally, Figure 3 reveals that the 0.01 flow ratio film has a

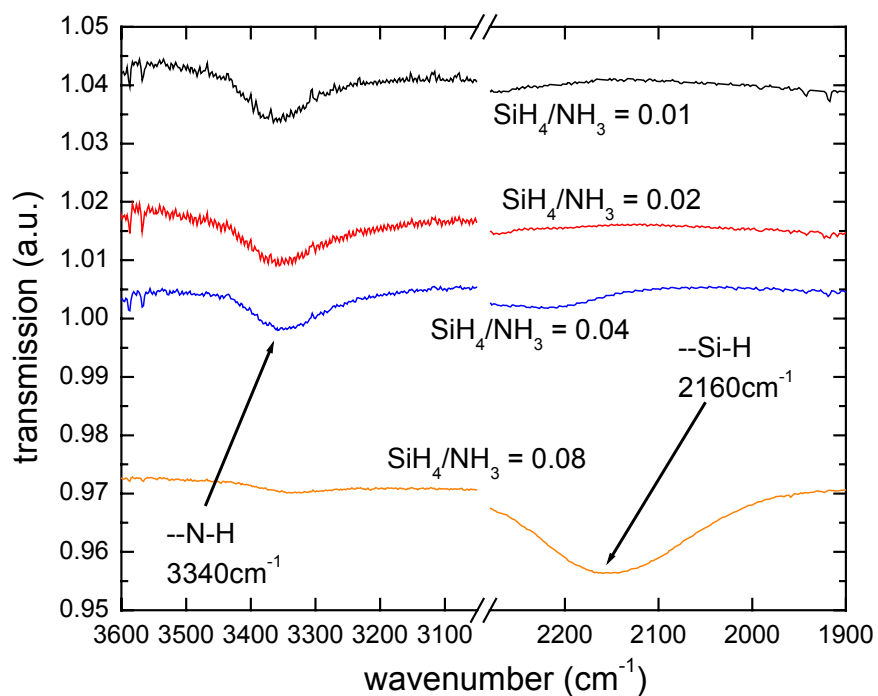


Figure 4. Normalized FTIR spectra of the same films as in Figure 3.

Table 1. Film growth conditions and resulting thickness/index.

SiH_4/NH_3	Q_S (sccm)	Q_N (sccm)	t (nm)	n
0.01	8	8	62	1.8
0.02	16	8	128	1.8
0.04	32	8	287	1.9
0.08	32	4	129	2.5

prominent Si-O-Si feature that is diminished or absent in films grown at higher flow ratios.

To complement these FTIR measurements, Rutherford Backscattering (RBS) and Hydrogen Forward Scattering (HFS) measurements were made to determine the stoichiometry and hydrogen content (with greater accuracy) of a select number of SiN_x films. The films chosen for analysis were the 0.01 and 0.08 flow ratio films, in addition to two films grown at a flow ratio of 0.06 (all other conditions identical),[†] one of which was subjected to a post-deposition H₂ treatment. The post-deposition H₂ treatment was carried out under conditions identical to SiN_x deposition, but with the replacement of SiH₄ and NH₃ with H₂ at the same 100 mTorr total pressure. The rationale for this treatment was to determine whether additional H (produced by H₂ decomposition on the wire) could be incorporated into the as-grown SiN_x.

Table 2 provides a summary of the RBS, HFS, and FTIR film analysis. As expected, the RBS data reveal an increase in the Si/N ratio in the film as the SiH₄/NH₃ flow ratio increases. All values are greater than the value of 0.75 expected of stoichiometric silicon nitride, although the value of ~ 1 obtained with a flow ratio of 0.01 is attributed to the presence of SiO₂. There is a slight decrease

[†] FTIR analysis of the 0.06 flow ratio films revealed that H was bonded predominantly to Si, as in the 0.08 case.

Table 2. Summary of RBS and HFS film analysis.

SiH_4/NH_3	t (nm)	n	Si/N [RBS]	[H] (at.%) [HFS]	atomic density (cm^{-3}) [RBS]	oxygen content (at%)
0.01	62	1.8	0.99	9.3%	8.2×10^{22}	23%
0.06	209	2.2	1.3	16%	7.5×10^{22}	0%
0.06 + H_2	185	2.1	1.1	16%	8.4×10^{22}	0%
0.08	129	2.5	2.2	18%	6.2×10^{22}	0%

in the Si/N ratio after the post-deposition H_2 treatment, suggesting an etching effect of H on the Si of these Si-rich films. Revealed by HFS is an increase in the overall atomic percentage of H as the flow ratio (or Si/N ratio) increases, supporting the idea that SiH_4 is the primary source of H under these growth conditions.

Interestingly, the post-deposition H_2 treatment appeared to have little effect on the atomic percentage of H in the film, and may only have served to etch the Si-rich film. The films also exhibited a decrease in atomic density (as determined with RBS, using the known film thickness) as the proportion of Si/N increased, consistent with the considerably larger covalent radius of Si.² The film subjected to the H_2 treatment showed an increase in atomic density, suggesting that H etched excess Si from the film, and then densified. Finally, it is noteworthy that

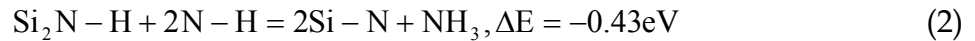
the 0.01 flow ratio film contains a large percentage of oxygen (23%), while it is below the detection limit in films grown at higher flow ratios. This result is consistent with the earlier FTIR measurements showing an Si-O-Si feature in the 0.01 flow ratio film. It has also been observed by Stannowski *et al.*,⁹ using similar techniques, that nitride films deposited with a small flow ratio of 0.02 undergo post-deposition oxidation, likely due to absorption of H₂O molecules. The authors infer that films grown under these conditions must be porous to allow for H₂O absorption.

5.3.4 Annealing of Hydrogenated SiN_x

For applications where hydrogenated SiN_x is to be used as a passivation coating, the mobility of bound hydrogen is critical because the degree of passivation (as measured in minority carrier lifetime) is thought to depend on the amount of hydrogen released from the SiN_x film into the underlying Si substrate.¹⁴ In order to observe the effects of H release from N versus Si, the 0.02 and 0.08 flow ratio films from the previously described films were selected. Following a similar experimental approach as taken by Yelundur,¹⁴ we chose to anneal each of these films for 5 minutes at temperatures of 400°C, 600°C, and 800°C. Between each anneal, the sample was allowed to cool to room temperature, after which FTIR measurements were made to monitor to release of

H from the SiN_x film. Figure 5 shows the FTIR spectra at the various annealing temperatures for each of these films, along with an estimate of the H concentration, determined by the aforementioned method of Lanford and Rand.² Figure 5a shows a steady reduction in the H bonded to N (0.02 flow ratio film) as the anneal temperature is increased, with an overall reduction of 70% after the 800°C anneal. Figure 5b reveals only a slight reduction in the H bound to Si (0.08 flow ratio film) up to 600°C, with a drastic reduction of 80% after the 800°C anneal.

These results are in qualitative agreement with results of Boehme *et al.*¹⁵ For films deposited with a small flow ratio SiH₄/NH₃ (N-rich), the activation energy for the H-bond concentration reduction was 450 meV, while it was 800 meV for large flow ratios (Si-rich). The larger activation energy for films grown at large flow ratios is consistent with the observation that higher temperatures were required for H-loss to occur in such films. For N-rich films in which there are few Si-H bonds available, the H-loss mechanism was proposed to be:¹⁵



where NH₃ is the diffusing, H-carrying species. Conversely, in Si-rich films where there are few N-H bonds available, the loss mechanism is likely to be:¹⁵



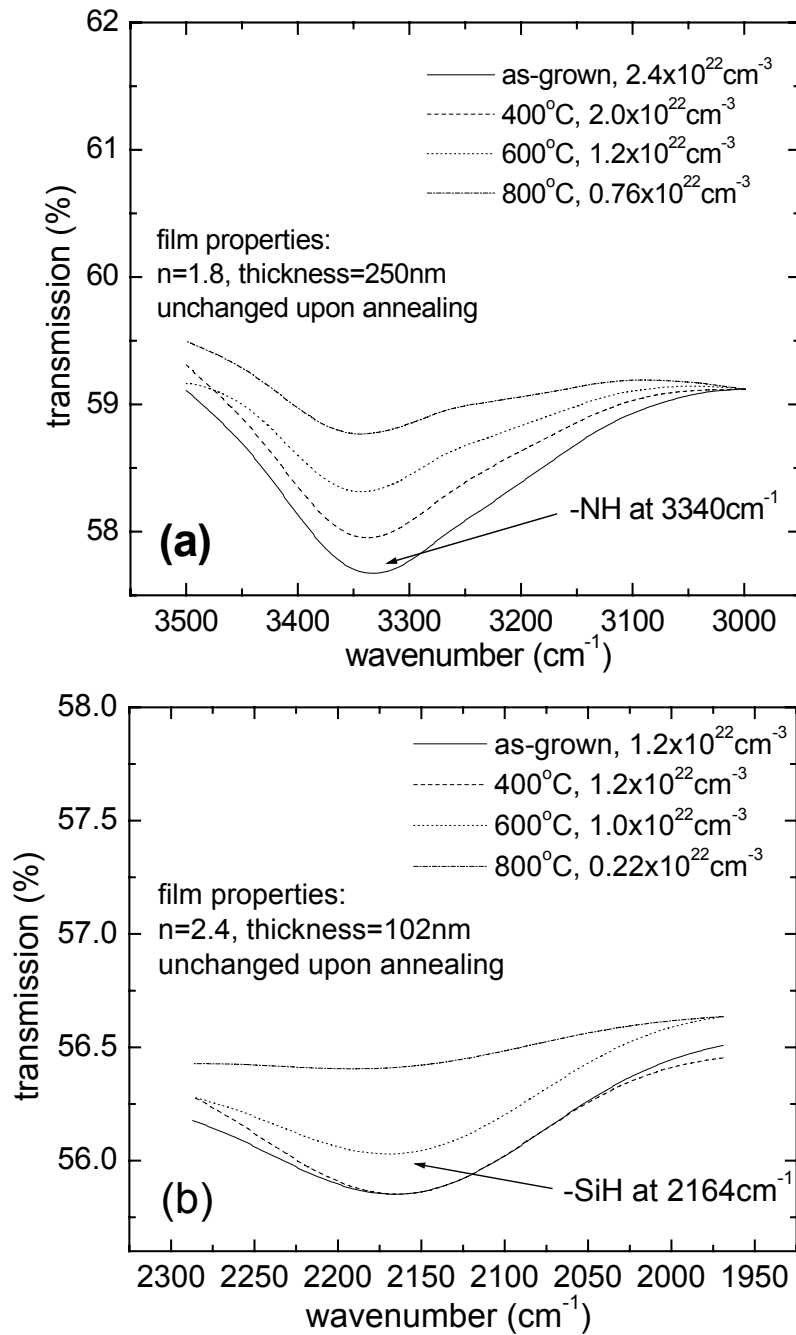


Figure 5. FTIR spectra at various annealing temperatures (5 minute anneal at each temperature) for (a) film grown with a flow ratio of 0.02 SiH_4/NH_3 , and (b) film grown with 0.08 SiH_4/NH_3 ; corresponding hydrogen concentrations at each temperature are listed.

As this second reaction is slightly more energetically favorable, it would be expected to result in a larger degree of H-loss for the same annealing treatment. Indeed, the Si-rich film showed an 80% reduction in H-content, compared to the 70% observed with the N-rich film.

5.3.5 Multiple Internal Reflection FTIR: Hydrogen-Defect Passivation

The previous section demonstrated that large fractions of bound hydrogen can be liberated from silicon nitride films upon annealing. Questions remain, however, about whether this hydrogen is simply released into the environment (as H₂) or is driven into the bulk c-Si beneath. To investigate this issue, the technique of Multiple Internal Reflection FTIR (MIR-FTIR) was used. This technique involves passing an infrared beam through a sample with a prism geometry, at an angle exceeding the critical angle for total internal reflection, as illustrated in Figure 6.¹⁶ This internal reflection results in a much longer absorption path length (~ cm) than a straight through transmission measurement, allowing trace vibrational features to be detected. In addition, operation near liquid-helium temperatures can enable 0.35 cm⁻¹ resolution¹⁷ and reduce interference from phonon modes of the bulk Si.

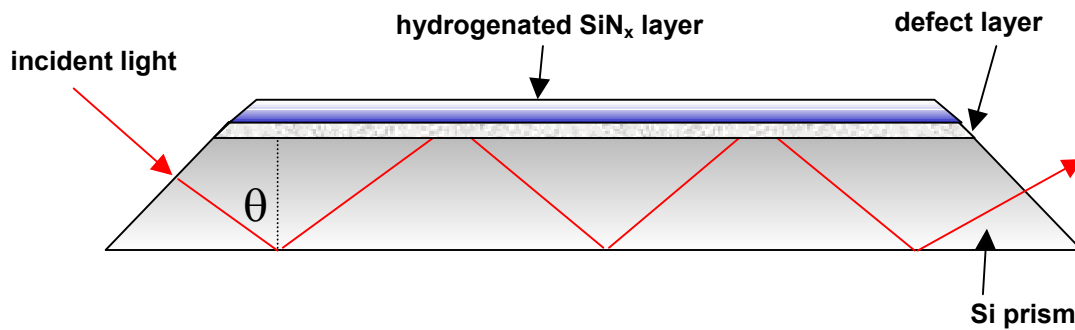


Figure 6. Schematic of Multiple Internal Reflection technique used to probe hydrogenation of defects.

The specific features being examined were platinum-hydrogen complexes (Pt-H, Pt-H₂) and vacancy-hydrogen complexes (V-H_x, x=1-4). Platinum-hydrogen complexes have been well studied, with their vibrational features and charge states assigned.¹⁷ Platinum is also a representative transition-metal impurity that may be present in Si and can act as a sink for H. Vacancies are one of the most important intrinsic defects in Si¹⁸ and their hydrogenated complexes have also been well studied.¹⁹ The formation of such complexes has profound effects on the optical properties of the material,¹⁹ and thus, their observation would provide strong evidence in favor of passivation induced by H-release from the nitride coating.

A series of four float zone Si samples were analyzed by our collaborators Jiang and Stavola:²⁰ 1) p-type with [B] = $2 \times 10^{15} \text{ cm}^{-3}$ and Pt impurities (prepared by high temperature diffusion at 1250°C to a level of 10^{17} cm^{-3}), 2) n-type with [P] = $3 \times 10^{16} \text{ cm}^{-3}$ and Pt impurities of the same level, 3) p-type of the same dopant level with no impurities, and 4) n-type of the same dopant level with no

impurities. A Pt-diffusion was chosen to create a sink for H-atoms and evaluate what fraction of the H leaving the nitride film diffuses into the c-Si substrate beneath. For those substrates that were undiffused, it was thought that the native vacancies in the doped Si could act as H atom sinks. Different dopants were used because of the known greater abundance of vacancies in p-type versus n-type Si.¹⁸

The Si samples underwent the same cleaning/etching procedure described in section 5.2. Then, a nitride coating of approximately 86 nm, with an index of 2.30 (Si-rich), was deposited at 300°C on all four samples by HWCVD. Previous results (section 5.3.3) showed a H-content in the range from 16-17 atomic % for films with this index.

The nitride coated samples were then measured by FTIR, revealing no H in the bulk. Samples were subsequently annealed at temperatures of 400°C, 500°C, 600°C, and 700°C for 10 minutes, between which FTIR measurements were made. Figure 7 shows the FTIR spectra of the p-Si Pt-diffused sample at the various annealing temperatures. Peaks on the left are attributed to Pt-H complex formation, originating from the H-released by the nitride layer (the Si-H is shown by the peaks on the right side of the spectra). There was no evidence for the formation of Pt-H complexes after the 400°C anneal; however, anneals at the higher temperatures show the appearance of Pt-H in the bulk. It is worth noting that Pt-H is thermally stable up to about 650°C,²¹ and thus anneals carried out at

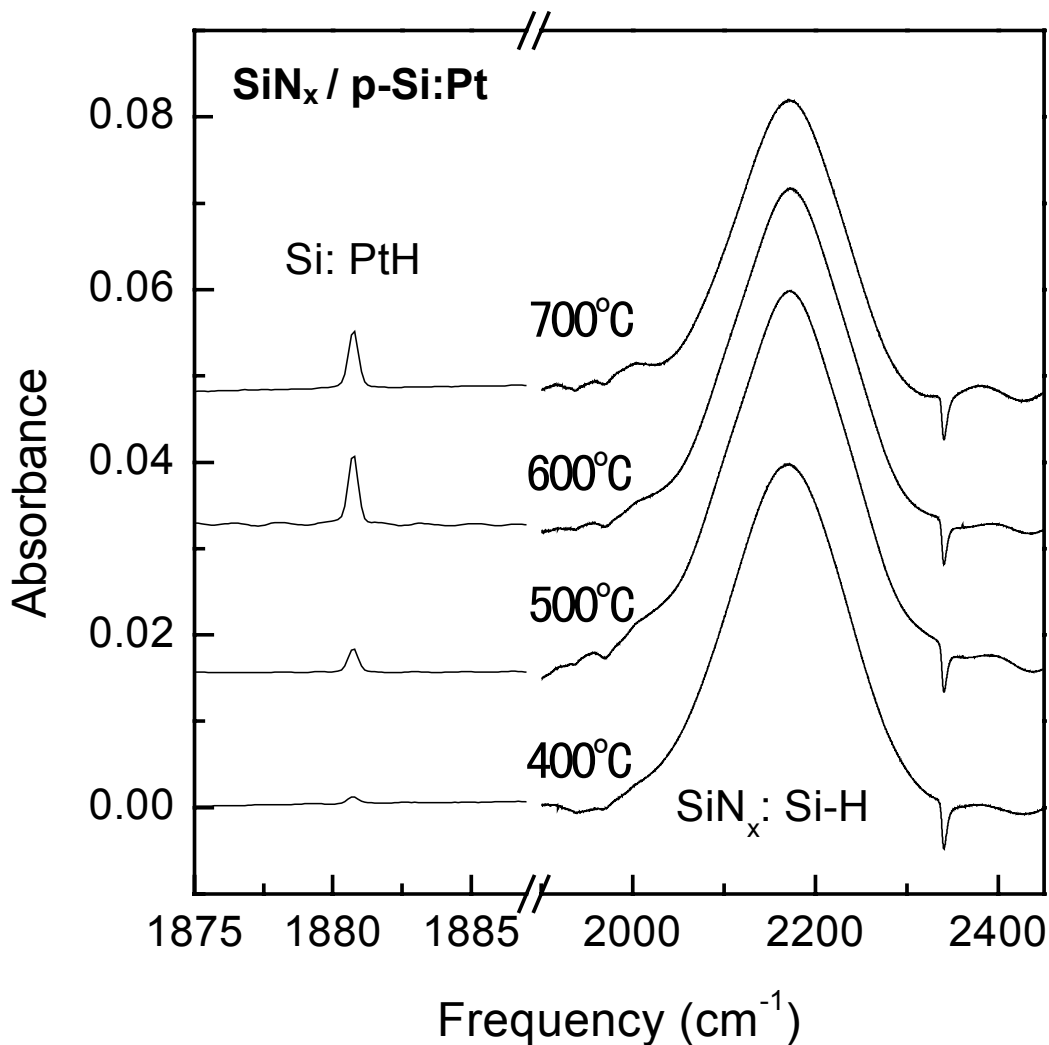


Figure 7. FTIR spectra for p-Si Pt-diffused sample obtained by the ATR technique; leftmost peaks are attributed to the formation of Pt-H complexes, while those on the right come from the Si-H of the nitride top layer.

higher temperatures show a reduction in this feature, presumably due to out-diffusion of H₂ from the sample. The temperature dependence observed for the appearance of the Pt-H complex is consistent with the H-release behavior from the nitride film previously discussed (5.3.4); specifically, Si-rich nitride layers show little H-release until a temperature of 600°C. From Figure 7, the H-loss is

estimated to be 5% of the total at 600°C, while the total loss is 23% after the 700°C anneal.

From previous calibration¹⁷ of the intensity of the Pt-H lines, a Pt-H concentration of $5.8 \times 10^{12} \text{ cm}^{-2}$ is determined for the 600°C anneal (the areal concentration of Pt, in cm^{-2} , is proportional to the area of the IR absorption line). This amount represents only 0.15% of the H released from the nitride layer at this temperature (which itself is only 5% of the total present in the nitride). After the 700°C anneal, the Pt-H concentration drops to $4.9 \times 10^{12} \text{ cm}^{-2}$. Through successive thinning of this sample to monitor H introduction, the Pt-H concentration is found to drop to $3.1 \times 10^{12} \text{ cm}^{-2}$ at a depth of 390 μm . This, in turn, leads to a bulk Pt-H concentration of $5 \times 10^{13} \text{ cm}^{-3}$. Assuming a uniform distribution of H throughout the sample, a hydrogenated layer thickness of 1.1 mm is calculated.

The n-type Pt-diffused sample showed similar characteristics as the p-Si sample, but with approximately a factor of two lower H-incorporation into the bulk. In both the diffused and undiffused samples, there was no evidence for vacancy-H complexes. It is possible that such complexes would be observed in samples that underwent Al-alloying on the backside. This alloying is believed to produce vacancies at the backside that can migrate and increase the chemical potential gradient for H into the bulk Si, in addition to assisting in the dissociation of molecular hydrogen.¹⁴ As a result, samples that undergo a “co-firing”, where the Al-back contact is formed and the nitride film releases H

simultaneously, have produced significant enhancements in minority carrier lifetime, attributed to the synergy between these two processes.¹⁴

No B-H or P-H complexes were observed in any of the four samples analyzed. The former is believed to be unstable under the high annealing temperatures used here,²² while the latter has only been observed in samples treated by a H plasma.²²

When compared with the Pt bulk concentration of order 10^{17} cm⁻³, it is seen that approximately 0.1% of the Pt is passivated in the Pt-diffused samples. This degree of passivation is approximately one order of magnitude lower than that observed for wet chemical methods of hydrogenation,¹⁷ but it is possible that some of the H lies in other defects that were not probed or are inaccessible by this FTIR technique. The question that remains is whether this level of defect hydrogenation can result in significant enhancement in minority carrier lifetime. Results of Rohatgi *et al.*²³ suggest that the degradation threshold (i.e., the impurity concentration level at which solar cell performance starts to degrade) for a number of metals such as Cr, Mn, Fe, and Ni is of order 10^{14} cm⁻³ or lower. Thus, it is conceivable that this process, even without further enhancement by Al-alloying, may improve minority carrier lifetime in a solar cell.

5.3.6 Silicon Nitride Deposition onto String Ribbon Silicon Substrates

It is clear from the preceding section that H-defect passivation occurs to some degree during annealing of nitrified Si samples. The remaining questions are 1) what effect this annealing treatment has on the electronic properties of a resulting solar cell, and 2) how hot-wire CVD nitride films compare with their plasma CVD counterparts. The first question will be addressed later in this section. To answer the second question, hot-wire nitride films were deposited onto String Ribbon²⁴ substrates provided by *Evergreen Solar, Inc.* (Marlboro, MA). The samples were p-type (resistivity of 3 Ω -cm), with a thin phosphorous-diffused n-type layer on top. Due to the large area of the substrates used (15 cm x 8 cm), a filament array had to be used to achieve thickness uniformity, and is illustrated schematically relative to the substrate in Figure 8. Further description of this filament array can be found in Appendix A. It has been observed⁸ that if the filament spacing is at most half the filament-to-substrate distance, then there is little non-uniformity associated with the filament array. With this design criterion in mind, the 20 cm long filaments were spaced a maximum of 2 cm apart, with a wire-to-substrate separation of 5 cm. It is worth noting that the wire array DSMC simulations of section 4.2.1 predicted the same optimal wire spacing. The initially grown sample shown in Figure 8 was still slightly non-

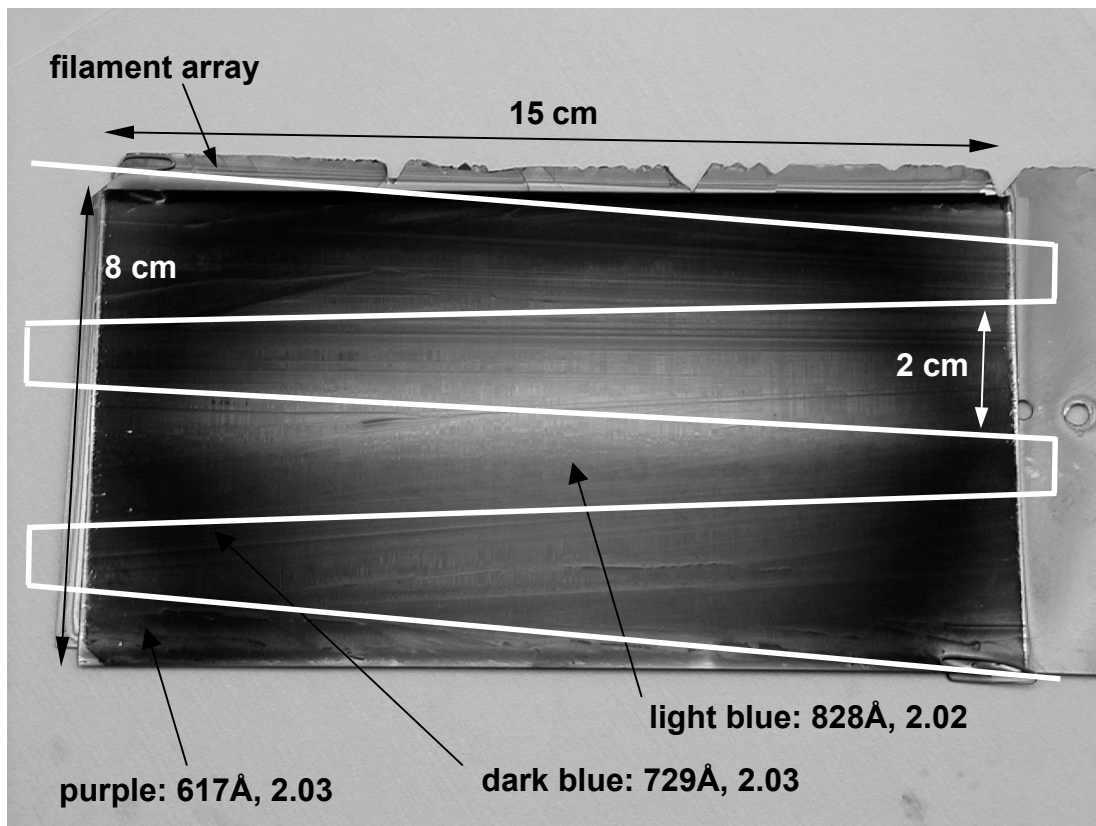


Figure 8. String-ribbon silicon substrate with an illustration of the relative location of the filament array. The array is spaced 5 cm from the substrate, with a maximum filament spacing of 2 cm. Select points are shown with their apparent color, thickness, and index of refraction, determined by ellipsometry (at a wavelength of 633 nm).

uniform, with a 200 Å thickness variation from center to edge in the long direction (center thickness of ~ 800 Å); there was no thickness variation, however, in the short direction. Subsequent samples were made more uniform in thickness (variation of ~ 100 Å) by translating the sample across the wire array over the course of deposition. The remaining thickness nonuniformity can be attributed to lower wire temperatures near the ends of the array (due to

conductive heat losses to the wire spacers), as the desorption rate of film precursors decreases exponentially with wire temperature.

Three nitride samples with an average center thickness of 830 Å were chosen for subsequent processing by *Evergreen Solar, Inc.* The nitrated samples had a thick film of a commercially available aluminum paste deposited on back, and a front Ag grid of commercially available Ag paste was deposited on the nitrated surface. The samples were then annealed in a belt furnace using a “slow firing” process (peak temperature of 700°C with a peak dwell time of 30 seconds) to sinter and form the contacts as well as to release H from the nitride layer. The cell's electrical properties were then measured.

Table 3 provides the short circuit current density (J_{SC}), open circuit voltage (V_{OC}), fill-factor (FF), and efficiency (η) for the best hot-wire (HW) nitride cell versus the best plasma nitride cell (using the same “slow firing” anneal process) produced by *Evergreen Solar, Inc.* The hot-wire nitride cell is comparable in all electrical properties (with the exception of J_{SC}) to the plasma nitride cell. As J_{SC} should increase with the degree of defect passivation, further improvements might be expected with the use of more uniform nitride coatings.

Table 3. Comparison of electrical properties for hot-wire versus plasma nitride cells.

cell type	J_{sc} (mA/cm ²)	V_{oc} (mV)	FF	η (%)
HW nitride	29.99	579	0.712	12.4
plasma nitride	30.92	584	0.709	12.8

5.4 Conclusions

It was demonstrated that the decomposition rate of NH_3 on tungsten is low relative to SiH_4 , explaining the large excess flow of NH_3 needed to produce stoichiometric silicon nitride films. The NH_3 decomposition reaction is catalyzed by the wire, with an activation energy of 31 kcal/mole. Varying the ratio of SiH_4/NH_3 from 0.01-0.08 produced films ranging in refractive index from 1.8-2.5, with hydrogen content ranging from 9-18 atomic %. Transmission measurements using FTIR revealed a transition in the bonding of H (going from N to Si) in SiN_x as the flow ratio was increased beyond 0.06 SiH_4/NH_3 . As this ratio was increased, the overall H-content increased in the film, suggesting that SiH_4 is the primary source of H under these conditions. A film deposited with a low flow ratio of SiH_4/NH_3 of 0.01 revealed a prominent Si-O-Si feature suggesting oxidation, a result further confirmed with RBS, indicating 23% oxygen incorporation in the film.

Post-deposition H₂ treatments were found to have little impact on the overall atomic percentage of H in the film, but did appear to have an etching effect with the Si-rich samples used. Annealing studies revealed different kinetics for H release from Si versus N, consistent with experimental results from the literature. Samples consisting of a thin hydrogenated nitride layer on a platinum-diffused silicon substrate were analyzed by MIR-FTIR techniques. Platinum-hydrogen complexes were observed in the bulk silicon after annealing treatments similar to those for which hydrogen loss was observed in the nitride layer. The bulk concentration of these complexes was estimated to be of order 10¹⁴ cm⁻³, potentially significant enough to improve the minority carrier lifetime in a fabricated solar cell. No dopant-hydrogen or vacancy-hydrogen complexes were observed in the samples analyzed. Finally, photovoltaic cells produced with hot-wire-grown silicon nitride layers show comparable electrical properties to those produced with plasma nitride layers.

References

1. H. Sato, A. Izumi, and H. Matsumura, *Appl. Phys. Lett.* **77**, 2752-2754 (2000).
2. W. Lanford and M. Rand, *J. Appl. Phys.* **49**, 2473-2477 (1978).
3. A. Aberle, *Sol. Ener. Matl. Sol. Cells* **65**, 239-248 (2001).
4. B. Vogl, A. Slade, S. Pritchard, M. Gross, C. Honsberg, J. Cotter, and S. Wenham, *Sol. Ener. Matl. Sol. Cells* **66**, 17-25 (2001).
5. H. Matsumura, *Jap. J. Appl. Phys.* **37**, 3175-3187 (1998).
6. B. Nelson, E. Iwaniczko, A. Mahan, Q. Wang, Y. Xu, R. Crandall, and H. Branz, *Thin Solid Films* **395**, 292-297 (2001).
7. J. Moschner, J. Schmidt, and R. Hezel, 29th IEEE Photovoltaic Specialists Conference (New Orleans, LA) 2002.
8. A. Ledermann, U. Weber, C. Mukherjee, and B. Schroeder, *Thin Solid Films* **395**, 61-65 (2001).
9. B. Stannowski, M. van Veen, and R. Schropp, *Mat. Res. Soc. Symp. Proc.* **664**, A17.3.1 (2001).
10. J. Holt, M. Swiatek, D. Goodwin, and H. Atwater, submitted to *J. Appl. Phys.* (2002).
11. F. Qi, L. Sheng, Y. Zhang, S. Yu, and W.-K. Li, *Chem. Phys. Lett.* **234**, 450 (1995).

12. R. Sanderson, *Chemical Bonds and Bond Energy* (Academic Press, New York) 1976).
13. S. Kaluri and D. Hess, *Appl. Phys. Lett.* **69**, 1053 (1996).
14. V. Yelundur, A. Rohatgi, A. Ebong, A. Gabor, J. Hanoka, and R. Wallace, *J. Elec. Matl.* **30**, 526-531 (2001).
15. C. Boehme and G. Lucovsky, *J. Vac. Sci. Tech. A* **19**, 2622 (2001).
16. E. Rudkevich, D. Savage, W. Cai, J. Bean, J. Sullivan, S. Nayak, T. Kuech, L. McCaughan, and M. Lagally, *J. Vac. Sci. Technol. A* **15**, 2153 (1997).
17. M. Weinstein, M. Stavola, K. Stavola, S. Uftring, J. Weber, J. Sachse, and H. Lemke, *Phys. Rev. B* **65**, 035206-1 (2001).
18. G. Watkins, *Deep Centers in Semiconductors* (Gordon and Breach, New York), 1986.
19. Y. Park, S. Estreicher, C. Myles, and P. Fedders, *Phys. Rev. B* **52**, 1718 (1995).
20. F. Jiang and M. Stavola, in *Hydrogen Passivation From SiN_x:H Films: What is Really Happening in the Si?*, 12th Workshop on Crystalline Silicon Solar Cell Materials and Processes (Breckenridge, Colorado) 2002.
21. S. Uftring, M. Stavola, P. Williams, and G. Watkins, *Phys. Rev. B* **51**, 9612 (1995).
22. M. Stavola, private communication, August 19th, 2002.
23. A. Rohatgi, J. Davis, R. Hopkins, and P. McMullin, *Solid-State Electronics* **26**, 1039 (1983).

24. R. Wallace, J. Hanoka, A. Rohatgi, and G. Crotty, *Sol. Ener. Matl. Sol. Cells* **48**, 179-186 (1997).

Chapter 6 *In situ* Silane Generation by
Hot-Wire Atomic Hydrogen
Etching of Solid Silicon
Sources

Abstract

Experiments aimed at selective hydrogen etching of a cooled silicon target to generate silane and deposit a silicon film onto a heated substrate are described. Crystalline silicon was found to be unsuitable as a target material, in agreement with a number of reports in the literature. Selective etching and net growth was only possible with the use of an amorphous silicon target, for which etch rates of up to 2.5 nm/min were measured. A design modification that may enable the use of crystalline silicon targets is described.

6.1 Introduction

The etching effect of atomic hydrogen on amorphous and crystalline silicon has long been known, with one of the first studies carried out by Veprek and Marecek;¹ this study also happened to be the first to demonstrate microcrystalline silicon growth. In this study they demonstrated transport of Si and Ge by means of a hydrogen plasma, speculating that the transport occurred through the formation of volatile hydride species. Twenty years later, direct measurements by Abrefah and Olander² showed that the predominant species created by atomic hydrogen etching of crystalline silicon is SiH₄. They further demonstrated that the etch rate, specifically of Si(111), shows an inverse dependence on temperature; at substrate temperatures below 1000 K, however, the etching probabilities of Si(111) and Si(100) were shown to be identical.

These results suggest that it is possible to grow silicon films by first etching a cooled silicon target to produce SiH₄, then decomposing this SiH₄ on a hot filament, followed by deposition of the decomposition products onto a heated silicon substrate. Such a process was recently demonstrated by Masuda *et al.*,³ referring to it as “Catalytic Chemical Sputtering.” In their study, they used a Si(100) substrate as the target material and deposited onto a variety of substrates, including Si(100), Si(100) with a variable thermal oxide thickness, and fused-quartz having a silicon seed layer.

If such a technique could be suitably optimized, it would have the potential to replace the hazardous and costly usage of SiH_4 gas. In addition, there exists the possibility of using less refined materials such as solar-grade silicon (obtained as a by-product from the semiconductor industry for use in solar cells) and metallurgical-grade silicon (produced by the reduction of silica, with approximately 1.5 atomic % metal impurities) as etching targets. It has not yet been demonstrated, however, whether selective etching of the silicon occurs over the alkali and transition metal impurities. Should selective etching be demonstrated, the technique could prove revolutionary to both the photovoltaic and semiconductor industries.

6.2 Experiment

With the initial promising results of Masuda *et al.*³ (from this point forward referred to just as Masuda or the Masuda study), a design similar to theirs was implemented, as illustrated in Figure 1. The idea was to both verify their results, and explore other areas of the parameter space (e.g., pressure, flow rate) in order to optimize the target etch rate and the resulting net growth rate. This design differs from the standard hot-wire reactor setup only in the addition of a water-cooled block to keep the source material (Si(100) in this case) under 100°C ; the temperature was measured by a thermocouple bonded to the Si substrate with

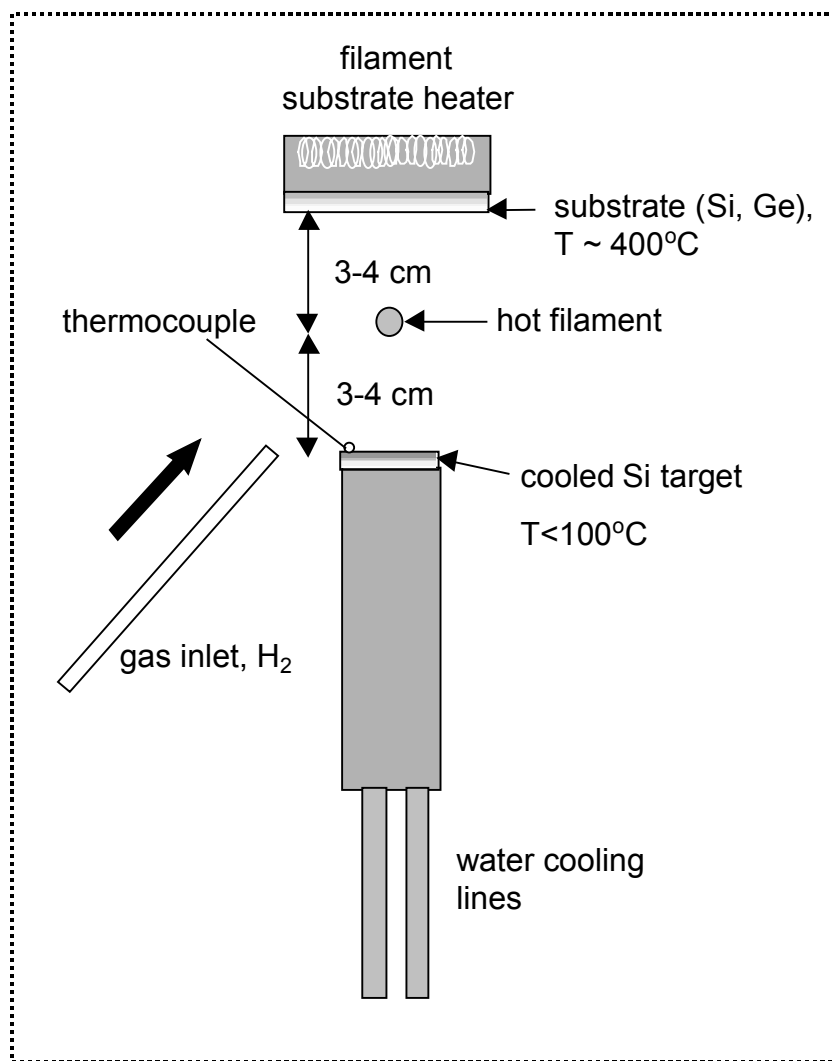


Figure 1. Schematic of *in situ* silane generation source.

conductive silver paint. Hydrogen gas is introduced through 0.25 inch stainless steel tubing into the reactor (pressures between 50-200 mTorr, flow rates between 10-80 sccm) where it is decomposed into atomic H on a tungsten filament held between 1800°C-2000°C. This atomic H diffuses to the heated substrate as well as the cooled target, placed equidistant from the filament. It should be noted that the reactor walls were etched with atomic hydrogen (conditions of 200 mTorr H₂, wire temperature of 2100°C, time period ~ 12 hours) prior to experiments to

remove previously deposited amorphous silicon; by doing this, it could be insured that the cooled target was the sole source of the SiH_4 generated in the chamber.

Provided a large enough temperature gradient is maintained, the net etching rate at the cooled target should exceed that at the heated substrate. Masuda reported a H etching rate of 230 nm/min at 80°C, dropping to 0.6 nm/min at 420°C. This high etching rate at lowered temperatures generates SiH_4 that may diffuse from the cold target to the hot filament, decomposing primarily to Si (section 2.3.1) that subsequently diffuses to and deposits on the heated substrate. Under these conditions, Masuda reported a net growth rate of 1.6 Å/s ($\sim 0.01 \mu\text{m}/\text{min}$).

6.3 Results

Initial film growth experiments used the same conditions as in the Masuda study. A hydrogen pressure of 100 mTorr, at a flow rate of 10 sccm, was used. The substrate was maintained at 400°C and the Si(100) target below 100°C. Both Si(100) and Ge(100) were used as deposition substrates, the latter to enable relatively thin films to be detected by ellipsometry (based on the differing indices of refraction). Substrates went through a standard surface preparation consisting of 1) sonication in acetone/methanol for 10 minutes each to degrease the

substrates, 2) UV-ozone treatment for 10 minutes to remove residual hydrocarbons, and 3) dip in 5% hydrofluoric acid (in H₂O) to remove the thermally-grown oxide and to H-terminate the surface. These conditions were unsuccessful in producing films of measurable (by use of a stylus profilometer, with a resolution of ~ 50 Å) thickness on Si(100) substrates. For the Ge(100) substrate, a fairly regular array of etch pits was created on the surface, as can be seen in Figure 2. These features are attributed to anisotropic etching by H. The particular case illustrated was for a total exposure time of 80 minutes. The possibility that contaminants may have built up on the substrates during their transfer to the reactor (e.g., native oxide regrowth, hydrocarbons) was considered. In this case, there would be an incubation time (before the onset of film growth) associated with its removal. Indeed, in the Masuda study, an incubation time of 1 hour was observed for substrates having a 55 nm thermal oxide. Exposure times of up to 15 hours were used, which would have been more than adequate to remove a possible contamination layer. As before, however, immeasurably thin films on Si(100) and etch pits on Ge(100) were obtained.

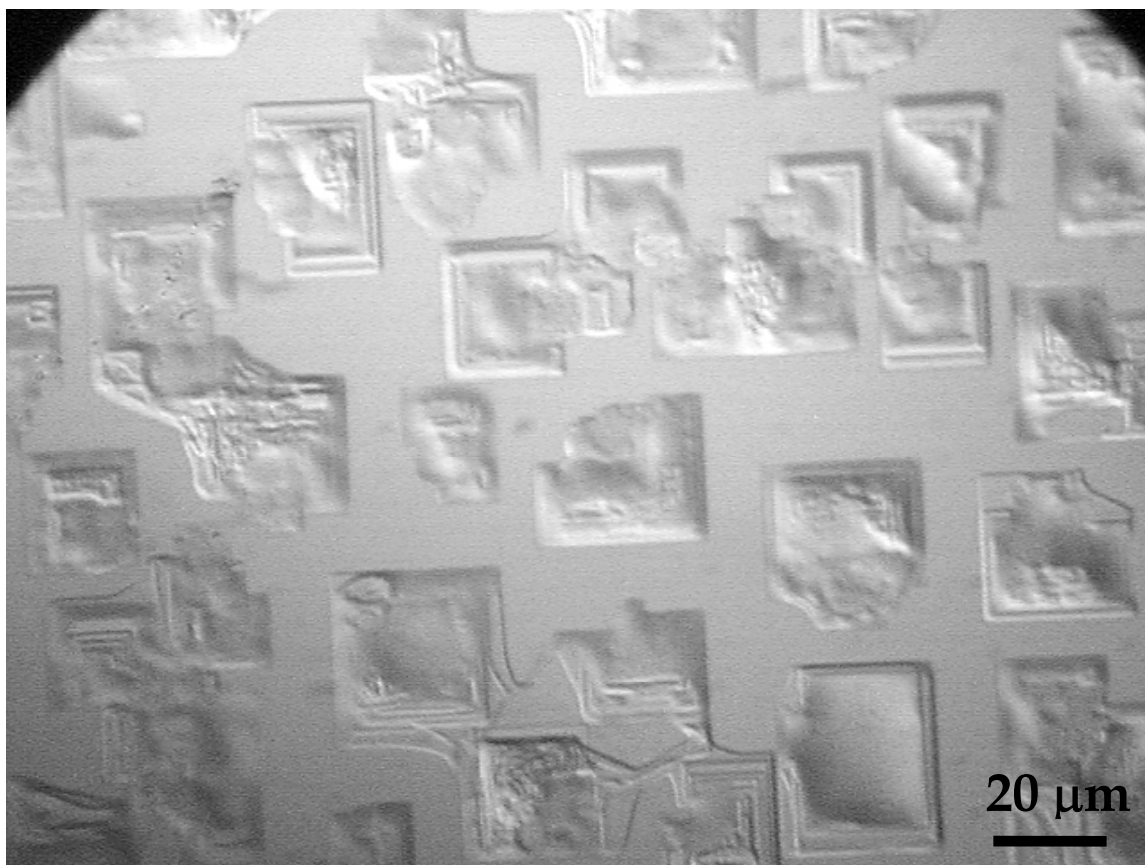


Figure 2. Optical micrograph of etch pits created on Ge(100) substrate during exposure to atomic H for a period of 80 minutes; feed gas conditions were 100 mTorr/10 sccm of H₂.

A more direct method of etch rate determination that avoids the potential problems of surface contamination involves the use of a quartz crystal deposition monitor (Inficon XTC/2, East Syracuse, New York). This monitor was used in the reactor, placed at a distance from the wire comparable to that of the target (3-4 cm). A thick (~ 100 nm) a-Si film was deposited onto the water-cooled monitor (with a temperature < 100°C, from previous thermocouple measurements) using standard hot-wire conditions (100 mTorr of 1% SiH₄ in He mixture at 13 sccm) to provide a sacrificial layer for subsequent etch rate determinations. Given the

faster etch rate of amorphous versus crystalline silicon (Otobe *et al.*⁴ report a difference of one order of magnitude), the determined etch rates represent an upper bound to that which would be expected from the crystalline silicon targets previously used.

After the a-Si deposition took place, H₂ was introduced into the reactor

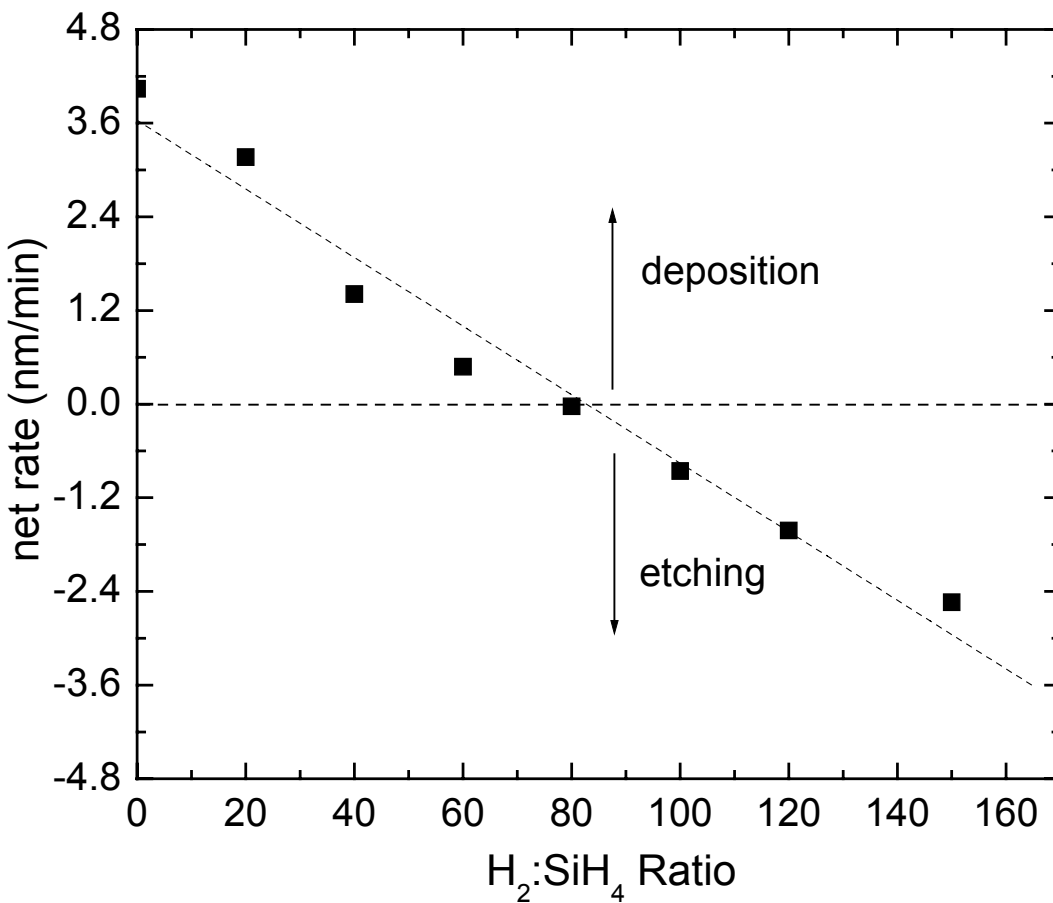


Figure 3. Transition from deposition to etching that occurs upon H₂-dilution.

(keeping the background SiH₄) incrementally, creating a progressively more H₂-diluted SiH₄ mixture; H₂ flow rates were up to 20 sccm at 150 mTorr partial pressure (150:1 dilution). The effects of this dilution can be seen in Figure 3. A transition from deposition to etching is observed at a dilution of 80:1. The gas ambient for dilution ratios of 100 and higher is taken to be representative of that in the Masuda study, namely, a highly H₂-diluted SiH₄ mixture (with the trace SiH₄ generated by atomic H etching); Masuda's reported net growth rate at the heated substrate of 1.6 Å/s (10 nm/min) is consistent with a SiH₄ partial pressure of a few mTorr, as is the case here (0.67 Å/s or 4.0 nm/min at a SiH₄ pressure of 1 mTorr). Figure 3 shows that the etch rate ranges from 0.9-2.5 nm/min as the dilution increases from 100:1 to 150:1.

With knowledge of the a-Si etch rate, another film growth experiment was carried out (removing the quartz crystal monitor). In this case, an a-Si layer (~100 nm thickness) was deposited onto the cooled c-Si target. Subsequent etching was carried out at a similar pressure of 146 mTorr H₂, but a higher flow rate of 80 sccm; the higher flow rate was motivated by the results of Wanka *et al.*,⁵ suggesting an increase in etch rate by a factor of 4 by increasing the flow rate from 20 sccm to 80 sccm. A Ge(100) substrate was used for subsequent ellipsometry measurement of the film thickness and index. Similar target and substrate temperatures were used as before ($T_{\text{target}} < 100^\circ\text{C}$, $T_{\text{sub}} = 400^\circ\text{C}$), and the exposure time was 1.5 hours. In this case, a measurable film of 50 nm thickness

was obtained. Its measured index of refraction of 3.9 is consistent with that of crystalline silicon (whether $\mu\text{c-Si}$ or poly-Si is uncertain). Subsequent attempts at film growth under these high flow rate conditions using a c-Si target were unsuccessful, however.

6.4 Discussion

The amorphous etch rates (0.9-2.5 nm/min) obtained by the quartz crystal measurements are well below that reported by Masuda for crystalline Si (50-230 nm/min for $T_{\text{sub}} = 100\text{-}150^\circ\text{C}$) in a similar temperature regime. If it is assumed that the c-Si etch rate for our experiment is at least one order of magnitude lower than that for a-Si (i.e., 0.25 nm/min), as suggested by Otobe,⁴ this results in the removal of 225 nm of material over the span of 15 hours (the maximum H-exposure time used). If it is further assumed that the yield (defined here as the ratio of the net growth rate at the substrate to the etch rate at the target) for this process is 4% (the Masuda value), the resulting film thickness is 9 nm. This thickness is consistent with the present results obtained for c-Si target etching, and is near the resolution limit of the profilometer used for thickness determination. The higher etch rates expected for a-Si consequently led to a measurably thick film of 50 nm after only 1.5 hours. For an assumed yield of 4%, a higher amorphous etch rate of 14 nm/min (as compared with the quartz crystal

measurement of 2.5 nm/min) would be calculated; this difference may be accounted for, however, by variation between the quartz crystal temperature and that of the target substrate.

Considering the discrepancy between the present results and those of Masuda, it is useful at this point to place these results in the context of previous studies of H etching (by plasma, hot-wire, or other methods) of amorphous and crystalline Si. Results of Otobe *et al.*,⁴ using a very high frequency (VHF) plasma system, show that the c-Si etch rate is insensitive to temperature over a range from 100°C-300°C, while a-Si shows a factor of 4 reduction in etch rate over the same range. The conditions of these experiments are not significantly different from those of the present study, namely an H₂ pressure of 200 mTorr and a flow rate of 54 sccm. The absolute etching rates obtained were 3 nm/min (3×10^{-3} μm/min) for a-Si and 0.3 nm/min (3×10^{-4} μm/min) for c-Si. The a-Si etch rate obtained by Otobe is comparable to the quartz crystal measurements previously described, but that for c-Si is several orders of magnitude less than reported by Masuda.

Results of Wanka⁵ show relatively high etch rates of up to 160 nm/min (0.16 μm/min) for a-Si (for 150 mTorr H₂, 80 sccm, and T_{sub} = 25°C), dropping only to 100 nm/min (0.1 μm/min) at the highest substrate temperature (400°C).

Unpublished results by Fontcuberta i Morral⁶ reveal negligible etch rates for μc-Si, rates of up to 6 nm/min (0.006 μm/min) for a-Si, with a variation of only 15%

for temperatures between 100°C-250°C; these results were obtained for an H₂ pressure of approximately 1 Torr under low power plasma conditions.

Table 1 summarizes the results of the present studies along with those previously mentioned. Absolute etching rates for a-Si range from 0.3 nm/min up to 160 nm/min, the differences due perhaps to target temperature variations and/or intrinsic differences between the techniques used (i.e., higher degree of H₂ dissociation and thus higher H-flux). The majority of results for μ c-Si and c-Si reveal small or negligible etching rates when compared with a-Si under similar conditions. The two exceptions are the Masuda results and those of Abrefah and Olander.² However, the latter involves molecular beam etching where the incident H flux could be expected to differ from that in a plasma or hot-wire system, and the etch rate cited was extrapolated from low pressure data ($\sim 10^{-4}$ Torr); it is not clear that the etch rate should be linear in pressure over several orders of magnitude, considering the multiple competing processes that are taking place (e.g., bulk diffusion, H₂ recombination).

Why the Masuda results differ so substantially from the majority of results in the literature is unclear. The picture that emerges from these results, however, is that it is difficult to obtain selective etching and growth by a process similar to ours at high rates; a temperature gradient between the target and substrate alone does not seem adequate. Thus, another process must be devised that separates out the etching and deposition steps, as it is clear that the optimal conditions for

Table 1. Comparison of etch rates for amorphous and crystalline silicon – (100), unless otherwise noted. Pressures and flow rates are those of pure hydrogen. The etch rate for Holt *et al.* (a-Si) was calculated based on the resultant growth rate, assuming a 4% yield. Abrefah *et al.*² calculate the etching rate reported in this table by extrapolating data from $\sim 10^{-4}$ Torr.

<i>Author/ Technique</i>	<i>Material</i>	<i>P (mTorr)</i>	<i>Q (sccm)</i>	<i>T_{substr} (°C)</i>	<i>Etch rate ($\mu\text{m}/\text{min}$)</i>
Otobe <i>et al.</i> ⁴ / VHF plasma 5W/144 MHz	a-Si	200	54	150	3.0×10^{-3}
Same	c-Si	200	54	150	3.0×10^{-4}
present author/ hot-wire (film growth)	a-Si	146	80	<100	~ 0.014 calculated
Same (film growth)	c-Si	100 150	10 80	100 100	$< 10^{-5}$ $< 10^{-5}$
Same (quartz crystal)	a-Si	150	20	<100	2.5×10^{-3}
Fontcuberta i Morral ⁶ / low P plasma	a-Si	1000	140	100	6.0×10^{-3}
Same	$\mu\text{c-Si}$	1000	140	100	Negligible
Wanka <i>et al.</i> ⁵ / hot-wire	a-Si	150	80	400	0.1
Same	a-Si	150	80	25	0.16
Same	a-Si	150	20	400	0.03
Masuda <i>et al.</i> ³ / hot-wire	c-Si	100	10	80	0.25
Abrefah <i>et al.</i> ² / molecular beam	c-Si (111)	100	n/a	25	4.0 from low P data

H-etching are substantially different from those for high rate growth. Specifically, a high flux atomic H source is needed (by hot-filament or plasma methods) that can be directed at the target material. The degree of H_2 dissociation in this source should be as high as possible to insure that the residual H_2 pressure in the chamber is as low as possible. The smaller the H_2 pressure in the chamber, the lower will be the H flux from the wire to the heated substrate, thus reducing the amount of competitive etching. After high rate etching is achieved, the etch products (SiH_4) would be subsequently decomposed by a hot filament placed near the heated substrate. The schematic of this process would differ from Figure 1 only in the addition of this atomic H source placed in close proximity (< 1 cm) to the cooled target.

6.5 Conclusions

Etching of cooled crystalline silicon substrates was negligible under a variety of pressures and flow rates explored with hot-wire chemical vapor deposition. The vast majority of other reports from the literature also suggest negligible etching of crystalline silicon under similar conditions, albeit with different techniques. Direct etching rate determination using a water-cooled quartz crystal monitor revealed a-Si etch rates of up to 2.5 nm/min at a H_2 to SiH_4 dilution of 150:1. Then, using an a-Si layer deposited onto a cooled Si(100)

substrate as a target, a net growth rate of 0.6 nm/min onto a heated Ge(100) substrate was obtained, with a calculated etch rate of ~ 14 nm/min; the index of refraction was consistent with crystalline silicon.

Coupled with the present experimental observations and those in the literature, it appears that a single hot filament is inadequate to selectively etch a cooled c-Si target with H atoms and concurrently decompose those etch products and deposit onto a heated substrate at high rates. This may be due to both the negligible etch rate at the cooled target and competitive etching at the heated substrate. A number of results in the literature suggest c-Si etch rates are relatively insensitive to temperature, in contrast to results presented by Masuda. As a result, a high flux pure atomic H source (e.g., one produced by a hot filament or microwave plasma) directed at the target substrate is proposed as an addition to the present design. This may enable the use of c-Si (and potentially less refined polycrystalline material such as metallurgical silicon) as a target material, with potentially higher etching rates and higher net deposition rates onto the substrate than obtained with the current design.

References

1. S. Veprek and V. Marecek, *Solid State Electronics* **11**, 683-684 (1968).
2. J. Abrefah and D. Olander, *Surface Science* **209**, 291-313 (1989).
3. A. Masuda, K. Kamesaki, A. Izumi, and H. Matsumura, *Mat. Res. Soc. Symp. Proc.* **664**, A4.5 (2001).
4. M. Otobe, M. Kimura, and S. Oda, *Jpn. J. Appl. Phys.* **33**, 4442-4445 (1994).
5. H. Wanka and M. Schubert, *J. Phys. D: Appl. Phys.* **30**, L28-L31 (1997).
6. A. Fontcuberta i Morral, unpublished data (2002).

Chapter 7 Conclusions and Future Work

7.1 Wire Surface Kinetics

Atomic Si was determined to be the predominant radical species desorbed from a new tungsten filament at temperatures above 1500 K. A strong dependence of the radical desorption kinetics on the history of the tungsten filament was observed. While new filaments show an 8 kcal/mole apparent activation energy for SiH_3 desorption, an aged filament shows a value of 110 kcal/mole, suggesting it no longer acts as a catalyst. Chemical analysis of aged wires show surface Si concentrations as high as 15 atomic %, with interior concentrations of approximately 2 atomic %. These results suggest that careful attention must be paid both to the temperature and silane exposure time experienced by the filament. If silicide formation can be suppressed, the silane decomposition rate, and consequently film growth rate, will be optimized.

Future studies could focus on other filament materials such as tantalum, molybdenum, and iridium. Some of these materials may prove superior because of the absence of a stable silicide phase under typical hot-wire conditions. These materials may also retain their ductility after high temperature annealing, reducing the likelihood of premature wire breakage that is a common problem

with the hot-wire process. Another interesting filament material from the standpoint of chemical resistivity and high temperature operation is graphite. Graphite is believed to be chemically inert, not reacting with precursor gases like silane or germane, thus reducing the likelihood of embrittlement that occurs with metallic filaments.¹ Its high melting temperature and chemical stability is also believed to result in less film contamination.¹ What has not been established, however, is whether graphite catalyzes the decomposition reaction of silane and other precursor gases.

7.2 Gas-Phase Experiments

The average residence time of stable gas species (i.e., Ar) was determined to be of order 10 seconds for representative hot-wire CVD film growth conditions (~ 200 mTorr dilute (1%) SiH₄). Subsequent stirred tank reactor calculations predict the onset of agglomerate (Si_xH_y, x > 1) formation for residence times greater than 10 seconds under these conditions, with the onset shifting to smaller times as the pressure increases. The radical SiH₂ was detected in large quantities relative to other species in the hot-wire reactor; however, this was attributed to heterogeneous pyrolysis on the walls. Ions were detected in only trace quantities (< 0.1%) relative to radical species in the hot-wire reactor. Disilicon species

(principally Si_2 , Si_2H , and Si_2H_6) were also trace in abundance ($\sim 1\%$) relative to radical species.

A number of directions can be defined for future studies. Safety considerations dictated the use of He-diluted silane in these studies, but the majority of researchers in the hot-wire field use pure silane (occasionally with some H_2 -dilution). The distribution of gas species could be different, and the onset of gas-phase chemistry will be at lower pressures in such an environment. To detect silane agglomerates produced at high pressures, a higher mass range spectrometer (up to 1000 amu) is needed, as well as multiple stages of pumping to insure that the base pressure remains low enough for operation of the electron multiplier ($< 10^{-5}$ Torr). Careful design of the sampling orifices (preferably, a conical geometry) at each stage is also an important consideration if radical sensitivity is to be optimized; the sensitivity for radical detection with the system used in the present studies was compromised by the use of a flat pinhole orifice. With such improvements, direct measurements of silane agglomerates might be possible, and this data would be useful to validate a number of silane pyrolysis mechanisms proposed in the literature.^{2,3}

7.3 Computations and Simulations of Gas-Phase Processes

An energetically feasible pathway for the reaction of Si and SiH₄ was proposed, involving the formation of Si₂H₂ and H₂. Uncertain is the rate of an intermediate spin-state transition, however, which remains an area for future investigation. The radical SiH₃ was predicted by direct particle simulations to be largest in abundance for conditions producing both amorphous and polycrystalline films in experiments. The H flux appears to be the most significant in dictating the amorphous-to-microcrystalline transition that occurs upon H₂-dilution. Two-dimensional DSMC simulations reveal that wire arrays can be used to improve film growth uniformity. For conditions where disilicon species formation is to be suppressed, continuum simulations predict maximum growth rates of 10 nm/s for dilute (1%) silane conditions and 50 nm/s for pure silane. Again, experimental data to validate some of these model predictions (by mass spectrometry, quartz crystal growth rate measurements) would be a useful complement.

Regarding the Si₂H₂ radical, a recent study has investigated the decay kinetics of this species, produced by photolysis of Si₂H₆ in this study.⁴ A lower limit to its self-reaction was determined (1.7×10^{-10} cm³/s), and it was determined to be unreactive towards closed-shell non-polar molecules (e.g., SiH₄, Si₂H₆).

Uncertain still, however, is the loss rate of this species at the (amorphous silicon-coated) walls. Also, direct measurements of this species in ambients of interest to hot-wire CVD of silicon (pure or dilute SiH_4), where the main production route is probably through reaction of Si and SiH_4 , are lacking. Measurements must typically infer the kinetics of this reaction through analysis of the decay rate of Si, although the myriad of other decay routes (other than through SiH_4) make this method questionable. Additional *ab-initio* and kinetic calculations to complement the work started in this thesis (specifically, examining the kinetics of the spin-state transition of the intermediate H_3SiSiH) might be the only feasible way to address this problem.

7.4 HWCVD of Silicon Nitride

Silicon nitride films were produced with refractive indices ranging from 1.8-2.5 and hydrogen content from 9-18 atomic %, making them suitable for antireflection/passivation coating applications. A transition in the hydrogen bonding from predominantly N-H to Si-H was observed as the SiH_4/NH_3 flow ratio was increased from 1% to 8%. Differences in H-release kinetics were observed for the two types of H-bonding, consistent with experimental results from the literature. In platinum-diffused silicon substrates capped by a hydrogenated nitride layer, platinum-hydrogen complexes (at a concentration of

10^{14} cm^{-3}) were observed in the bulk silicon after annealing treatments similar to those for which hydrogen loss was observed in the nitride layer; this constitutes the first such demonstration of H-passivation of bulk Si due to H-release from a silicon nitride layer. Also, photovoltaic cells with hot-wire nitride layers exhibited similar electrical properties to those produced with plasma nitride layers.

The present work on defect hydrogenation represents a first attempt at studying this effect *directly*. Previous studies have only *inferred* that defect hydrogenation was taking place based on improvements in minority carrier lifetime. The next steps in this study involve methods to increase the hydrogenation of the underlying bulk Si. One method involves Al-alloying the back side of the sample to inject vacancies that can both increase the atomic H solubility in the bulk Si, as well as assist in the dissociation of H_2 molecules.⁵ Another possibility to increase H-incorporation into the bulk Si (and reduce out-diffusion to the ambient) is to perform a forming gas ($\text{N}_2 + \text{H}_2$) anneal. This has the effect of reducing the chemical potential gradient of H_2 between the nitride layer and the surroundings, allowing a larger fraction of H_2 to diffuse into the Si. This forming gas anneal has resulted in noticeable improvements in efficiency (as compared with a pure N_2 anneal) for Al-alloyed ribbon Si cells.⁶ Coupled with methods for increasing the extent of Si hydrogenation, minority carrier lifetime measurements should also be performed that can directly correlate lifetime

improvement with defect hydrogenation. At present, it remains uncertain the extent to which the 10^{14} cm^{-3} level of Pt hydrogenation achieved in these studies would improve the lifetime.

The work involving deposition onto string ribbon Si substrates is in its initial stages and there are a number of experiments remaining to be performed. First, film uniformity could be improved with the use of a larger array of filaments. Whether improvements in film uniformity will make for significant improvements in cell electrical properties remains to be seen. Another area for future investigation involves the type of annealing treatment used – time and temperature. Samples produced in this study were subjected to a so-called “slow firing” anneal (peak temperature of 700°C with a peak dwell time of 30 seconds). Results of Yelundur *et al.*,⁷ however, suggest that a “spike firing” anneal (higher peak temperature for a shorter dwell time) can result in significant improvements in the cell efficiency. The key to effective passivation is to have a high enough temperature to release as much hydrogen from the nitride layer as possible, while keeping the dwell time sufficiently short so as not to thermally dissociate the defect-hydrogen complexes that form.

7.5 *In situ* Silane Generation by Hot-Wire Atomic Hydrogen Etching of Solid Silicon Sources

Hot-wire-produced atomic hydrogen etching of cooled ($T \sim 100^\circ\text{C}$) crystalline silicon substrates was negligible under a variety of pressures and flow rates. These results were in general agreement with the majority of reports in the literature, using a number of different techniques. Etch rates of up to 2.5 nm/min were measured for amorphous silicon at a temperature of approximately 100°C (150 mTorr H_2 , 20 sccm). Using this amorphous silicon film as the target source material, a net Si growth rate of 0.6 nm/min was obtained on a heated (400°C) Ge substrate.

As outlined in section 6.4, effective H etching of crystalline Si (whether Si(100) or a polycrystalline material like metallurgical Si) is only likely to be achieved with the use of a high flux pure atomic H source. Competitive etching at the heated substrate is likely the cause for the negligible growth rates observed when using crystalline Si targets. With the use of this high flux H source, subsequent experiments can evaluate the possibility of refining metallurgical silicon. Even if only a modest degree of refining is exhibited, the resultant films may be suitable for photovoltaic applications. The silicon nitride work of section 5 has shown that metal impurity hydrogenation is possible, and this could enable the use of relatively "metal-rich" films in photovoltaic devices.

References

1. A. Madan, S. Morrison, and J. Xi, "Hot wire chemical vapor deposition method and apparatus using graphite hot rods," U.S. Patent No. 6,427,622 (MV Systems, Inc, USA), 2001.
2. S. Girshick, M. Swihart, S. Suh, M. Mahajan, and S. Nijhawan, *J. Electrochem. Soc.* **147**, 2303 (2000).
3. A. Onischuk and V. Panfilov, *Uspekhi Khimii* **70**, 368 (2001).
4. Y. Nakajima, K. Tonokura, K. Sugimoto, and M. Koshi, *Intl. J. Chem. Kinet.* **33**, 136-141 (2001).
5. V. Yelundur, A. Rohatgi, A. Ebong, A. Gabor, J. Hanoka, and R. Wallace, *J. Electron. Matl.* **30**, 526-531 (2001).
6. B. Sopori, X. Deng, J. Benner, A. Rohatgi, P. Sana, S. Estreicher, Y. Park, and M. Robertson, *Sol. Ener. Matl. Sol. Cells* **41/42**, 159 (1996).
7. V. Yelundur, A. Rohatgi, A. Gabor, J. Hanoka, and R. Wallace, 9th Workshop on Crystalline Silicon Solar Cell Materials and Processes (Breckenridge, Colorado), p. 223-227 (1999).

Appendix A HWCVD Chamber Pictures and Design Considerations

This appendix serves to provide more detailed information about the hot-wire reactor, along with a discussion of design considerations implemented in a newer system. Figure 1 is a photo of the reactor taken from the front, indicating

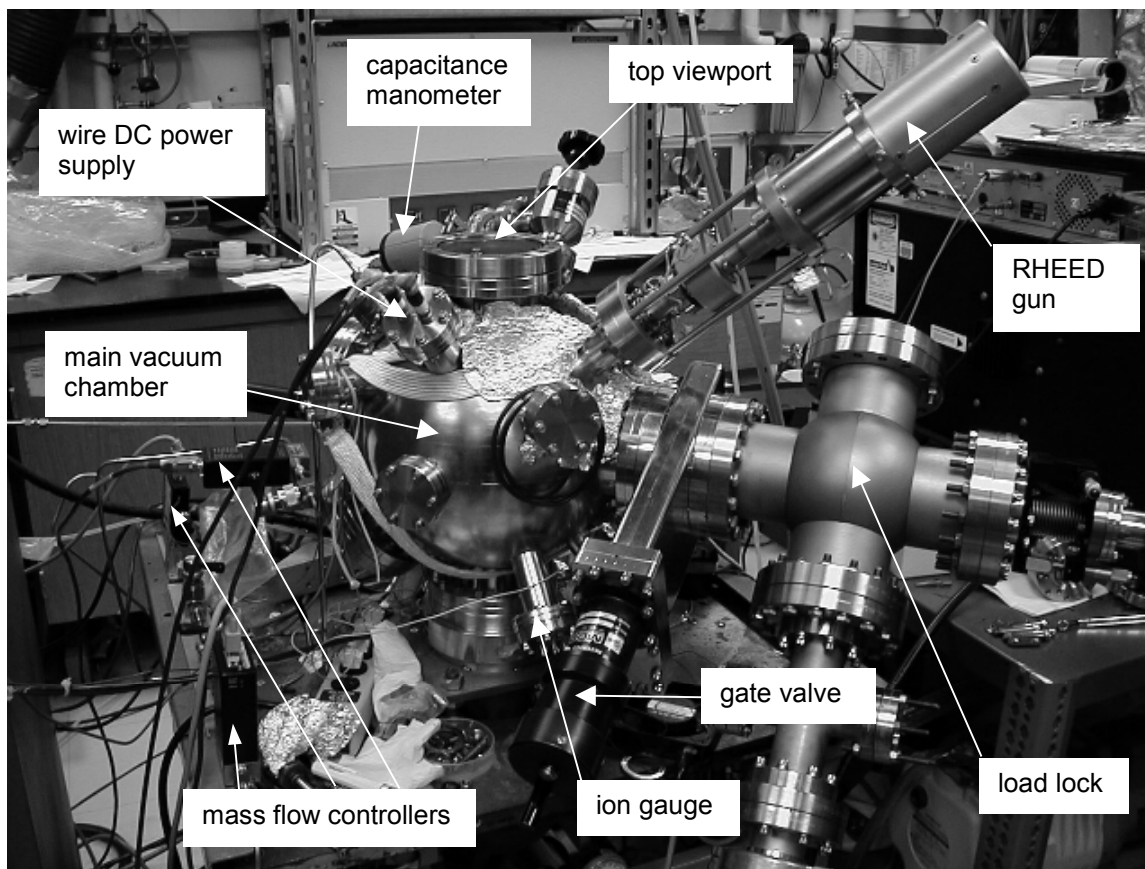


Figure 1. Front view of the hot-wire reactor.

the important features. A series of three mass flow controllers are used to introduce the precursor gases (1% SiH₄ in He, NH₃, and H₂). A capacitance manometer is used to monitor pressures in the range from 1 mTorr – 20 Torr, while an ion gauge is used for pressures below 1 mTorr. A DC power supply is used for resistive heating of the wires used in the reactor. Samples are introduced through the load lock (antechamber) illustrated and isolated from the main vacuum chamber by use of the gate valve. A RHEED gun can be used for monitoring the crystallinity of substrates and/or films *in situ* prior to and after growth, although this technique was not used for the work presented in this thesis. A viewport at the top of the chamber allows one to monitor samples as they are mounted on the substrate heater or during film growth.

Figure 2 is a photo of the chamber, taken from the rear. Visible from this angle are the substrate heater, main chamber butterfly valve (used to control the effective pumping speed), and linear motion feedthrough (used to translate the wire near the substrate during film growth). The gas inlet is also shown in Figure 2, consisting of a 0.25 inch stainless steel tube directed onto the filament(s) in the interior of the chamber. Figure 3 is a top view image through the viewport of the chamber with the wire on. For growth onto small-area samples (< 10 cm²), a single filament of 12 cm length (0.5 mm diameter) is used and held in place by the assembly shown; the wire is oriented normal to the plane of the viewport in

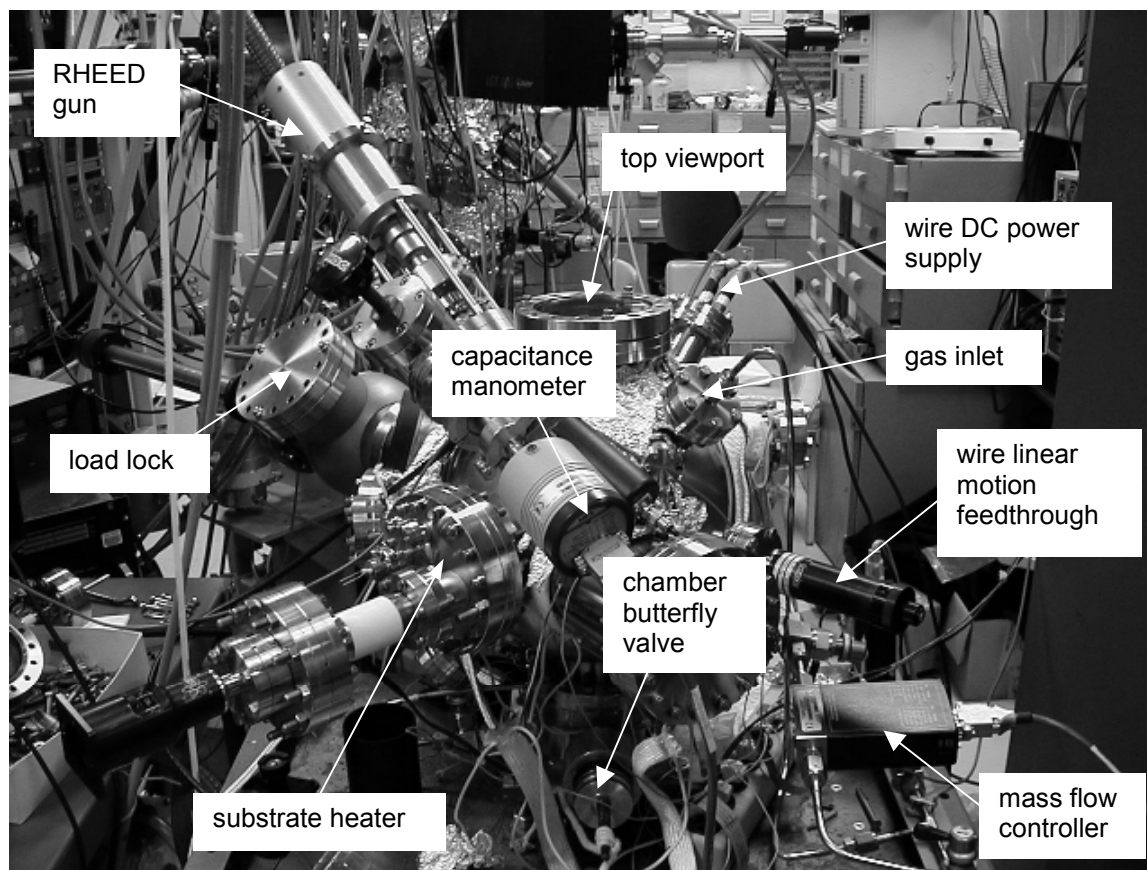


Figure 2. Rear view of the hot-wire reactor.

this photo. Ceramic standoffs are used to hold the DC power leads in place and electrically isolate the wire from the assembly.

For growth onto large-area samples ($\sim 100 \text{ cm}^2$), a filament array was constructed, shown in Figure 4. The array consists of a single 0.25 mm diameter tungsten filament strung in a “zig-zag” manner between 10 ceramic standoffs, spaced 20 cm in the long direction and 2 cm in the short direction. The maximum spacing between filament strands was approximately 2 cm (and a minimum of 1 cm). On the basis of results by Ledermann *et al.*,¹ as well as DSMC

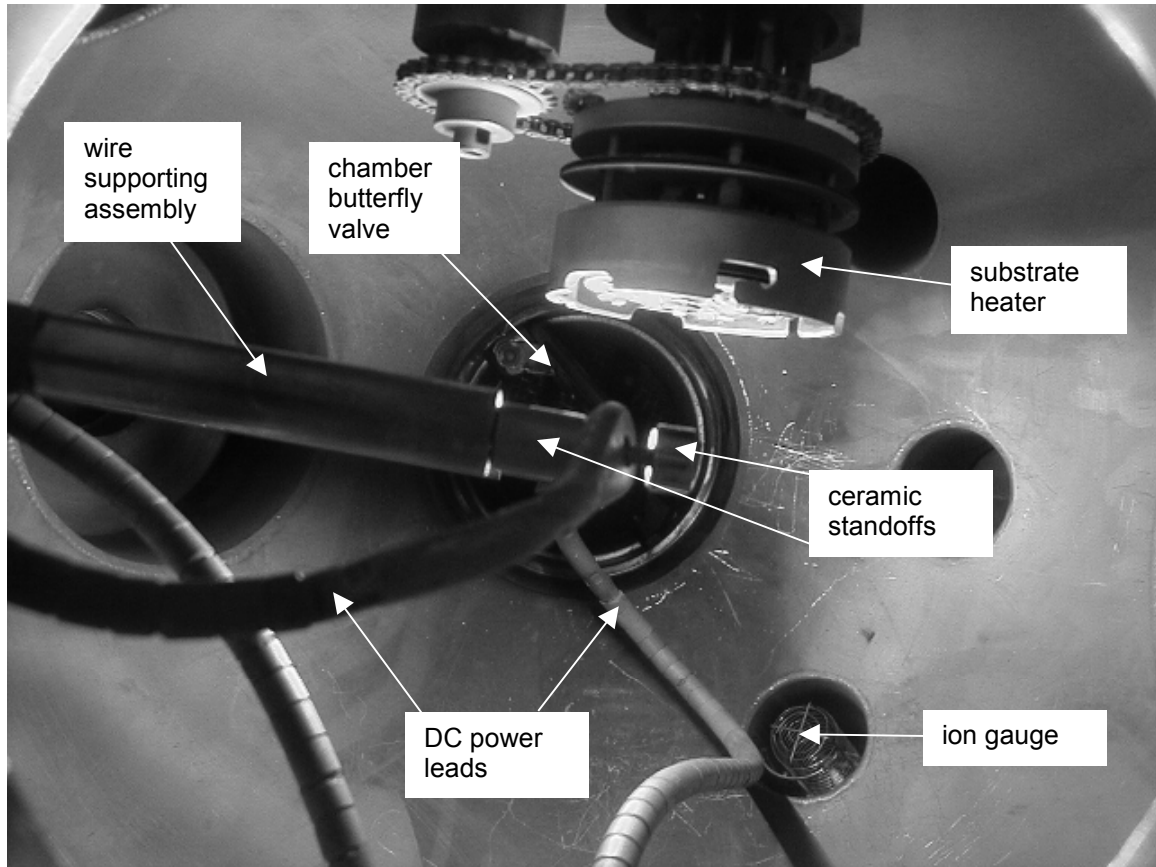


Figure 3. Top view of the hot-wire reactor through the viewport, with the wire on. The wire is oriented normal to the plane of the photo.

simulations in section 4.2.1, the filament array to substrate distance was fixed at 5 cm to prevent non-uniformity associated with the filament spacing; the criterion is that the wire spacing should be no larger than twice the filament-to-substrate distance. For a size comparison, the String Ribbon substrate (15 cm x 8 cm) that was used for deposition with this array is also shown in Figure 4.

A persistent problem with the hot-wire technique is the heat loss that occurs at the ends of the filaments, resulting in embrittlement (due to silicide formation,

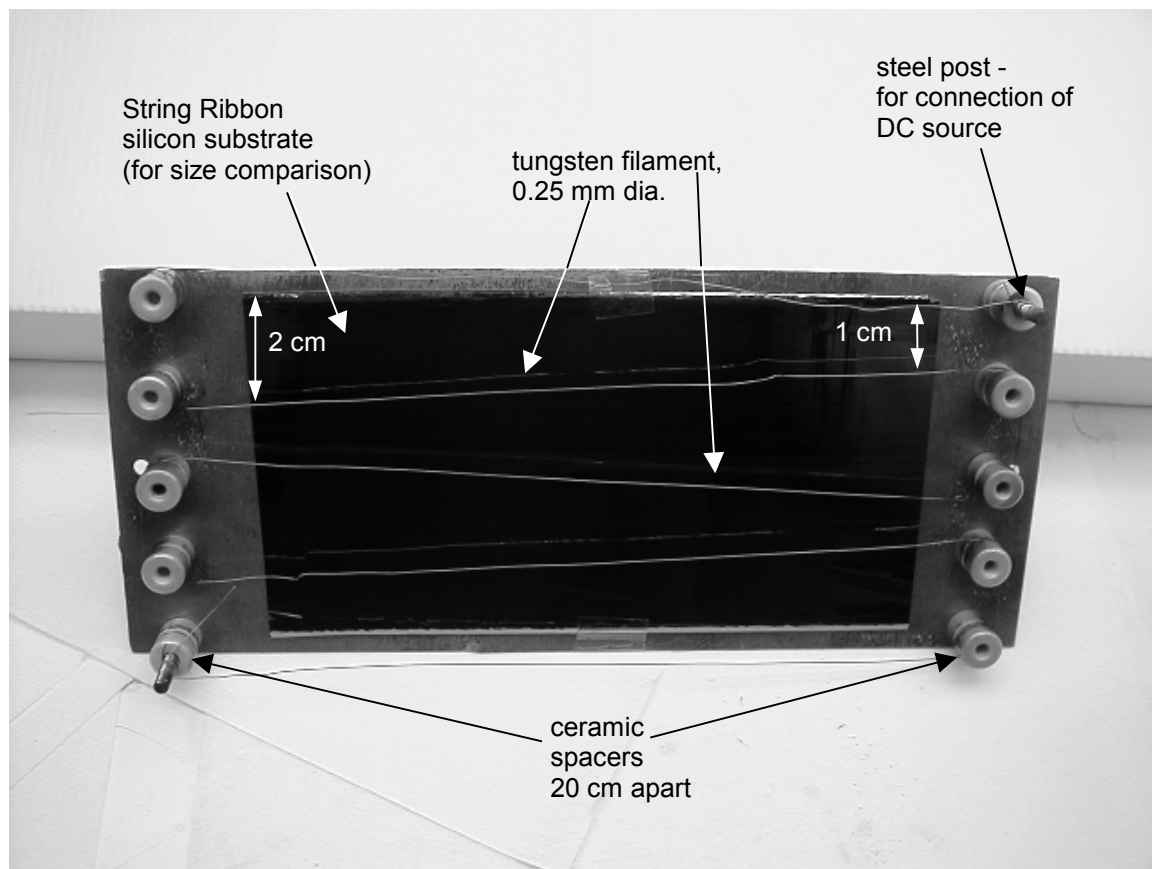


Figure 4. Wire array used for growth onto large area ($> 100 \text{ cm}^2$) samples.

section 2.4) and eventual breakage. A method to combat this problem was developed by the group at ANELVA Corporation in Japan, in collaboration with the Japan Advanced Institute of Science and Technology (JAIST), for a 1 m^2 deposition system.² Their design consists of a combined showerhead-catalyzer unit, illustrated in Figure 5. For 1 m^2 deposition, uniform distribution of the precursor gases around the filament array becomes critical (for the relatively small area samples used in this work, 100 cm^2 , a single gas tube sufficed). The idea behind the design is to use a series of shorter filaments, centered around a

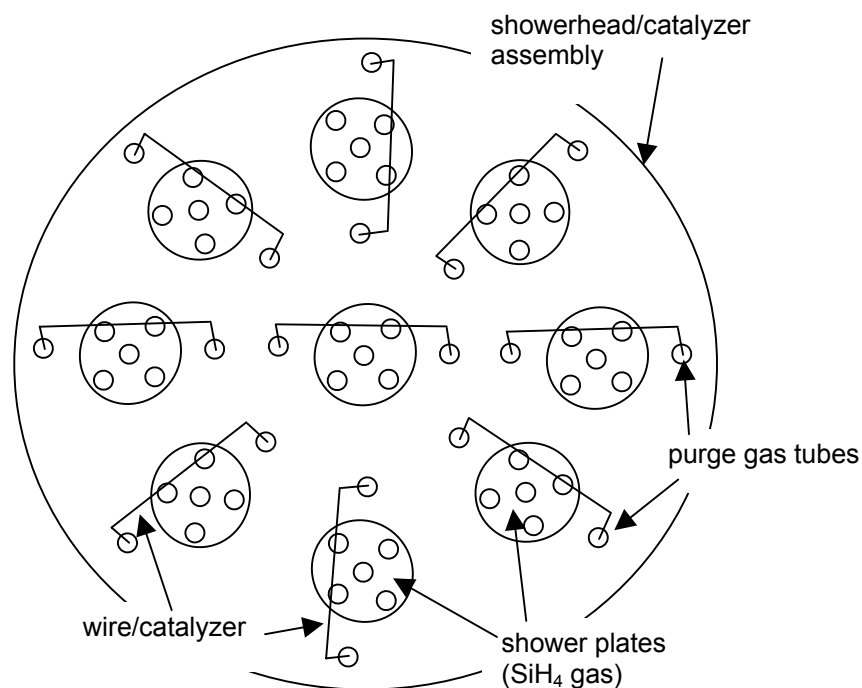


Figure 5. Schematic of showerhead-catalyzer assembly developed by the ANELVA/JAIST group. Adapted from Matsumura.³

shower plate through which the SiH₄ is introduced, with the terminal regions separated from the flow of SiH₄ gas by tubes through which a purge gas (e.g., H₂) may flow. Even in the absence of a purge gas, it was demonstrated² that silicide formation could be suppressed, presumably because the SiH₄ gas was decomposed and products deposited onto the interior walls of the purge gas tube before it could reach the cold ends near the terminals. In cases where a purge gas can be tolerated or is in fact desired during deposition (e.g., H₂ during microcrystalline growth), SiH₄ decomposition inside the tube could be suppressed entirely. For large-area (~ 1 m²) deposition where filament breakage

and replacement leads to significant downtime in the process, the aforementioned designs are a critical step forward in the industrialization of the hot-wire technique.

References

1. A. Ledermann, U. Weber, C. Mukherjee, and B. Schroeder, *Thin Solid Films* **395**, 61-65 (2001).
2. K. Ishibashi, M. Karasawa, G. Xu, N. Yokokawa, M. Ikemoto, A. Masuda, and H. Matsumura, *Abstracts of the 2nd International Conference on Cat-CVD (Hot-Wire CVD) Process (Denver, Colorado)*, p. 75-80 (2002).
3. H. Matsumura, , Kanazawa, Japan, 2000, p. 1-14.

Appendix B Wire, Substrate, and Gas-Phase Reactions Used in Modeling Studies

Tables 1 and 2 provide a summary of the relevant wire and substrate reactions used in both the DSMC and Continuum models. References are

Table 1. Assumed irreversible wire reactions, along with reaction probabilities.

Wire Reaction	Probability
(1) $\text{SiH}_4 \rightarrow \text{Si} + 4\text{H}$	0.7
(2) $\text{H}_2 \rightarrow 2\text{H}$	0.14

Table 2. Assumed irreversible surface reactions, along with reaction probabilities. H(s) represents a hydrogenated surface site, --(s) represents an open site, Si(s) is a silicon atom that has been incorporated into the film, and $\text{SiH}_3(\text{s})$ is a tri-hydride surface site.

Surface Reaction	Probability
(1) $\text{H} + \text{H}(\text{s}) \rightarrow (1/2)\text{H}_2 + \text{H}(\text{s})$	1.0
(2) $\text{SiH}_x + \text{H}(\text{s}) \rightarrow \text{Si}(\text{s}) + \text{H}(\text{s}) + (x/2)\text{H}_2, 0 \leq x \leq 2$	0.7
(3) $\text{Si}_n + \text{H}(\text{s}) \rightarrow n\text{Si}(\text{s}) + \text{H}(\text{s})$	0.7
(4) $\text{SiH}_3 + \text{H}(\text{s}) \rightarrow \text{SiH}_4 + \text{--}(\text{s})$	0.1
(5) $\text{SiH}_3 + \text{H}(\text{s}) \rightarrow \text{Si}(\text{s}) + \text{H}(\text{s}) + (3/2)\text{H}_2$	0.18
(6) $\text{H}_2 + \text{--}(\text{s}) \rightarrow \text{H}(\text{s}) + (1/2)\text{H}_2$	1.0

provided in section 4.2.1. It is worth noting here that the DSMC code handles non-integral amounts of H₂ by using a counter to keep track of the total. Once an integral amount is accumulated (e.g., 2 X (3/2) H₂ = 3 H₂), the H₂ molecules are reintroduced into the gas-phase; this insures an H-balance in the gas-phase.

Table 3 provides a complete list of all 19 reversible gas-phase reactions used

Table 3. Gas-phase reactions used in the DSMC simulation. The rate constant is given by: $k = AT^n \exp(-E_a/RT)$. Reactions (1)-(10) constitute the bimolecular portion of the mechanism, while reactions (11)-(19) are the remaining reactions that require a third body, denoted by (+M).

Reaction	A (cm ³ /mole-s)	n	E _a (cal/mole)
(1) SiH ₄ + H = SiH ₃ + H ₂	7.8E14	0.0	4491
(2) SiH ₄ + SiH ₂ = H ₃ SiSiH + H ₂	1.3E13	0.0	0
(3) SiH ₂ + SiH ₂ = Si ₂ H ₂ + H ₂	6.5E14	0.0	0
(4) SiH + H ₂ = SiH ₂ + H	4.8E14	0.0	23640
(5) SiH + SiH ₄ = H ₃ SiSiH + H	1.6E14	0.0	0
(6) Si + H ₂ = SiH + H	1.5E15	0.0	31800
(7) Si + SiH ₄ = Si ₂ H ₂ + H ₂	4.0E14	0.0	0
(8) SiH ₃ + SiH ₃ = SiH ₂ + SiH ₄	6.3E13	0.0	0
(9) SiH ₃ + SiH ₃ = H ₂ + H ₃ SiSiH	7.0E12	0.0	0
(10) Si + Si ₂ H ₆ = SiH ₂ + H ₃ SiSiH	1.3E15	0.0	12600
(11) SiH ₄ (+M) = SiH ₂ + H ₂ (+M)	3.1E09	1.67	54710
(12) Si ₂ H ₂ (+M) = Si ₂ + H ₂ (+M)	3.1E09	1.67	54710
(13) H ₃ SiSiH (+M) = H ₂ SiSiH ₂ (+M)	2.5E13	-0.22	5381
(14) Si ₃ H ₈ (+M) = SiH ₄ + H ₃ SiSiH (+M)	3.7E12	0.99	50850
(15) Si ₃ H ₈ (+M) = SiH ₂ + Si ₂ H ₆ (+M)	7.0E12	0.97	52677
(16) Si ₂ H ₆ (+M) = H ₂ + H ₃ SiSiH (+M)	9.1E9	1.83	54197
(17) Si ₂ H ₆ (+M) = SiH ₄ + SiH ₂ (+M)	1.8E10	1.75	50203
(18) H ₃ SiSiH (+M) = Si + SiH ₄ (+M)	1.4E13	0.54	57548
(19) Si + Si (+M) = Si ₂ (+M)	2.5E16	0.0	1178

in the original mechanism. The reactions involving atomic H come from the data of Woiki *et al.*,¹ while the other reactions (except (12)) are from the silane pyrolysis mechanism of Ho *et al.*² The kinetics of reaction (12) were estimated, by analogy with the unimolecular decomposition reaction of SiH₄ (reaction (11)). In DSMC simulations, the inclusion of additional species and gas-phase reactions has a computational penalty associated with it. Additional particles must be added to the simulation if trace species are to be resolved, and the computation timescales in proportion with the number of particles. Thus, if the number of reactions can be reduced and particular species eliminated from the mechanism, a significant savings in simulation run-time can be achieved.

For typical hot-wire CVD conditions, where the total pressure is under 300 mTorr, with SiH₄ partial pressures under 30 mTorr, only bimolecular reactions are important.³ The gas collision rate is too low for stabilization of 3-body reactions or for unimolecular decomposition to take place at a significant rate. In this case, only reactions (1)-(10) in Table 3 need to be included in the simulation mechanism. At even lower pressures, particularly for the dilute (1%) SiH₄ conditions used in the experiments of this thesis, the direct reactions of Si and H with SiH₄ were found to be the most important reactions ((1) and (7)). In this case, a typical DSMC simulation requires about 100,000 particles and takes only a few hours to achieve an acceptably low level of statistical scatter; this contrasts with the 1,000,000 particles and tens of hours that would be required for a

simulation employing the entire bimolecular mechanism. Of course, there is relatively little computational penalty associated with including the entire mechanism in continuum simulations, and thus, all 19 reactions are used in that case.

References

1. D. Woiki, L. Catoire, and P. Roth, *AIChE Journal* 43, 2670-2678 (1997).
2. P. Ho, M. Coltrin, and W. Breiland, *J. Phys. Chem.* 98, 10138 (1994).
3. D. Goodwin, *Proc. Electrochem. Soc.* (San Diego, California) p. 227, 1998.